UNIVERSITÀ DI PISA

DIPARTIMENTO DI INGEGNERIA CILVILE E INDUSTRIALE

CORSO DI LAUREA MAGISTRALE IN INGEGNERIA AEROSPAZIALE

AEROSPACE ENGINEERING

MASTER THESIS

DEVELOPMENT OF FLIGHT CONTROL LAWS FOR A SMALL-SCALE HELICOPTER

Supervisors:

Ing. Francesco Schettini

Prof. Roberto Galatolo

Prof. Eugenio Denti

Ing. Giampietro Di Rito

Author:

Roberto Fiorenzani

Academic year 2015

To my parents

ABSTRACT

University of Pisa is performing a research finalized to develop Rotary Unmanned Aerial Vehicles (RUAV) starting from a small commercial RC helicopters. These vehicles will be capable to perform planned missions in autonomous or automatic flight, including the take-off and landing phase, also thanks to sense and avoid system capabilities. At the moment the activities are focused on a small helicopter, T-REX 500 ESP, equipped with a GPS, inertial sensor and a data acquisition system, available at the department.

This thesis will focus on the development and verification of the control laws. As first step, a linear model will be developed and validated, by comparing the open loop responses with those ones provided by a complex non-linear model, carried out in a parallel work, and flight time histories. This linear model will be based on the aerodynamic derivatives to be evaluated in the trim conditions, obtained by means of a specific model. The linear model will be used to synthetize the control laws that should guarantee the automatic control of the speed components along the three body axes. To this end, several controller solutions will be studied and compared in order to identify the best architecture. The developed controllers will be verified in different flight condition by means of a simulation tests.

Notations

A	Rotor area
a	cl_alpha
$\mathbf{a_1}$	No fethering plane and rotor angle (xz)
$\mathbf{A_1}$	Cyclic command (yz)
$\mathbf{a_{1s}}$	Rotor and shaft angle (xz)
$\boldsymbol{\alpha_d}$	Rotor and velocity angle (xz)
$\mathbf{A_t}$	Tail rotor area
$\mathbf{B_1}$	Cyclic command (xz)
$\mathbf{b_1}$	No fethering plane and rotor angle (yz)
$\mathbf{b_{1s}}$	Rotor and shaft angle (yz)
$\mathbf{C_{ms}}$	Rotor moment coefficient
$\mathbf{C_t}$	Thrust coefficient
δ	cd0
DL	Disk load
$\mathbf{D_0}$	coeff. di resistance
e	offset hinge
f	Longitudinal position center of mass (x axis)
l	Lateral position center of mass
γ	Lock's number
h	Longitudinal position center of mass (z axis)
$\mathbf{H_D}$	Force parallel to the rotor
$\mathbf{h_t}$	Tail rotor position (z)
$\boldsymbol{\lambda_h}$	inflow in hovering
$\boldsymbol{\lambda_i}$	inflow
$\mathbf{l_t}$	Tail rotor position (x)
μ	Ratio horizzontal speed
$\mathbf{M_s}$	Moment due hingeless rotor
Ω	velocità angolare
R	Main rotor radius
ρ	Air density

$\mathbf{R_t}$	Tail rotor radius
$\boldsymbol{\sigma}$	Rotor solidity
$\boldsymbol{\sigma_t}$	Tail rotor solidity
$\mathbf{T_D}$	Force perpendicular to the rotor
$\mathbf{V_{tip}}$	Velocity at rotor tip
W	weight
wc	Non-dimentional weight

Introduction

This thesis is part of a larger study of the University of Pisa on Rotary Unmanned Aerial Vehicle of small dimension.

These vehicles have unique capabilities, such as vertical take-off and landing, maintain hovering for an extended period of time and high flight maneuvering; therefore them developing is in a growing interest.

The T-REX 500 ESP is the vehicle owned in department, where the identification of the non- linear system has been developed.

The purpose of this thesis is the development of flight control laws for the automatic flight mode.

In the automatic flight mode the pilot does not command the swash plate, but the motion of the vehicle by assign the velocity along the three body axis and the control ensure the stability during the flight checking the attitudes and the velocities.

A particular function of the automatic mode is the hovering, where, without commands of the pilot, the helicopter maintaining the stability in a specific geographic point by the feedback signals of the GPS and inertial sensor equipped on board.

In forward flight the pilot can assign velocity target (longitudinal, lateral and vertical speed) to change the state of flight.

The develop of the control laws pass throw the study of a liner model, necessary to find the transfer functions of the system.

In chapter 1, a generic description of the RUAV is provided, with a presentation of the T-REX 500 ESP and its identification of the non-linear model.

In chapter 2, the mathematical models, that are the cornerstone of the dynamic of the helicopter, are introduced; in particular the equation of flapping of the main rotor and the theory at the base of the generation of the thrust force.

In the chapter 3, the calculation of trim and aerodynamic derivatives is developed; the solution is reported for different value of the coefficient of forward speed μ.

In chapter 4, the linear system has been defined, a description of the behavior of the helicopter has been shown and the stability augmentation system by the mechanical feedback of the fly-bar has been described; the linear model has occurred with the non-linear system by checking the response to the same commands registered in a flight test; the results of the trim are implemented in the non-linear system with a Simulink tool to verify the equilibrium.

In chapter 5, the response in open loop to the commands known in literature have been studied, than the structure of controls in hovering, longitudinal velocity *u*, vertical velocity *w* and roll attitude ϕ have been developed and they have been validated with simulation in different flight conditions.

In the last chapter 6, the conclusion and the future step are illustrated.

INDEX

LIST OF FIGURE

LIST OF TABLE

1. INTRODUCTION TO RUAV

The acronym RPAS (Remotely Piloted Air System) is a flying system unmanned, controlled by radio or satellite from a fixed or mobile center on ground (Ground Control Station, GCS) that can be deployed even at a great distance from theater of operations.

The unmanned machine can be simplified by a system to increase stability (Stability Augmentation System, SAS) on board, or entirely entrusted to an appropriate system for the management of the flight that completely replaces the human operator; the first case is a flight in automatic mode and the second it is called stand-alone mode and the mission will be carried out according to the plans of flight plan.

The name Unmanned Aerial System (UAS) indicates the same concept to previous definition of RPAS, while the definition of Unmanned Aerial Vehicle (UAV) refers to the only segment of flight, not including all the elements constituting the complete system, such as the Ground Control Station (GCS).

There are various advantages in terms of weight and cost for UAVs compared to traditional systems with the pilot on board; such systems, in fact, do not have the need to have an area sufficiently broad in the fuselage to accommodate the pilot and do not require a cumbersome board instrumentation.

The maneuverability of conventional aircraft are also bound to the limits physiological pilots in terms of accelerations measured in "g". Removing the pilot from the aircraft eliminates all typical requirements required by the presence on board the pilot, bringing the human-machine interface to the ground.

The UAVs are two times more small and up to a quarter lighter than a traditional airplane with equivalent functions, which allow you to take on a greater payload and have a greater maneuverability.

For all these reasons, these systems, initially developed for purely military purposes, are becoming more widespread in the civil field.

These systems are often preferred to carry out some particular types of mission that are identified as Dirty, Dull, Dangerous:[10]

- Dirty: the environment is contaminated by nuclear pollution, chemical or bacteriological, such as to be harmful to the health of the crew;
- Dull: typically long-lasting as the monitoring and reconnaissance, in which the capacity of resistance and effectiveness of the human pilot poses a limit to the duration of the mission;
- Dangerous: the aircraft overfly hostile areas, that threatening the safety of the crew.

There are many types of UAV classified by endurance, altitude and weight, with fixed or rotary wing; to these last the definition is RUAV (Rotary Unmanned Aerial Vehicle).

The aircraft RUAV, in spite of a greater structural complexity and lower autonomy than fixed-wing aircraft, have some important characteristics, preferable in certain circumstances.

These machines are, in fact, endowed with the ability of vertical takeoff and landing (VTOL, Vertical Take-Off and Landing) that allows you to take advantage in the reduced space launch operations and recovery.

They are able, moreover, to be able to operate at cruise speed relatively low, and to be able to stay in the air at a fixed point (hovering).

1.1 T-REX 500 ESP

The helicopter model available in the department is the T-REX 500 ESP (figure 1.1) suitable for aerobatics and high performance flight but for this work only very low altitude, acceleration and speeds of flight will be considered; the research is ensuring the stability of the system in a small part of the flight envelope.

Figure 1.1: T-REX 500 ESP

To notice that the vertical and horizontal stabilizer surfaces of this helicopter are small and perforated, they only ensure the protection of the tail rotor, and therefore will be neglected in subsequent calculations.

Other dynamics that were not considered, since these are already controlled by standard systems present on the helicopter, are the variations of the angular speed of the main rotor (a control system over the power delivered by the electric motor ensures a constant rotation) and the yaw dynamic (a gyroscope measures the rate of yaw and it controls the collective of the tail rotor to maintain the heading except the presence of a pilot command that automatically disables the “heading lock”).

The helicopter is made of plastic material and carbon fiber, that ensure the structural strength and the low weight; the following table 1.1 summarizes the main characteristics.

This machine has a strongly rapid dynamics, but the presence of a fly-bar helps the pilot to stabilize the helicopter dynamics.
For a more specific description see [6] and [1].

Parameter	Value
Mass	2.14 kg
Weight	20.99 N
Rotor solidity	0.056 [ ]
Tail rotor solidity	0.121 [ ]
Main rotor radius	0.485 m
Flybar radius	0.235 m
Main rotor angular speed	240.7 rad s^{-1}
Tail rotor radius	0.105 m
clα	4.5 [ ]
a_t	1.5 [ ]
a_fb	1.5 [ ]
Main rotor chord	0.0423 m
Flybar chord	0.039 m
Main rotor inertia	0.01 kg m^2
Flybar inertia	7.8e-04 kg m^2
Vertical distance of main rotor from center of gravity	0.289 [ ]
Longitudinal distance of main rotor from center of gravity	-0.025 [ ]
Lateral distance of main rotor from center of gravity	0
Vertical distance of tail rotor from main rotor	-0.012/R [ ] (R means main rotor radius)
Longitudinal distance of tail rotor from main rotor	0.575/R [ ]

Helicopter equivalent flat surface	Sx=0.038 m^2; Sy=0.07 m^2; Sz=0.06 m^2;
Blade stiffness	50 N m rad^{-1}
Helicopter inertia	Ixx=0.02 kg m^2; Iyy=0.065 kg m^2; Izz=0.066 kg m^2; Ixz=-9*10^-4 kg m^2; Ixy=-7*10^-4 kg m^2; Iyz=0 kg m^2;

Table 1.1: T-REX 500 ESP main characteristics

1.2 Non-linear system

A non-linear RUAV simulation model has been developed in department to be used to validate the control laws before the flight tests.

As generally in literature, the calculation of a linear system is useful to the controllers synthesis; to validate the linear system the response of the two models to the same commands must match itch others as shown in the following chapter.

Here the non-linear dynamic model is shown quickly (to a more specific description see [1]).

The non-linear system has been developed in Matlab Simulink and it is composed of:

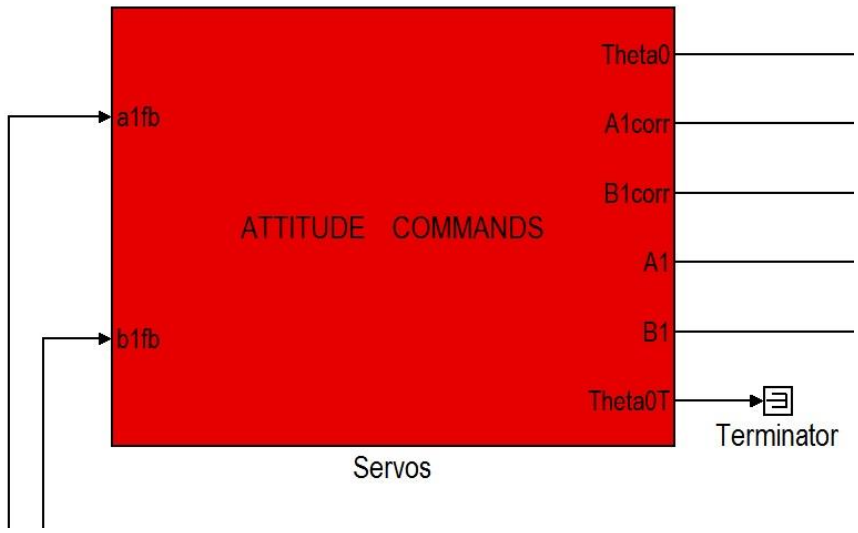

Figure 1.2 : Block of Attitude commands

In the "Attitude command's block" the electric commands, coming from the radio controller that moves the servo, are elaborated to find the angles of the swash-plate and calculate the commands known in literature θ_0, A_1, B_1 corrected by the dynamic of the fly-bar.

The tail command is now under study but the helicopter has its own gyro-control system that guarantee the heading-lock without any commands from the pilot to the tail; see the thesis [1] to upgrades.

The output goes in the following block:

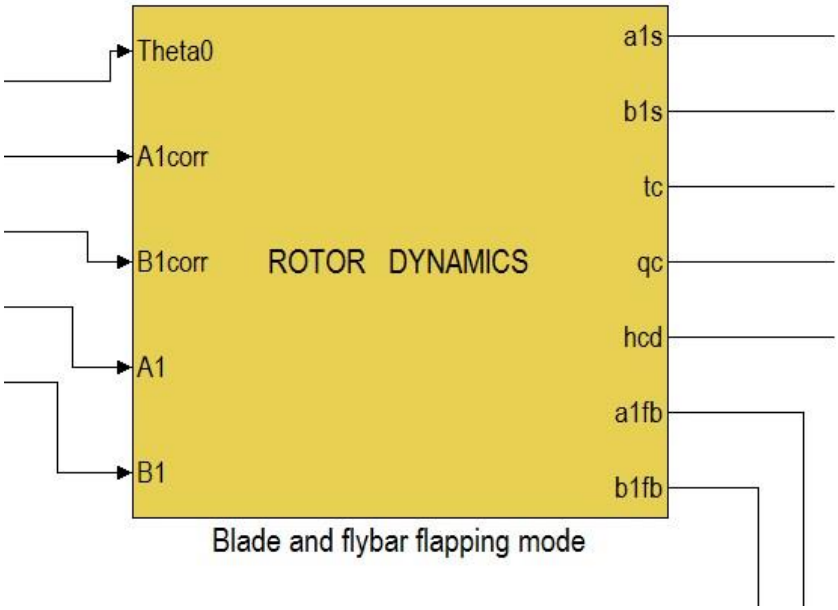

Figure 1.3 : Block of rotor and fly-bar dynamics

In the block “Rotor dynamics” are calculated the positions of the rotor and of the fly-bar compared to the shaft, on the basis of the commands and the flight conditions inputs, and the forces and torque generated by the main rotor.

The fly-bar’s outputs are used like feedback to the block of “Attitude commands” as seen previously.

The rotor’s output are used to calculate forces and moments to the helicopter axis in the following block:

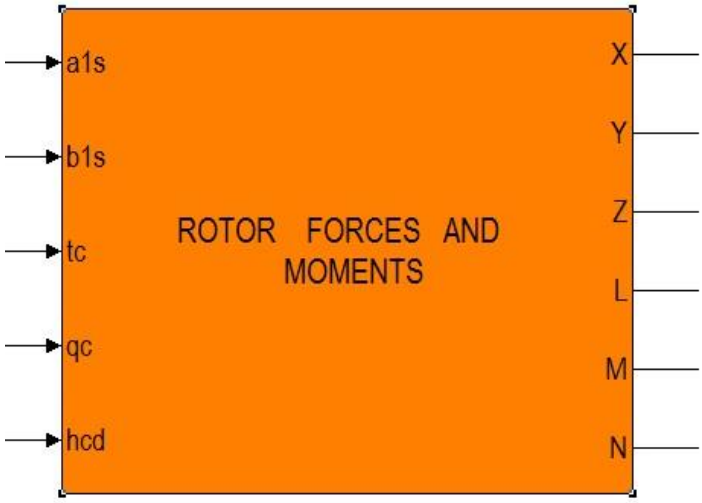

Figure 1.4 : Block of forces and moments

In the "Rotor forces and moments" the helicopter characteristics (weight, distances, inertia,…) are loaded and the rotor's forces and moments are transformed in the axes body.

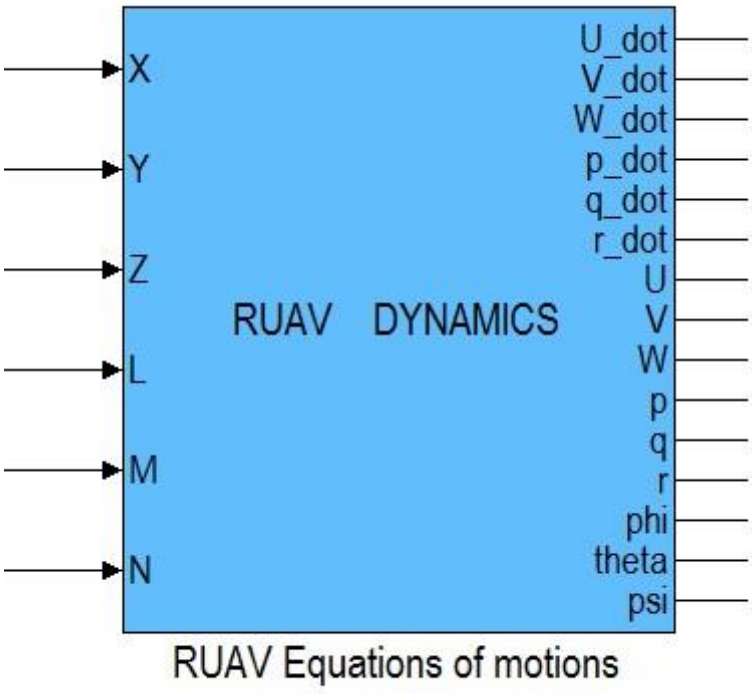

Figure 1.5 : Block of RUAV dynamic

In “Ruav dynamics” the forces and moments are used in the equations of rigid body dynamic and by integration the linear velocities, the angular speeds rate and the angular attitudes in body axes are found.

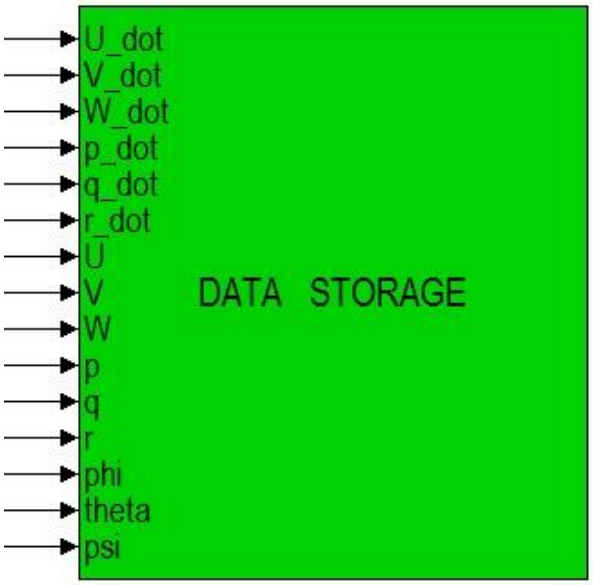

Figure 1.6 : Block of data storage

In the last block “Data storage” all the results from the simulation are transformed in inertial axes and are saved to plot the simulation results.

2. MATHEMATICAL MODELS

2.1 The flapping equation

Consider a single blade as shown in Figure 2.1 and let the flapping hinge be mounted a distance eR from the axis of rotation.

The shaft rotates with constant angular velocity Ω and the blade flaps with angular velocity $\dot{\beta}$.

The considered reference system is on the blade, parallel to the principal axes, origin at the hinge, with the *i* axis along the blade span, the *j* axis perpendicular to the span and parallel to the plane of rotation, and the *k* axis completing the right-hand set.

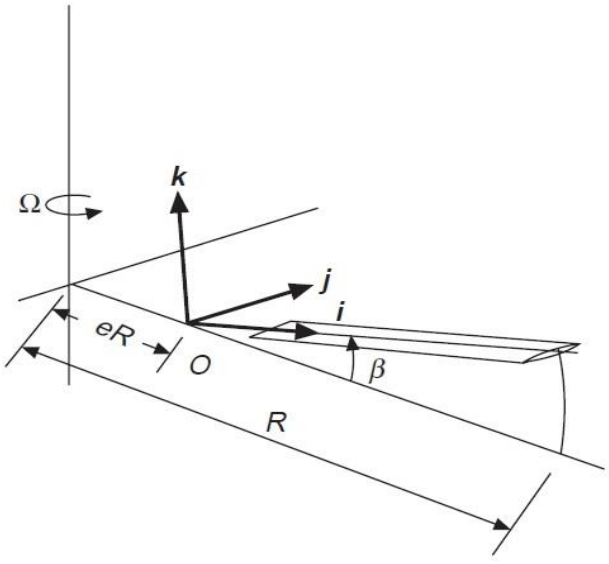

Figure 2.1 : Flapping blade and reference axes [2]

A very good approximation is to treat the blade as a lamina.

As a consequence, if *A* is the moment of inertia about *i*, and *B* the moment of inertia about *j*, the moment of inertia *C* about *k* is equal to *A* + *B*.

The angular velocity components $\omega 1, \omega 2, \omega 3$ about these axes are:

$$\omega_1 = \Omega \sin \beta, \qquad \omega_2 = -\dot{\beta}, \qquad \omega_3 = \Omega \cos \beta \tag{2.1}$$

The flapping motion takes place about the j axis, so putting the above values in the second of the 'extended' Euler's equations, and using $A + B = C$, gives

$$B\ddot{\beta} + \Omega^2(B \cos \beta + M_b e x_g R^2) \sin \beta = M_A \tag{2.2}$$

where $M_A = -M$ is the aerodynamic moment in the sense of positive flapping and M_b is the blade mass.

For small flapping angles equation 2.2 can be written

$$\ddot{\beta} + \Omega^2(1 + \varepsilon)\beta = M_A/B \tag{2.3}$$

where $\varepsilon = M_b e x_g R^2/B$.

If a disturb is considered, the change of incidence $\Delta\alpha$ due to flapping is

$$\Delta\alpha = \frac{r\dot{\beta}}{(r+eR)\Omega} = \frac{-x d\beta/d\psi}{(x+e)} \tag{2.4}$$

where $x = r/R$.

The moment of the lift about the flapping hinge is "rdL" and the total aerodynamic moment, assuming the blade chord c to be constant, is

$$\frac{M_A}{B\Omega^2} = -\left(\frac{\gamma}{8}\right)(1 - e)^3\left(1 + \frac{e}{3}\right)\frac{\partial\beta}{\partial\psi} \tag{2.5}$$

where $\gamma = \rho a c R^4/B$ is called Lock's inertia number.

The flapping equation become

$$\frac{\partial^2\beta}{\partial\psi^2} + \left(\frac{n\gamma}{8}\right)\frac{\partial\beta}{\partial\psi} + (1 + \varepsilon)\beta = 0 \tag{2.6}$$

where $n = (1 - e)^3(1 + e/3)$.

Now considering a command

$$\theta = \theta_0 - A_1 \cos\psi - B_1 \sin\psi \tag{2.7}$$

the steady-state solution of the flapping motion is

$$\beta = \gamma\theta_0/8 - A_1 \sin\psi + B_1 \cos\psi \tag{2.8}$$

The term $\gamma\theta_0/8$ represents a constant flapping angle and corresponds to a motion in which the blade traces out a shallow cone, and for this reason the angle is called the coning angle and neglecting the higher harmonics the flapping can be expressed

$$\beta = a_0 - a_1 \cos\psi - b_1 \sin\psi \tag{2.9}$$

$$\text{therefor} \begin{cases} a_0 = \gamma\theta_0/8 \\ a_1 = -B_1 \text{ e} \\ b_1 = A_1 \end{cases} \tag{2.10}$$

If the rotor hub is pitching with angular velocity q, Fig. 2.2, the angular velocity components of the blade are:

$$\{q \sin\psi \cos\beta + \Omega \sin\beta,\ q \cos\psi - \dot{\beta},\ -q \sin\psi \sin\beta + \Omega \cos\beta\} \tag{2.11}$$

where ψ is the azimuth angle of the blade, defined as the angle between the blade span and the rear center line of the helicopter.

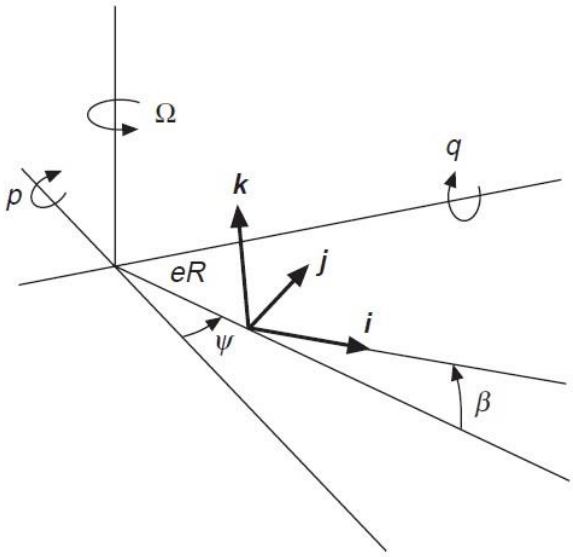

Figure 2.2 : Blade influenced by pitching and rolling rate [2]

By inserting these values into equation and neglecting q^2, which is usually very small compared with Ω^2, we finally obtain after some manipulation:

$$\ddot{\beta} + \Omega^2(1 + \varepsilon)\beta = M_A/B - 2\Omega q(1 + \varepsilon)\sin\psi + \dot{q}(1 + \varepsilon)\cos\psi \qquad (2.12)$$

The second term on the right is the gyroscopic inertia moment due to pitching velocity, and the third term is due to the pitching acceleration.

The change of incidence $\Delta\alpha$ is therefore

$$\Delta\alpha = (q\cos\psi - \dot{\beta})/\Omega = \hat{q}\cos\psi - d\beta/d\psi \qquad (2.13)$$

where $\hat{q} = q/\Omega$.

The moment due to the velocity $\dot{\beta}$ is already been considered.

The moment due to the pitching velocity q is found to be

$$(M_A)_{pitching} = \rho ac\Omega^2 R^4 \hat{q}\cos\psi/8 \qquad (2.14)$$

The flapping equation becomes now:

$$\frac{\partial^2\beta}{\partial\psi^2} + \frac{\gamma}{8}n\frac{\partial\beta}{\partial\psi} + (1 + \varepsilon)\beta = \frac{\gamma}{8}n\hat{q}\cos\psi - 2\hat{q}(1 + \varepsilon)\sin\psi \qquad (2.15)$$

and $\begin{cases} a_1 = -16\hat{q}/\gamma \\ b_1 = -\hat{q} \end{cases}$, $\hat{q} = \frac{q}{\Omega}$. (2.16)

When the rotor hub is rolling with angular velocity p, the equivalent equation to 2.15 may be derived in like manner and the extra term is: $2\Omega p\cos\psi + \dot{q}\sin\psi$.

If a longitudinal velocity is introduced the components at the blade, adding the contribution due the flapping and the induced velocity, are:

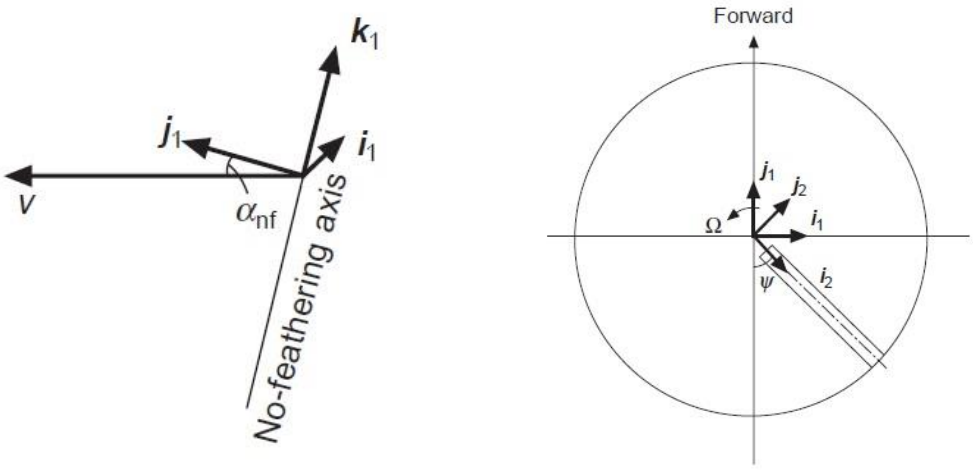

Figure 2.3 : Refereeing systems between wind and blade [2]

i direction: $V \cos \alpha_{nf} \cos \psi \cos \beta + V \sin \alpha_{nf} \sin \beta$

j direction: $-V \cos \alpha_{nf} \sin \psi - \Omega r$ (2.17)

k direction: $-V \cos \alpha_{nf} \cos \psi \sin \beta + V \sin \alpha_{nf} \cos \beta - \dot{r}\beta - v_i$

We define

$U_P = -V\beta \cos \alpha_{nf} \cos \psi + V \sin\alpha_{nf} - \dot{r}\beta - v_i$ (2.18)

$U_T = V \cos \alpha_{nf} \sin \psi + \Omega r$ (2.19)

$v_i = v_{i0}(1 + Kx\cos\psi)$ Glauert's formula (2.20)

with $v_{i0}$the inflow at the rotor center, $x = \frac{r}{R}$ and $K = \frac{4}{3}\frac{\frac{\mu}{\lambda}}{1.2+\frac{\mu}{\lambda}}$

and using

$\lambda' = (V \sin \alpha_{nf} - v_i)/\Omega R$ (2.21)

$\mu = (V \cos \alpha_{nf})/\Omega R$ (2.22)

$U_P = \Omega R(\lambda' - x\, d\beta/d\psi - \mu\beta \cos \psi)$ (2.23)

$U_T = \Omega R\,(x + \mu \sin \psi)$ (2.24)

considering the aerodynamic flapping moment

$M_A = \frac{1}{2}\rho a \int_0^R {U_T}^2(\theta + \frac{U_P}{U_T})\, cr\, dr$ (2.25)

we obtain, after some calculations, the differential equation of flapping in the form:

$$\frac{\partial^2\beta}{\partial\psi^2} + \frac{\gamma}{8}\left(1+\frac{4}{3}\mu\sin\psi\right)\frac{\partial\beta}{\partial\psi} + \left[1 + \varepsilon + \frac{\gamma}{8}\left(\frac{4}{3}\mu\cos\psi\right)\right]\beta = \frac{\gamma}{8}\left[\theta_0\left(1+\frac{8}{3}\mu\sin\psi\right) + \frac{4}{3}\lambda - K\lambda_i cos\psi + 2\mu\lambda\sin\psi - \mu\lambda_i K sin2\psi\right] \quad (2.26)$$

and the flapping coefficients in forward flight

$$a_0 = \frac{\gamma}{8(1+\varepsilon)}\left[\theta_0\,(1+\mu^2) + \frac{4}{3}\lambda\right] \quad (2.27)$$

$$a_1 = \frac{2\mu(\frac{4\theta_0}{3}+\lambda)}{1-\frac{\mu^2}{2}} + \frac{8}{\gamma}\frac{\varepsilon}{1-\frac{\mu^2}{2}}b_1 \quad (2.28)$$

$$b_1 = \frac{4(\mu a_0 + 0.75K\lambda_i)/3}{1+\frac{\mu^2}{2}} - \frac{8}{\gamma}\frac{\varepsilon}{1+\frac{\mu^2}{2}}a_1 \quad (2.29)$$

For all the dynamics of the rotor, the presence of a hinge with offset "e" has been considered, but the T-REX 500 has a hinge-less rotor and a way of studying the problem is to consider the deformation of the blades for zero offset and the moment generated proportional to the angle of flapping[3]:

$$M = k_\beta\beta \quad (2.30)$$

where k_β is the stiffness of the blade.

So, the flapping equation can be wrote $\ddot{\beta} + \Omega^2(1 + k_\beta/B\Omega^2)\,\beta = M_A/\mathrm{B}$, i.e. $\varepsilon = k_\beta/B\Omega^2$; (if we supposed to be an offset plus the blade stiffness $\varepsilon_{tot} = \varepsilon + k_\beta/B\Omega^2$).

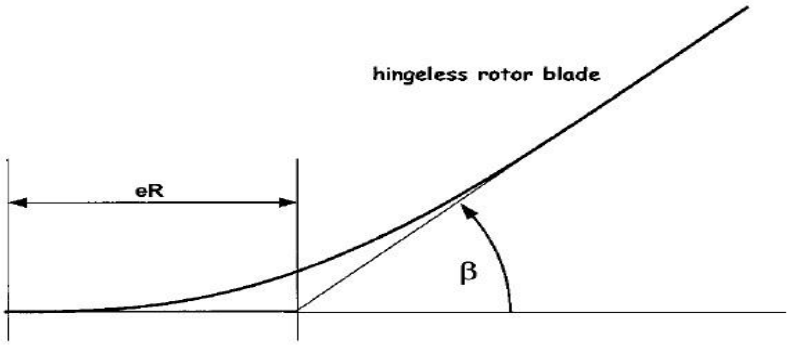

Figure 2.4 : Representation of hingeless blade [5]

2.2.1 Interpretation of flapping and feathering coefficients

The blade flaps of β angle around the hub plane and rotates of θ angle around the feathering axis.

Let us assume the following figure for a clockwise rotor to fix the meaning of the coefficients used.

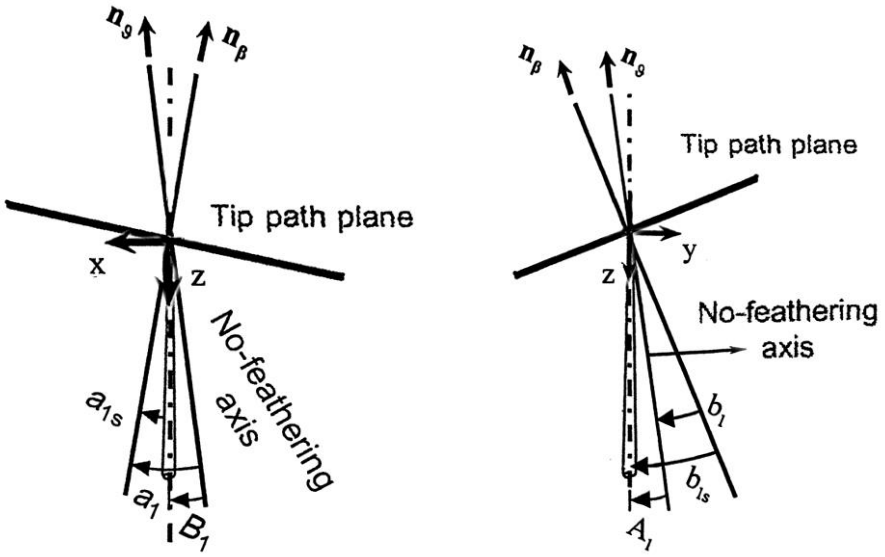

Figure 2.5 : Left and rear side view of helicopter with flapping and feathering coefficients [7]

The points occupied by the tip of the blade during the flapping are locked on the plane named tip path, that has the a_{1s} angle with the shaft in the longitudinal plane and b_{1s} in the lateral plane; while the no-feathering plane is represented by the position of the points where the blade has the same feather, it is represented by the angle B_1 in the longitudinal plane and A_1 in the lateral plane.

The tip path plane and the no-feathering plane differ them self of the flapping coefficients a_1 and b_1; they are coincident only in hovering.

2.2 Actuator disc momentum theory

Let us take a cylindrical control surface surrounding a control volume whose radius is R_1, which encloses the rotor, radius R, and its slipstream, radius R_2, Figure 2.6.

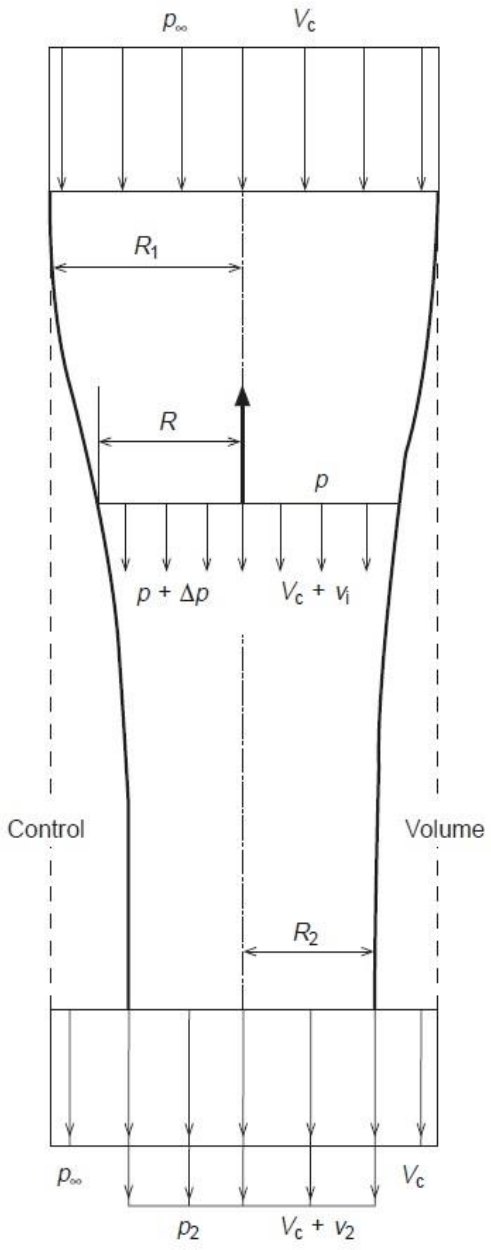

Figure 2.6 : Representation of control volume for actuator disc momentum theory [2]

The air velocity relative to the rotor is the rate of climb V_c and the pressure is p_∞. As the air approaches the rotor, the airspeed increases to $V_c + v_i$ at the rotor itself and there is a jump of pressure Δp which accounts for the rotor thrust $T = \Delta pA$, A being the rotor disc area.

The slipstream velocity continues to increase downstream of the rotor, reaching a value in the ultimate wake of $V_c + v_2$, where the slipstream radius is R_2 and the pressure p_2.

Let us assume, as for the classical actuator disc, that the pressure in the final wake is the same as the ambient pressure, i.e. that $p_2 - p_\infty = 0$.

We can write the following equations:

$$\dot{m} = \rho A(V_c + v_i) = \rho A_1 V_c = \rho A_2(V_c + v_2) \tag{2.31}$$

$$\dot{m}(V_c + v_2) - \dot{m}V_c = T \tag{2.32}$$

$$\frac{1}{2}\dot{m}\left[(V_c + v_2)^2 - {V_c}^2\right] = T(V_c + v_i) \tag{2.33}$$

After some simplifications we find:

$$v_2 = 2v_i \tag{2.34}$$

$$T = \dot{m}v_2 = 2\rho A(V_c + v_i)v_i \tag{2.35}$$

In hovering, when $V_c = 0$, the equation 2.32 simplifying in

$$T = \dot{m}v_2 = 2\rho A{v_i}^2 \tag{2.36}$$

and the inflow at fixed flight point has found to be

$$v_2 = \sqrt{\frac{T/A}{2\rho}} = v_0 \tag{2.37}$$

Generally we can write the equation 2.35

$${v_i}^2 + V_c v_i - \frac{T}{2\rho A} = 0 \tag{2.38}$$

and using the hovering inflow

$$\left(\frac{v_i}{v_0}\right)^2 + \frac{V_c v_i}{{v_0}^2} - 1 = 0 \tag{2.39}$$

2.3 Blade element theory

The relationship between the thrust and the induced velocity requires that either the thrust or the induced velocity are known.

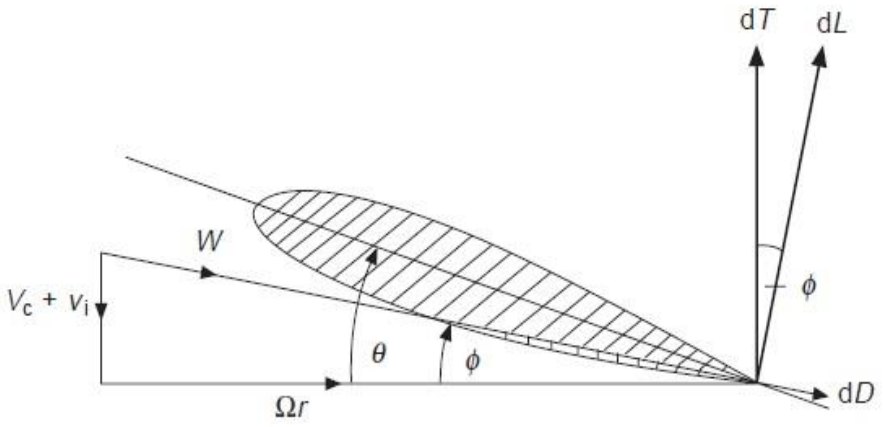

Figure 2.7 : Section of the blade [2]

Considering an element of blade of chord *c* and width dr located at a radius *r* from the axis of rotation.

The geometric pitch angle of the blade element relative to the plane of rotation is θ, the climbing speed is V_c, and the local induced velocity is v_i.

The direction of the flow relative to the blade makes an angle φ (the inflow angle) with the plane of rotation and for small φ,

$$\varphi = (Vc + vi)/\Omega r \quad (2.40)$$

$$W^2 \approx \Omega^2 r^2 \quad (2.41)$$

$$CL = a\alpha = a(\theta - \varphi) \quad (2.42)$$

$$dL \approx dT \quad (2.43)$$

where dT is the elementary thrust, the force perpendicular to the plane of rotation.

The total thrust is therefore

$$T = \frac{1}{2}\rho ab\Omega \int_0^R c(\theta - \varphi)r^2 dr \quad (2.44)$$

where b is the number of blades.

Defining

$\lambda_c = V_c/\Omega R,\ \lambda_i = v_i/\Omega R,\ x = r/R$ (2.45)

and if the chord, induced velocity and 'collective' pitch angle θ are constant along the blade,

$$T = 0.5\,\rho a c b \Omega^2 R^3 \left[\frac{\theta_0}{3} - \frac{1}{2}(\lambda_c + \lambda_i)\right] \quad (2.46)$$

where θ_0 is the constant (collective) pitch angle.

Defining a thrust coefficient by

$tc = T/\rho s A \Omega^2 R^2$ (2.47)

where $s = bc/\pi R$ is the rotor solidity, from the 2.46

$tc = (a/4)[2\theta_0/3 - (\lambda_c + \lambda_i)]$ (2.48)

Now from the momentum theory, the induced velocity and the thrust are related in non-dimensional form by

$\lambda_i^2 + \lambda_c\lambda_i - 0.5 s t_c = 0$ (2.49)

Therefore we have two equations in two unknowns.

If there is a longitudinal velocity, using the Glauert's formula, we can write

$\bar{v}_{i0}^4 + \bar{V}^2\bar{v}_{i0}^2 - 1 = 0$ (2.50)

where $\bar{v}_{i0} = \frac{v_{i0}}{v_0}$, $\bar{V} = \frac{V}{v_{i0}}$, $v_0 = \sqrt{(T/2\rho A)}$.

A Glauert's formula interpretation can be shown in the figure 2.8.

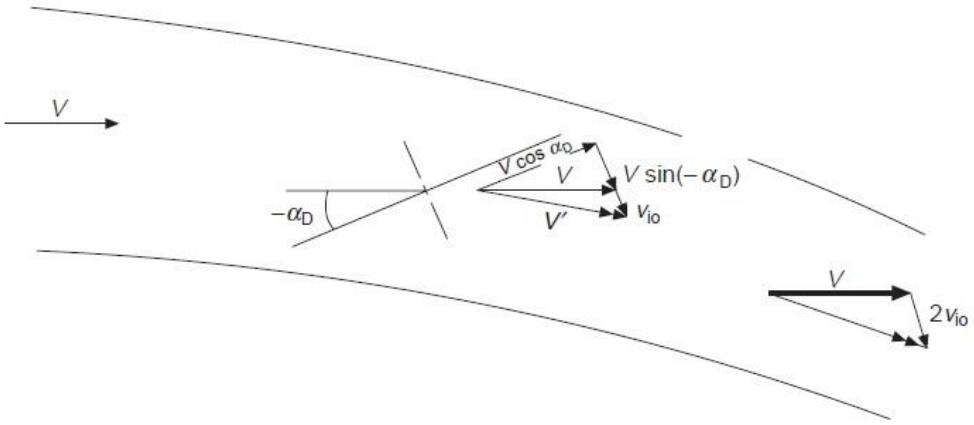

Figure 2.8 : Interpretation of Glauert's formula [2]

So the thrust coefficient is modified as[2]

$$t_c = (a/4)[2\theta_0/3(1 + 3\mu^2/2) + \lambda] \quad (2.51)$$

$$\lambda = \mu\alpha_d - \lambda_i \quad (2.52)$$

the in-plane H-force coefficient

$$h_c = (a/2)[\frac{\mu\delta}{2a} + \frac{1}{3}a_1\theta_0 + \frac{3}{4}\lambda a_1 - \frac{1}{2}\theta_0\lambda] \quad (2.53)$$

and the rotor torque coefficient

$$q_c = \frac{\delta(1+3\mu^2)}{8} - \lambda t_c - \mu h_c \quad (2.54)$$

3. TRIM AND AERODYNAMIC DERIVATIVES

The problem of trim is to determine the significant parameters characterizing the stationary straight flight of the helicopter on the longitudinal and on the lateral-directional.

3.1 Longitudinal trim

To analyze the condition of trim in the longitudinal plane, reference is made to Figure 3.1.

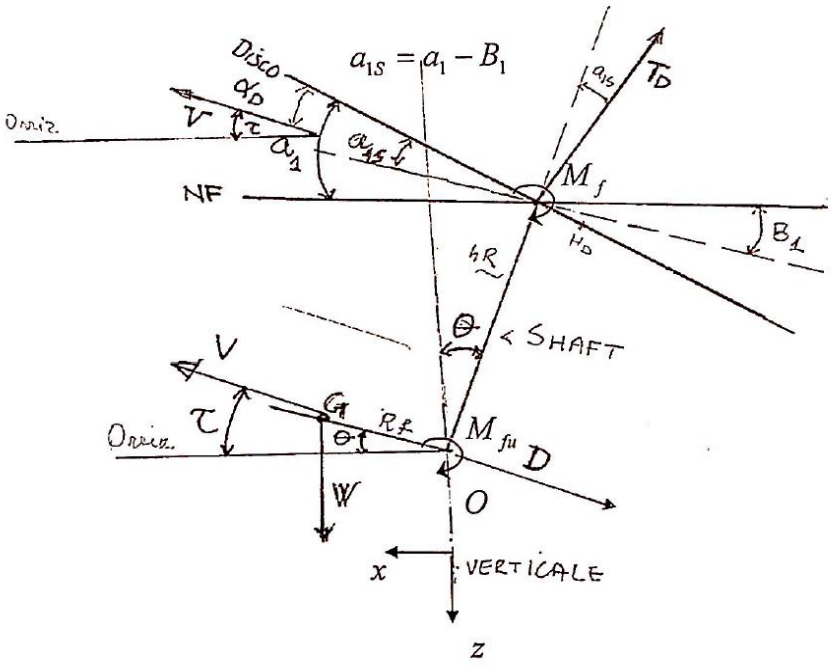

Figure 3.1: Longitudinal trim force and moments left side [7]

Equilibrium equations along the horizontal axis and the vertical axis and equation of the moment around the y axis[2][7]:

$$T_d \cdot \cos(\alpha_d + \tau) - H_d \cdot \sin(\alpha_d + \tau) - D \cdot \sin(\tau) - W = 0 \quad (3.1)$$

$$H_d \cdot \cos(\alpha_d + \tau) + T_d \cdot \sin(\alpha_d + \tau) + D \cdot \cos(\tau) = 0 \quad (3.2)$$

$$H_d \cdot \mathrm{h} \cdot \mathrm{R} \cdot \cos(a_{1s}) + T_d \cdot h \cdot R \cdot \sin(a_{1s}) - W \cdot f \cdot R \cdot \cos(\theta) + M_f + M_s \cdot a_{1s} = 0 \quad (3.3)$$

$$a_{1s} = a_1 - B_1 \quad (3.4)$$

By dividing to $s\rho AR^2\Omega^2$ with $\Omega=V_{tip}/R$ and linearizing (θ, a_{1s} ($\alpha_d+\tau$) and $H_d\sin(\alpha_d+\tau)$ are neigible):

$$t_{cd} = 0.5 \cdot \hat{V}^2 \cdot d_0 \cdot \sin(\tau) + w_c \text{ with } \hat{V} = \frac{V}{\Omega R} \quad (3.5)$$

$$h_{cd} + t_{cd} \cdot (\alpha_d + \tau) + 0.5 \cdot d_0 \cdot \cos(\tau) = 0 \quad (3.6)$$

$$h_{cd} \cdot \mathrm{h} + t_{cd} \cdot h \cdot (a_{1s}) - w_c \cdot f + C_{mf} + C_{ms} \cdot a_{1s} = 0 \quad (3.7)$$

where $C_{ms} = k_\beta / s\rho AR^2\Omega^2$.

The coefficients t_{cd} e h_{cd} are function of aerodynamics coefficients, of μ, θ_0 and the inflow, that is known from Glaeurt's theory.

The problem has coupled equations that need a iter-code to find the unknowns[7]: first of all we need to let $h_{cd} = 0.25\mu\delta$, from the 2.53, without considering the inflow and collective contribute, than we calculate α_d from the 3.6 and λ, from the 2.52, knowing λ_i with the Glauet's theory and the value of the collective command from the 2.51; at the end we upgrade the new h_{cd} value, introducing the collective command and the inflow, till the percent error is smaller than a prefixed constant as shown in the appendix A.

The flapping coefficients, the attitude and the commands which ensure the trim at the different velocities are fended and the corresponding rotor torque helpful to find the tail rotor thrust in the lateral trim.

3.2 Lateral trim

We refer to the figure 3.2

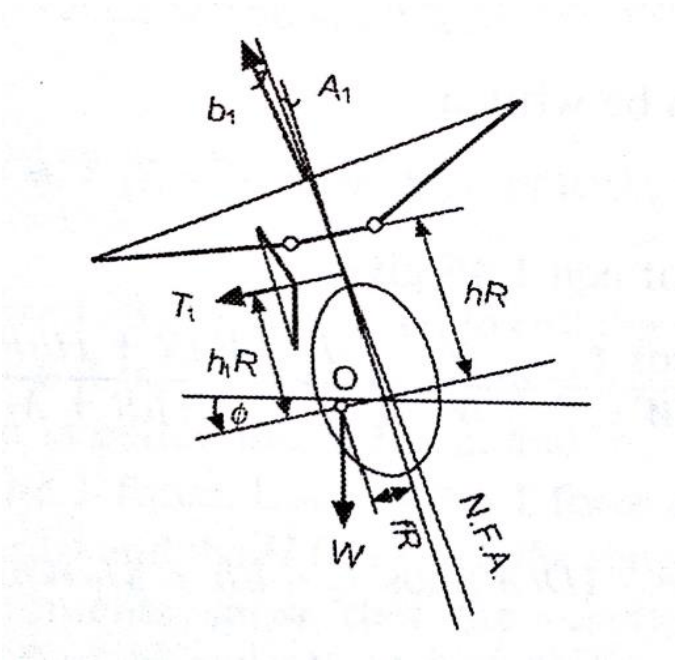

Figure 3.2: Lateral trim force and moments front side [2]

The equations of translation above y axis and the rotation around x axis are[2][7]:

$$T_t + T_d \cdot b_{1s} + W \cdot \varphi = 0 \tag{3.8}$$

$$T_t \cdot h_t \cdot R + (T_d + M_s) \cdot b_{1s} \cdot h \cdot R + W \cdot f_{lat} \cdot h = 0 \tag{3.9}$$

$$b_{1s} = A_1 + b_1 \tag{3.10}$$

Remember that the T-REX 500 has a clockwise rotor motion so in the figure 3.2 we must take A_1, b_1 and Tt negative, because it refers to a classic helicopter with anticlockwise rotor.

The tail rotor thrust Tt must compensate the rotor torque.

Defining l_t the distance of the tail rotor from the center of mass:

$$Q_c = q_c \cdot \rho \cdot s \cdot A \cdot \Omega^2 \cdot R^3 \tag{3.11}$$

$$T_t = -\frac{Q_c}{l_t} \tag{3.12}$$

3.3 Trim results

The results of the trim for the T-REX 500 are shown below.

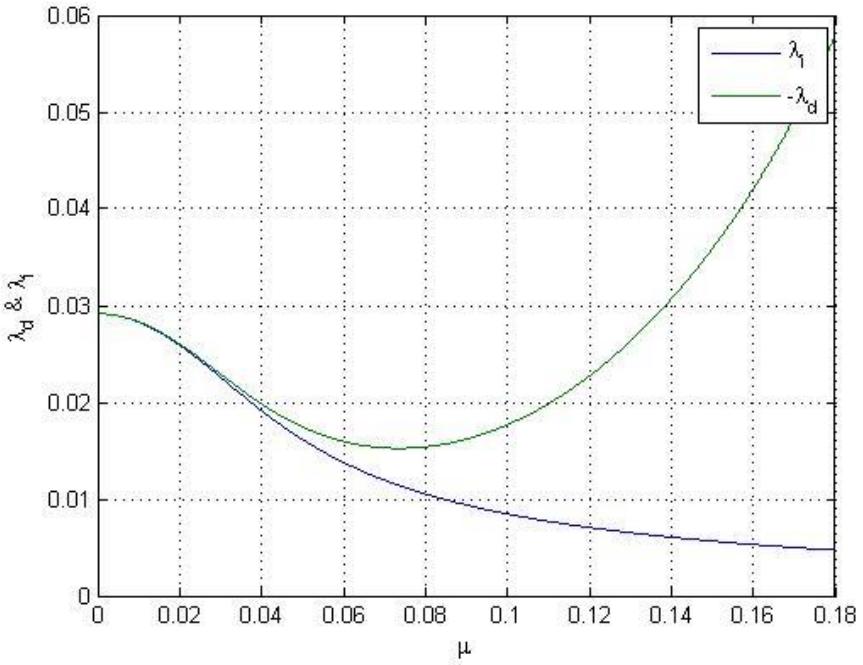

Figure 3.3: Inflow at the different flight speed

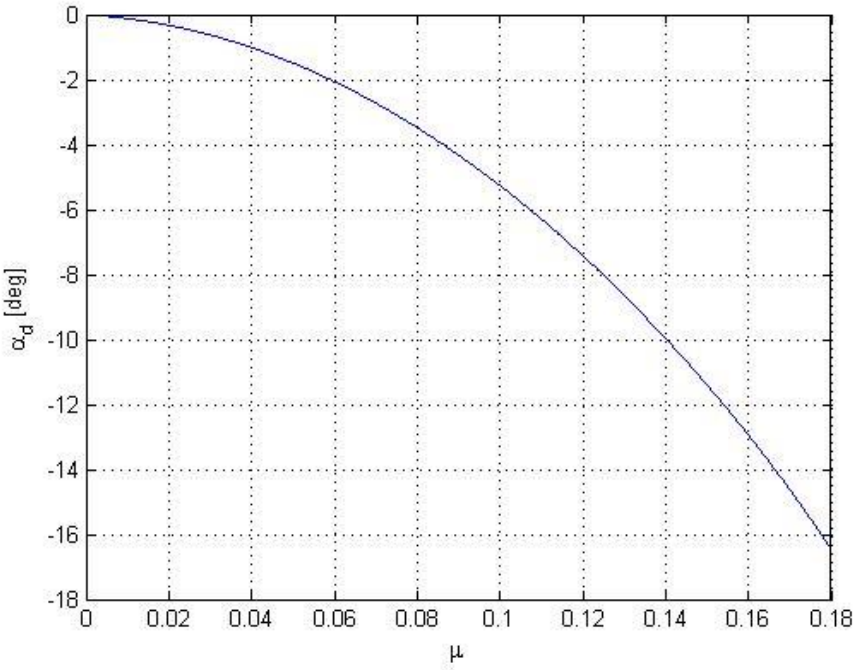

Figure 3.4: Attitude of the rotor at different flight speed

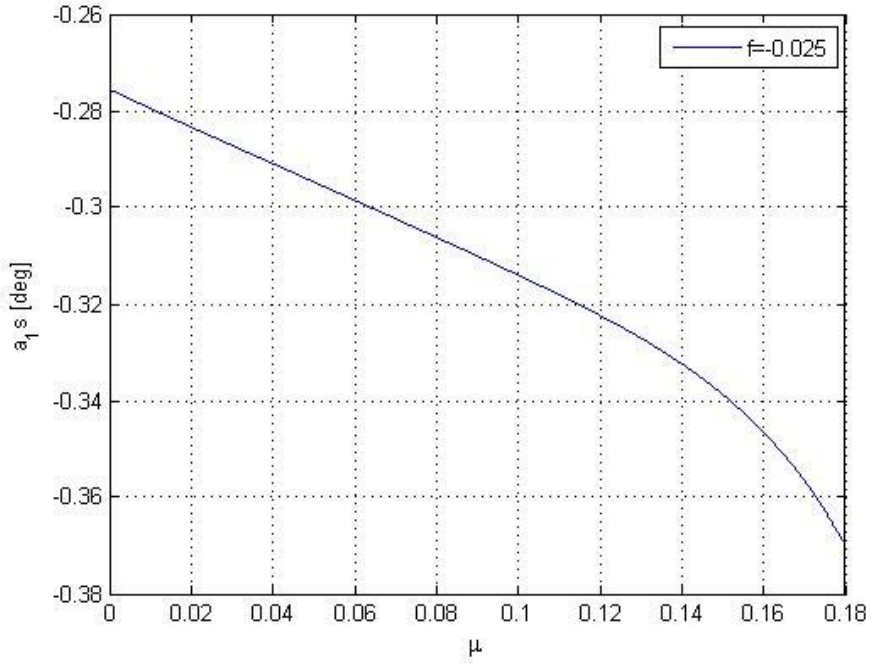

Figure 3.5: Angle between rotor and shaft at the different flight speed

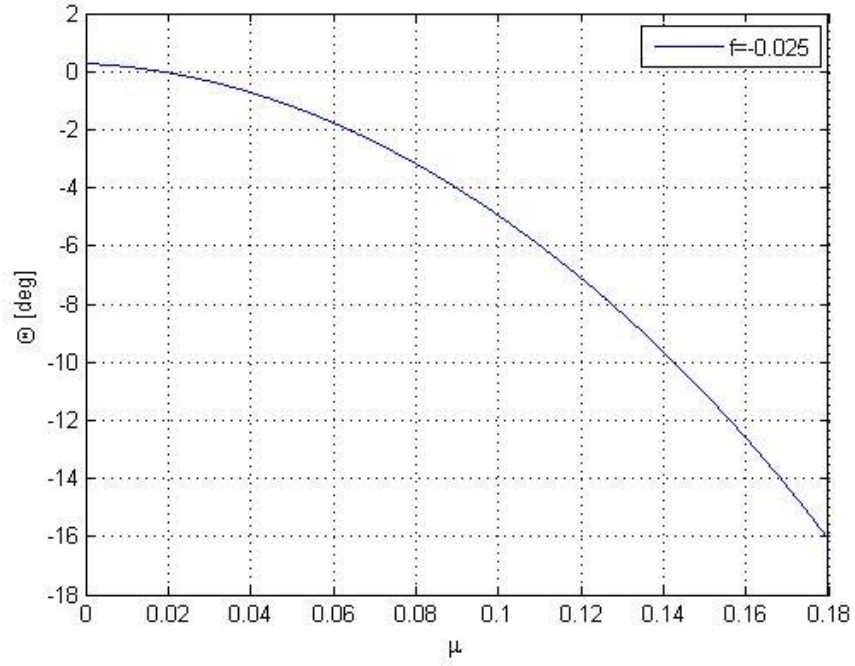

Figure 3.6: Attitude of helicopter at the different flight speed

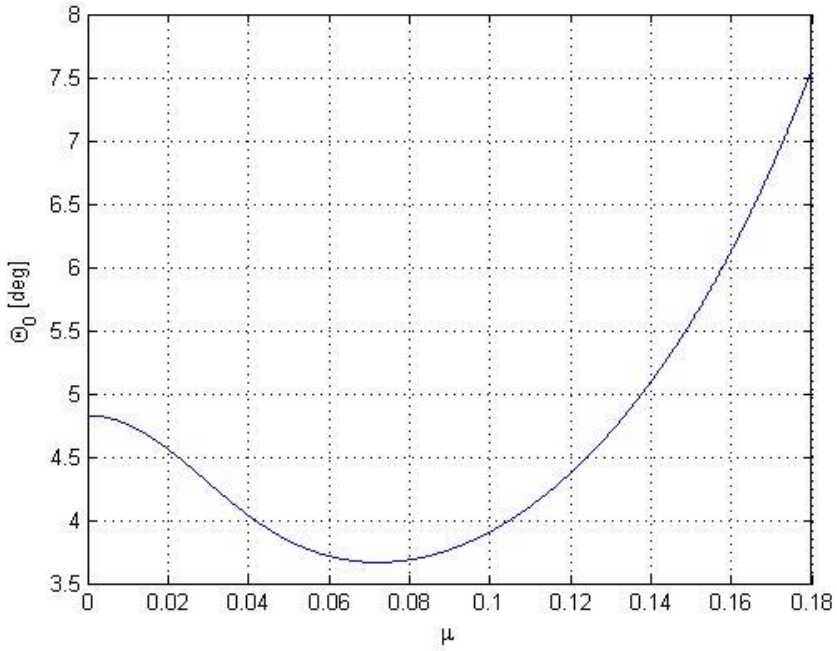

Figure 3.7: Collective command at the different flight speed

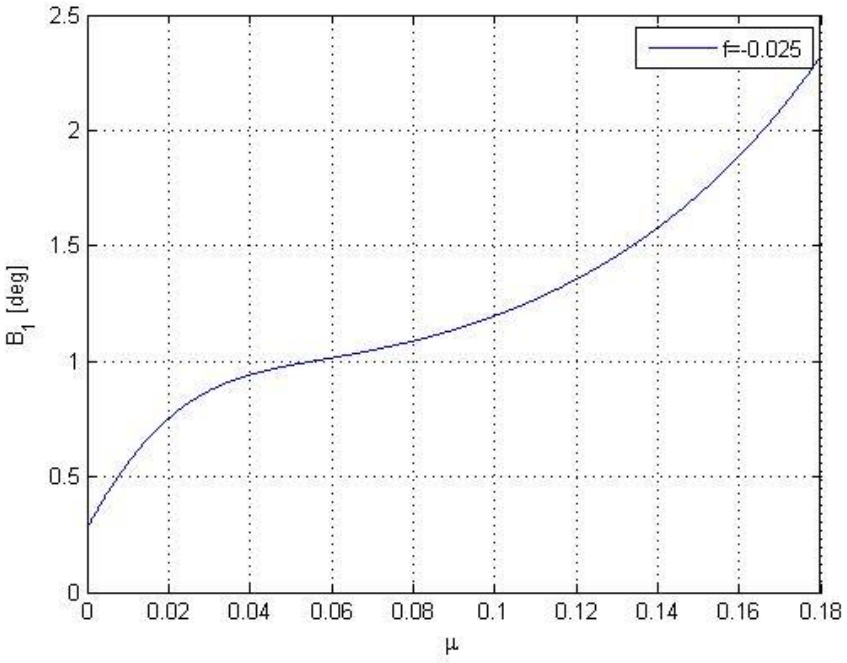

Figure 3.8: B_1 cyclic command at the different flight speed

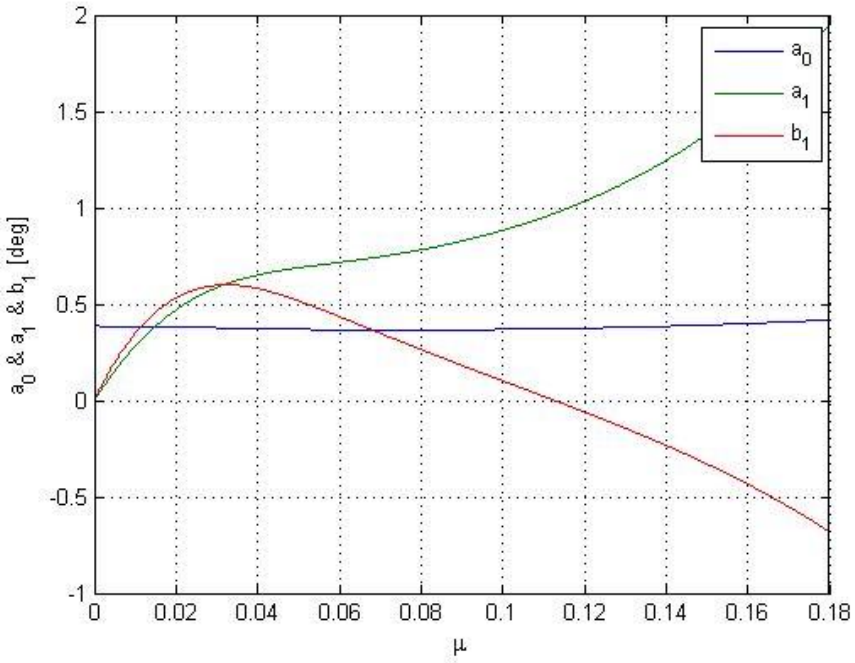

Figure 3.9: Blade flapping coefficients at the different flight speed

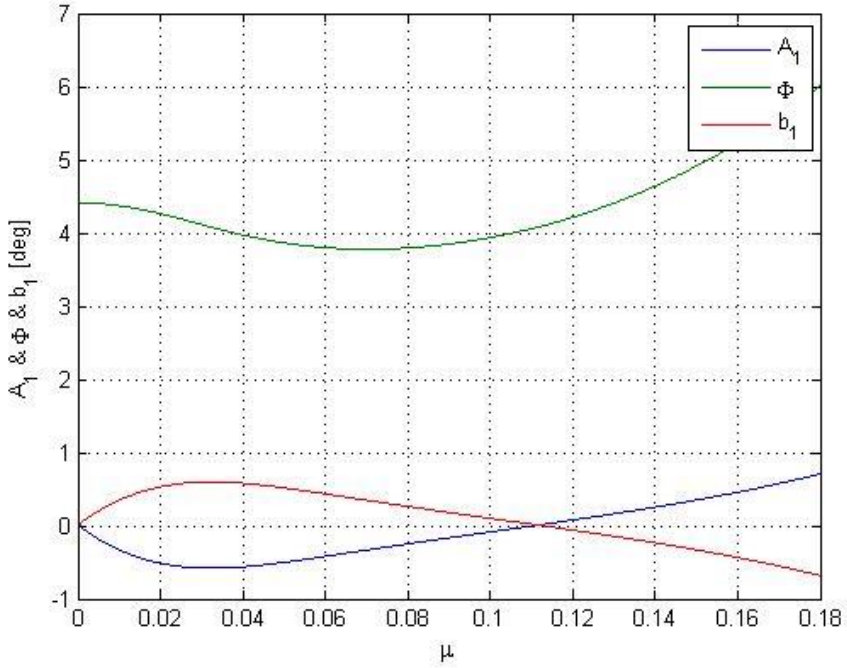

Figure 3.10: Lateral attitude and A_1 cyclic command at the different flight speed

3.3 Equations of motion

According to the high speed of rotation of the main rotor and its high frequency dynamic, to analyze the characteristics of dynamic stability of the helicopter we take the equations that govern the motion considering the helicopter as a point.

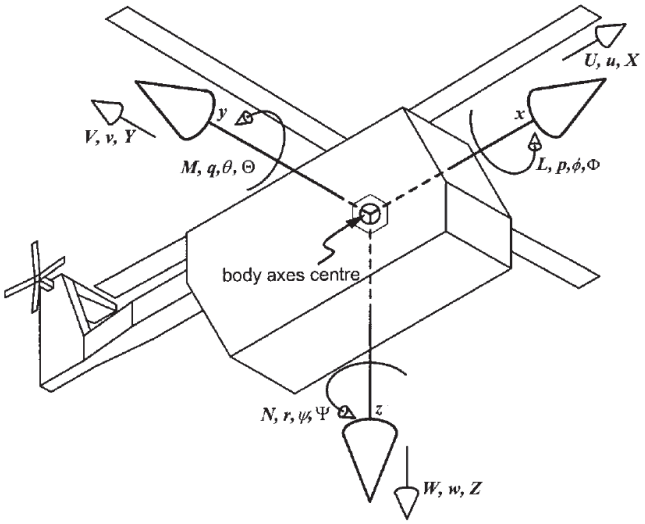

Figure 3.11: Representation of body axes [3]

$$\begin{cases} \vec{F} = m\left(\dot{\vec{V}} + \vec{\Omega} \times \vec{V}\right) \\ \vec{M} = I\dot{\vec{\Omega}} + \vec{\Omega} \times \left(I\vec{\Omega}\right) \end{cases} \text{[3] [8]} \tag{3.13}$$

To study these equations we make simplifying assumptions such as the theory of small perturbations and the angle β=0.

The velocity vector and angular velocity can be written:

$$\begin{cases} \vec{V} = (U + u)\vec{\imath} + v\vec{\jmath} + (W + w)\vec{k} \\ \vec{\Omega} = p\vec{\imath} + q\vec{\jmath} + r\vec{k} \end{cases} \tag{3.14}$$

The first equation has the components:

$$\begin{cases} m(\dot{u} + q(W + w) - vr) = X + W_x \\ m\big(\dot{v} + r(U + u) - p(W + w)\big) = Y + W_y \\ m\big(\dot{w} + pv - q(U + u)\big) = Z + W_z \end{cases} \tag{3.15}$$

Not to be confused W (velocity component according *k*) with W_i (weight component according to the axis *i*).

In wind axes(W=0) and linearizing [8]:

$$\begin{cases} \dot{u} = \frac{X_0 + \Delta x + W_{x0} + \Delta w_x}{m} \\ \dot{v} + rU = \frac{Y_0 + \Delta y + W_{y0} + \Delta w_y}{m} \\ \dot{w} - qU = \frac{Z_0 + \Delta z + W_{z0} + \Delta w_z}{m} \end{cases} \tag{3.16}$$

Similarly for the second cardinal and assuming that the inertia matrix is symmetric $I = \begin{bmatrix} A & F & E \\ & B & D \\ & & C \end{bmatrix}$ we can write:

$$\begin{cases} A\dot{p} - E\dot{r} = L \\ B\dot{q} = M \\ C\dot{r} - E\dot{p} = N \end{cases} \tag{3.17}$$

Through simplifying assumptions, the principal of all is that of small perturbations, we can manage these equations by linearizing the problem.

From the linearization and by imposing a condition of equilibrium initial (these steps will be explained later) there are two elements represented by: $\frac{\Delta\vec{F}}{m}$ e $\frac{\Delta\vec{M}}{I}$.

With the small perturbations they can be explicit with a development of Taylor stopped at the first order (taking the example of the component of the force along the X axis, the concept extends equally to the other components)[2][7][8]:

$$\Delta X = \frac{\partial X}{\partial u} u + \frac{\partial X}{\partial w} w + \frac{\partial X}{\partial q} q + \cdots \tag{3.18}$$

The terms $X_u = \frac{\partial X}{\partial u}, X_w, X_q$ ... are called aerodynamic derivatives.

3.4 Aerodynamic derivatives

Considering an equilibrium condition, it is calculate the variations of the forces and moments of the system due to the disturbance.

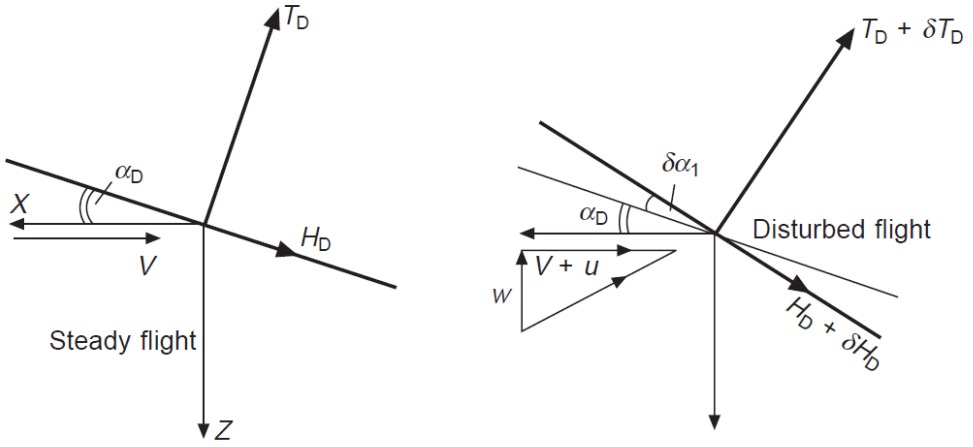

Figure 3.12: Disc and forces in steady and disturbed flight in longitudinal plane [2]

For longitudinal plane [2]:

$$\delta X = -(T_D + \delta T_D)\sin(\alpha_D + \delta a_1) - (H_D + \delta H_D)\cos(\alpha_D + \delta a_1) - T_D \sin\alpha_D - H_D \cos\alpha_D \approx -T_D \delta a_1 - T_D \alpha_D - \delta H_D \quad (3.19)$$

$$\delta Z = -(T_D + \delta T_D)\cos(\alpha_D + \delta a_1) + (H_D + \delta H_D)\sin(\alpha_D + \delta a_1) + T_D \sin\alpha_D - H_D \cos\alpha_D \approx -\delta T_D \quad (3.20)$$

To estimate the change in pitching moment consider the following figure 3.13:

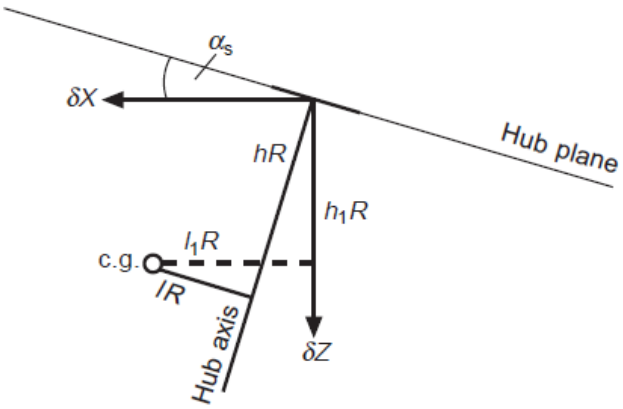

$$h_1 \approx h - l\alpha_s \quad l_1 \approx l + h\alpha_s \quad \alpha_s = \alpha_d - a_{1s} \quad (3.21)$$

Figure 3.13: Change of distance of center of mass to the rotor with the variation of helicopter attitude [2]

$$\delta M = -h_1 R\delta X + l_1 R\delta Z + M_s \delta a_1 + \delta M_f \tag{3.22}$$

So we have:

$$X_u = \frac{\partial X}{\partial u} = -T_D \frac{\partial a_1}{\partial u} - \alpha_D \frac{\partial T_D}{\partial u} - \frac{\partial H_D}{\partial u} \tag{3.23}$$

$$Z_u = \frac{\partial Z}{\partial u} = -\frac{\partial T_D}{\partial u} \tag{3.24}$$

and for the others generally:

$$X_i = \frac{\partial X}{\partial i} = -T_D \frac{\partial a_1}{\partial i} - \alpha_D \frac{\partial T_D}{\partial i} - \frac{\partial H_D}{\partial i} \tag{3.25}$$

$$Z_i = \frac{\partial Z}{\partial i} = -\frac{\partial T_D}{\partial i} \tag{3.26}$$

$$M_i = \frac{\partial M}{\partial i} = -h_1 R X_i + l_1 R Z_i + M_s \frac{\partial a_1}{\partial i} + (M_i)_f \tag{3.27}$$

Considering the presence of a tail plane and its incidence $\alpha_T = \alpha_{T0} + \theta - \tau_c - \varepsilon$ as shown in the figure 3.14, we must evaluate the contributions on pitching.

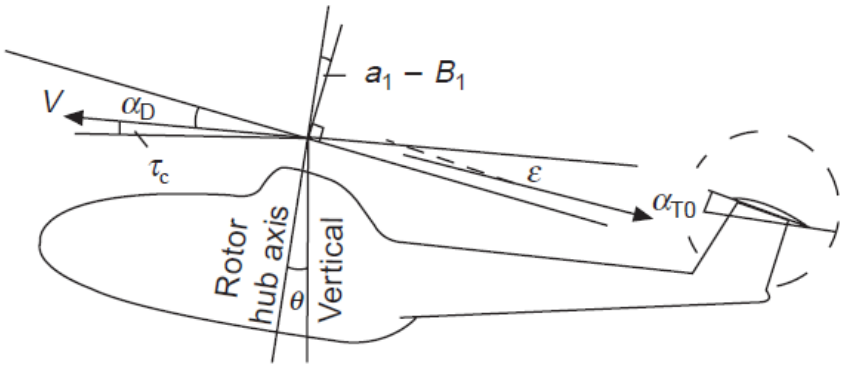

Figure 3. 14: Effect of the tail plane [2]

$$M_{u_T} = \frac{\partial M_T}{\partial u} = -\rho V S_T l_T R \left[C_{L_T} + \frac{1}{2} V \frac{\partial C_{L_T}}{\partial u}\right], \quad \text{with} \quad V \frac{\partial C_{L_T}}{\partial u} = -a_T V \frac{\partial \varepsilon}{\partial u} = -a_T \left[\frac{\partial v_i}{\partial V} - \frac{v_i}{V}\right] \tag{3.28}$$

$$M_{w_T} = \frac{\partial M_T}{\partial w} = -\frac{1}{2}\rho V^2 S_T l_T R \left[\frac{\partial C_{L_T}}{\partial w}\right], \text{ con } \frac{\partial C_{L_T}}{\partial w} = \frac{\alpha_T}{V}\left[1 - \frac{\partial \varepsilon}{\partial \alpha}\right] \tag{3.29}$$

If there is an angular velocity q the variation of incidence is $\Delta\alpha_T = l_T R\, {}^{q}/_{V}$ and the moment is $\Delta M_T = -\frac{1}{2}\rho a_T V S_T {l_T}^2 R^2 q$; so that:

$$M_{q_T} = \frac{\partial M_T}{\partial q} = -\frac{1}{2}\rho a_T V S_T {l_T}^2 R^2 \tag{3.30}$$

However, the TREX 500 tail plane is small and perforated and these contributions can be neglected; them can be useful for next and more specific study.

Similarly for the lateral plane and following the figure 3.15:

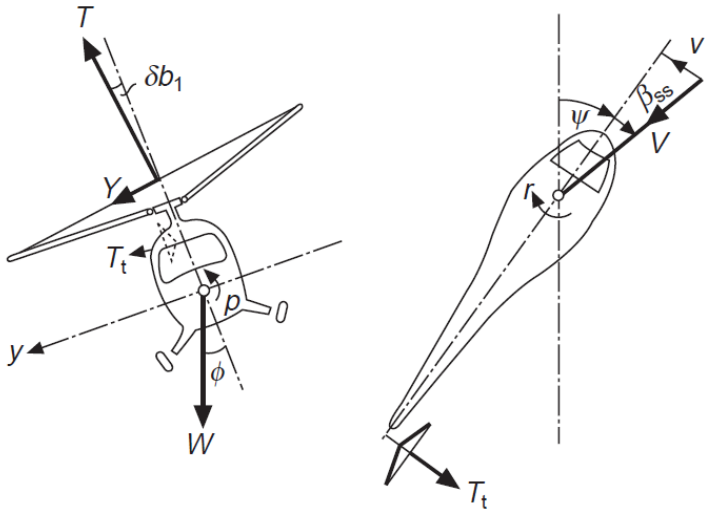

Figure 3.15: Disc and forces in disturbed flight in lateral plane [2]

$$\delta Y = T\delta b_1 + \delta T_t + \delta Y_f \tag{3.31}$$

$$Y_i = \frac{\partial Y}{\partial i} = T\frac{\partial b_1}{\partial i} + \frac{\partial T_t}{\partial i} + \frac{\partial Y_f}{\partial i} \tag{3.32}$$

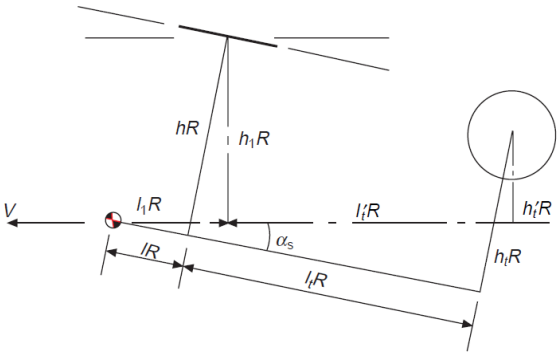

$$h_t{}' \approx h_t - l_t\alpha_s \qquad l_t{}' \approx l_t + h_t\alpha_s \tag{3.33}$$

Figure 3.16: Change of distance of the tail rotor to the center of mass with the variation of helicopter attitude [2]

$$\delta L = h_1 RT\delta b_1 + h_1 R\delta Y + M_s \delta b_1 + h_t{}' R\delta T_t \tag{3.34}$$

$$\delta N = -l_t{}' R\delta T_t + \delta N_f \tag{3.35}$$

It's better work in non-dimensional form to have a problem the more generally as possible:

$$\frac{\partial}{\partial \mathrm{u}} = \frac{\partial}{R\Omega \partial \hat{\mathrm{u}}} \approx \frac{\partial \lambda}{R\Omega \partial \mu} \tag{3.36}$$

then

$$x_u = \frac{X_u}{\rho s A R\Omega} = -t_c \frac{\partial a_1}{\partial \mu} - \alpha_{\mathrm{d}} \frac{\partial \mathrm{t}_c}{\partial \mu} - \frac{\partial \mathrm{h}_{cd}}{\partial \mu} \tag{3.37}$$

and similarly has being calculated the others non-dimensional aerodynamic derivatives as shown in the appendix A.

The following are the main results in non-dimensional form for the calculation of derivatives.

$$\frac{\partial \lambda}{\partial \mu} = \alpha_{\mathrm{nf}} - \frac{\partial \lambda_i}{\partial \mu}, \alpha_{\mathrm{nf}} = \alpha_{\mathrm{d}} - a_1 \tag{3.38}$$

$$\frac{\partial \lambda_i}{\partial \mu} = \frac{2\mu\theta_0 + \alpha_{\mathrm{nf}} - (4t_c/a\lambda_i)\bar{V}\bar{v}_i{}^3}{1 + (4/a)(t_c/\lambda_i)(1+\bar{v}_i{}^4)} \tag{3.39}$$

$$\frac{\partial \mathrm{t}_c}{\partial \mu} = \frac{2\mu\theta_0 + \alpha_{\mathrm{nf}} + \bar{V}\bar{v}_i{}^3/(1+\bar{v}_i{}^4)}{(4/a) + (\lambda_i/t_c)/(1+\bar{v}_i{}^4)} \tag{3.40}$$

$$\frac{\partial \mathrm{a}_1}{\partial \mu} = \frac{\mathrm{a}_1}{\mu} - \frac{2\mu}{1-\mu^2/2}\frac{\partial \lambda}{\partial \mu} \tag{3.41}$$

$$\frac{\partial \mathrm{h}_{cd}}{\partial \mu} = \frac{1}{4}\delta \tag{3.42}$$

$$\frac{\partial \mathrm{t}_c}{\partial \hat{\mathrm{w}}} = \frac{a}{4}\frac{\partial \lambda}{\partial \hat{\mathrm{w}}} = \frac{a}{4}\frac{1}{1 + (a/4)(\lambda_i/t_c) + \bar{v}_i{}^4} \tag{3.43}$$

$$\frac{\partial \mathrm{a}_1}{\partial \hat{\mathrm{w}}} = \frac{2\mu}{(1-\mu^2/2)}\frac{\partial \lambda}{\partial \hat{\mathrm{w}}} = \frac{2\mu}{(1-\mu^2/2)(1 + (a/4)(\lambda_i/t_c) + \bar{v}_i{}^4)} \tag{3.44}$$

$$\frac{\partial \mathrm{h}_{cd}}{\partial \hat{\mathrm{w}}} = \frac{a}{4}\frac{1}{1 + (a/4)(\lambda_i/t_c) + \bar{v}_i{}^4}\left(\frac{1}{2}a_1 - \mu\theta_0 + \frac{\mu\lambda_D}{1-\mu^2/2}\right) \tag{3.45}$$

$$\frac{\partial \mathrm{t}_c}{\partial \hat{\mathrm{q}}} = 0 \tag{3.46}$$

$$\frac{\partial \mathrm{a}_1}{\partial \hat{\mathrm{q}}} = -\frac{16}{\gamma}\frac{1}{1-\mu^2/2} \tag{3.47}$$

$$\frac{\partial \mathrm{h}_{cd}}{\partial \hat{\mathrm{q}}} = \frac{a}{4}\left(\frac{1}{2}\lambda + \mu \mathrm{a}_1 - \mu^2 \theta_0\right)\frac{\partial \mathrm{a}_1}{\partial \hat{\mathrm{q}}} \tag{3.48}$$

If a lateral disturb affect the helicopter, the rotor flapping will be rotated through angle β_{ss}, so that $\partial \mathrm{b}_1 = \mathrm{a}_1 \beta_{\mathrm{ss}} = v/\mu$ (positive because the rotor has a clockwise motion) [2][3]

$$\frac{\partial \mathrm{b}_1}{\partial \hat{\mathrm{v}}} = +\mathrm{a}_1/\,\mu \tag{3.49}$$

$$\frac{\partial \mathrm{y}_c}{\partial \hat{\mathrm{v}}} = -\mathrm{h}_c/\,\mu = -\frac{1}{4}\delta \tag{3.50}$$

$$\frac{\partial \mathrm{b}_1}{\partial \hat{\mathrm{p}}} = \frac{16}{\gamma}\frac{1}{1+\mu^2/2} \tag{3.51}$$

$$\frac{\partial \mathrm{T}_t}{\partial \hat{\mathrm{v}}} = -\frac{\partial \mathrm{T}}{\partial \hat{\mathrm{w}}} \tag{3.52}$$

$$\frac{\partial \mathrm{T}_t}{\partial \hat{\mathrm{p}}} = -h_t{}' R\frac{\partial \mathrm{T}}{\partial \hat{\mathrm{w}}} \tag{3.53}$$

$$\frac{\partial \mathrm{T}_t}{\partial \hat{\mathrm{r}}} = l_t{}' R\frac{\partial \mathrm{T}}{\partial \hat{\mathrm{w}}} \tag{3.54}$$

The application of longitudinal cyclic pitch tilts the no-feathering axis in the longitudinal plane and the incidence of the helicopter had been reduced by the same amount:

$$\frac{\partial}{\partial \mathrm{B}_1} = -\mu\frac{\partial}{\partial \hat{\mathrm{w}}} \tag{3.55}$$

Applying a collective command we have

$$\frac{\partial \mathrm{t}_c}{\partial \theta_0} = \frac{\mathrm{a}}{6}\frac{1+3\mu^2/2}{1+(a/4)(\lambda_i/t_c)+\bar{v}_i{}^4} \tag{3.56}$$

$$\frac{\partial \lambda_i}{\partial \theta_0} = \left(\frac{\lambda_i}{t_c}\right)\frac{\frac{\partial \mathrm{t}_c}{\partial \theta_0}}{1+\bar{v}_i{}^4} \tag{3.57}$$

$$\frac{\partial \mathrm{a}_1}{\partial \theta_0} = \frac{2\mu}{1-\mu^2/2}\left[\frac{4}{3} + \frac{\partial \lambda_i}{\partial \theta_0}\right] \tag{3.58}$$

$$\frac{\partial \mathrm{h}_{cd}}{\partial \theta_0} = \frac{a}{8}\left[\mathrm{a}_1\frac{\partial \lambda_D}{\partial \theta_0} + \lambda_D\frac{\partial \mathrm{a}_1}{\partial \theta_0} - 2\mu\left(\lambda_D + \theta_0\frac{\partial \lambda_D}{\partial \theta_0}\right)\right] \tag{3.59}$$

$$\frac{\partial \lambda_D}{\partial \theta_0} = \mu\frac{\partial \mathrm{a}_1}{\partial \theta_0} - \frac{\partial \lambda_i}{\partial \theta_0} \tag{3.60}$$

Following the results of the derivatives for the T-REX 500 are shown for the different speed of flight.

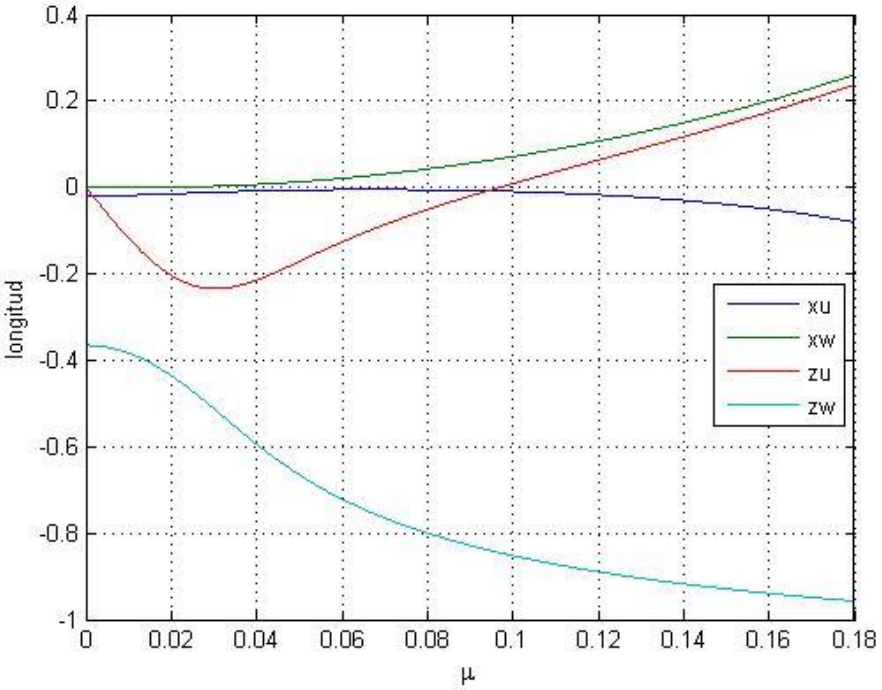

Figure 3.17: Longitudinal derivatives value at different flight speed

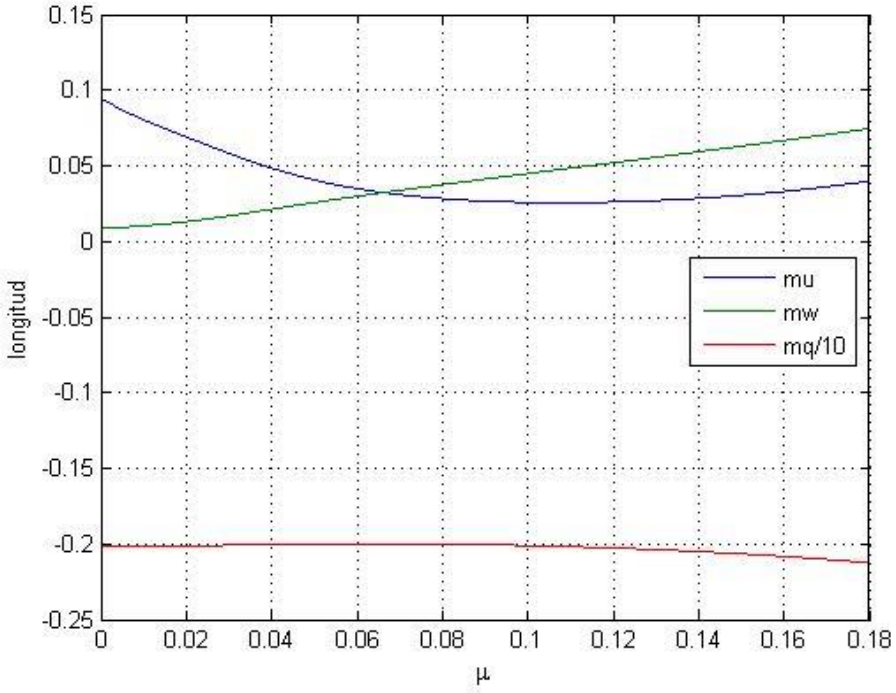

Figure 3.18: Longitudinal derivatives value at different flight speed

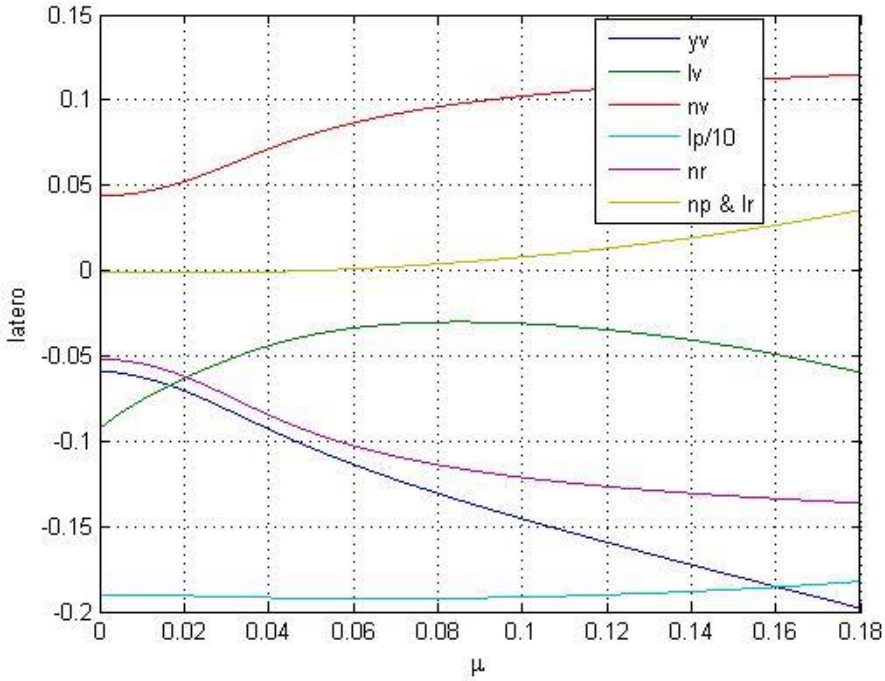

Figure 3.19: Lateral derivatives value at different flight speed

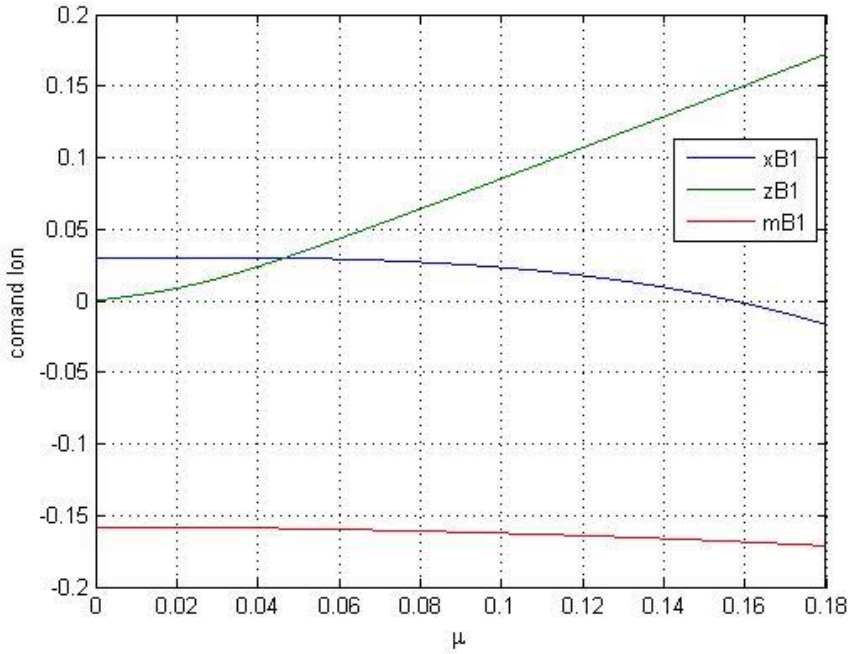

Figure 3.20: Longitudinal control derivatives value at different flight speed

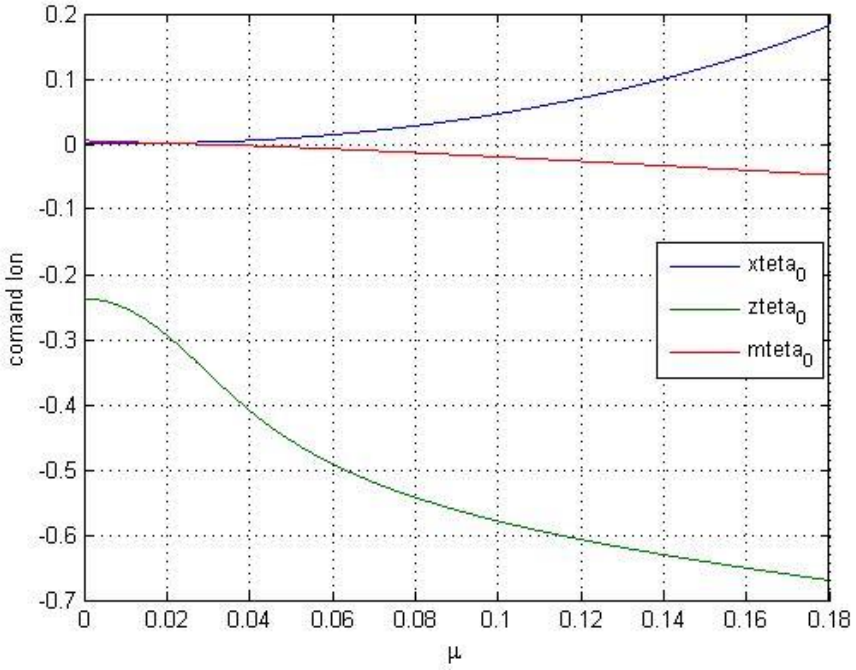

Figure 3.21: : Longitudinal control derivatives value at different flight speed

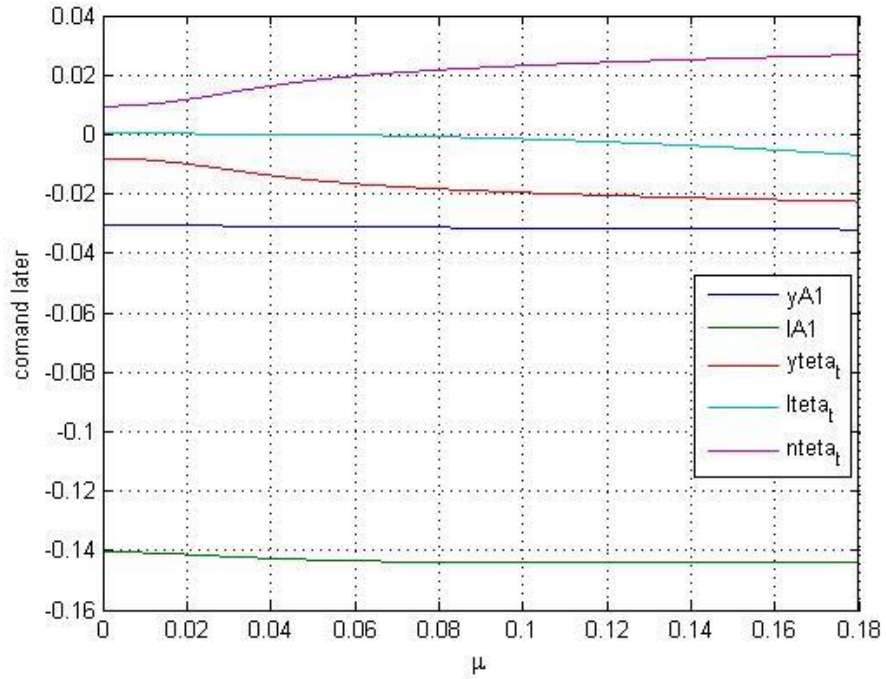

Figure 3.22: : Lateral control derivatives value at different flight speed

4. DYNAMIC OF HELICOPTER

4.1 LINEAR SYSTEM

The linear system can be represented in the knowing form:

$$\begin{cases} \{\dot{x}\} = [A]\{x\} + [B]\{u\} \\ y = [C]\{x\} + [D]\{u\} \end{cases}$$

Remembering the equations 3.16 and 3.17 and taking the advantage from the concept of aerodynamic derivative we can find a liner system that it will be useful for the developing of the flight control laws.

The system has been generated from the script on appendix A and has the following form:

X_u	X_w	X_q	-g	X_v	X_p	X_r	0	0
Z_u	Z_w	Z_q+U	0	Z_v	Z_p-V	Z_r	0	0
M_u	M_w	M_q	0	M_v	M_p	M_r	0	0
0	0	1	0	0	0	0	0	0
Y_u	0	Y_q	0	Y_v	Y_p	Y_r-U	g	0
L_u	L_w	L_q	0	L_v	L_p	L_r	0	0
N_u	N_w	N_q	0	N_v	N_p	N_r	0	0
0	0	0	0	0	1	0	0	0
0	0	0	0	0	0	1	0	0

Table 4.1: Matrix A of the linear system

$X_{\theta 0}$	X_{B1}	X_{A1}	$X_{\theta t}$
$Z_{\theta 0}$	Z_{B1}	Z_{A1}	$Z_{\theta t}$
$M_{\theta 0}$	M_{B1}	M_{A1}	$M_{\theta t}$
0	0	0	0
$Y_{\theta 0}$	Y_{B1}	Y_{A1}	$Y_{\theta t}$
$L_{\theta 0}$	L_{B1}	L_{A1}	$L_{\theta t}$
$N_{\theta 0}$	N_{B1}	N_{A1}	$N_{\theta t}$
0	0	0	0
0	0	0	0

Table 4.2: Matrix B of the linear system

and the vector of states

$$\{u, w, q, \theta, v, p, r, \phi, \psi\}'$$

The problem is highly coupled cause the asymmetry of the helicopter but to understand the evolution of flight it is useful separate the longitudinal and lateral dynamic.

4.2 Longitudinal plane

Starting from a steady state and applying a perturbation:

$$\begin{cases} X_0 = W \sin \tau_c \\ Z_0 = -W \cos \tau_c \end{cases} \tag{4.1}$$

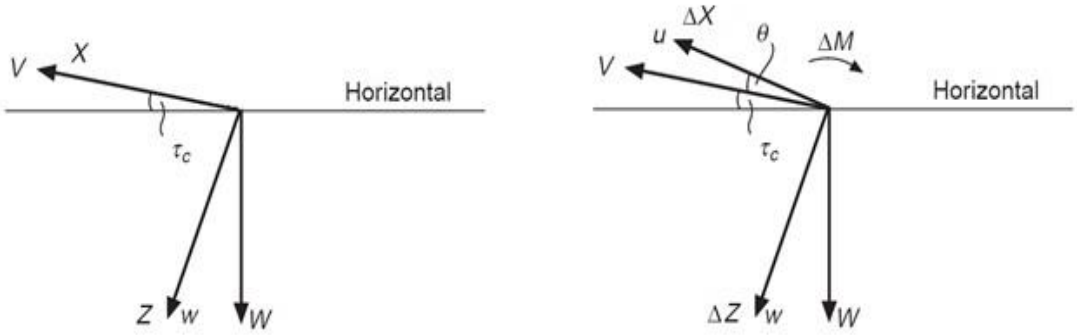

Figure 4.1: Perturbation of flight in longitudinal plane [2]

Using the aerodynamic derivatives and remembering:

$\vec{w} = mg \begin{pmatrix} -\theta \cos \tau_c \\ \phi \cos \tau_c \\ -\theta \sin \tau_c \end{pmatrix}$ [8]:

$$\begin{cases} \dot{u} + g\theta \cos \tau_c = X_u u + X_w w + X_q q + X_{B1} B_1 + X_\Theta \Theta \\ \dot{w} - qU + g\theta \sin \tau_c = Z_u u + Z_w w + Z_q q + Z_{B1} B_1 + Z_\Theta \Theta \\ \dot{q} = M_u u + M_w w + M_{\dot{w}} \dot{w} + M_q q + M_{B1} B_1 + M_\Theta \Theta \\ \dot{\theta} = q \end{cases} \quad (4.2)$$

Where the derivatives $X_{\dot{w}}$ e $Z_{\dot{w}}$ are neigible.

The poles of the system can be find using the Laplace's transformation:

$$\begin{bmatrix} s - X_u & -X_w & g \cos \tau_c \\ -Z_u & s - Z_w & -Us + g \sin \tau_c \\ -M_u & -(sM_{\dot{w}} + M_w) & s^2 - M_q s \end{bmatrix} \begin{pmatrix} u \\ w \\ \theta \end{pmatrix} = 0 \quad (4.3)$$

The characteristic equation has usually the roots [3][4]:

$$\left(s + \frac{1}{T_1}\right)\left(s + \frac{1}{T_2}\right)(s^2 + 2\zeta\omega_n s + {\omega_n}^2) \quad (4.4)$$

We can find from equation 4.4:

1- Vertical speed mode: it is a steady mode described by $\left(s + \frac{1}{T_1}\right)$, it's decoupled from the other modes and it is a heavily damped subsidence;
2- Forward mode: it is described by $\left(s + \frac{1}{T_2}\right)$ but it is coupled with pitch attitude and pitch rate;
3- Pitching oscillation: it is both speed and flight condition dependent, unstable for hinge-less rotor configurations that worsens at high speed.

4.2.1 Hovering stability

In hovering some derivatives can be neglect such as X_w, Z_u, Z_q, Z_w and M_w, the speed is U= 0 and the rate of climb $\tau_c = 0$; so the characteristic equation takes the form [3][4]:

$$(s - Z_w)\left(s^3 - \left(X_u + M_q\right)s^2 + X_u M_q s + M_u g\right) = 0 \qquad (4.5)$$

One real root is given by $(s - Z_w) = 0$; this represents a heavily damped motion such that if a helicopter is disturbed, by a vertical speed, the motion of lifting is rapidly damped.

The movement is a pure convergence without oscillation and confirms that the vertical motion is completely decoupled from the pitch.

The other real root represents the mode of pitch rate, coupled with speed and pitch oscillation.

In hovering the oscillation in pitch has the following explanation:

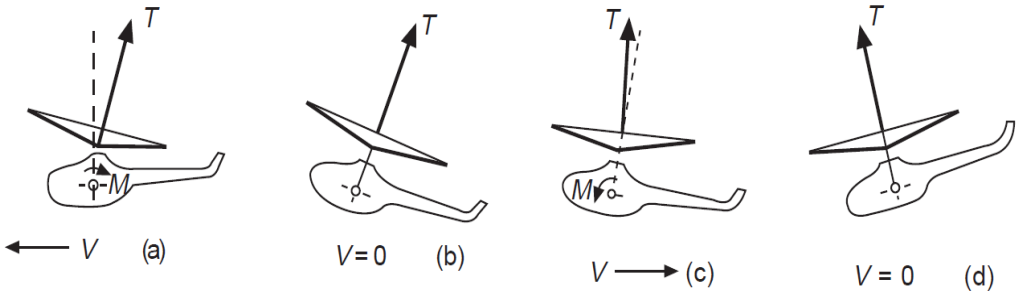

Figure 4.2: Representation of coupling in pitch and longitudinal speed [2]

Assume that the helicopter in hovering has an horizontal velocity disturbance, the change of relative speed to the rotor causes a backward rotation (a), which exerts a positive pitching moment.

At the same time it develops a rear component of the thrust vector that decelerates the aircraft up to stop (b).

At this point the helicopter is located to a new trim angle and the moment generated vanishes, but the component of traction towards brings behind the

aircraft to a translation which introduces a new disorder in speed with consequent rotation of the rotor in forward and generation of a positive pith moment (c).
The component of forward command the motion until arresting the helicopter with a new trim angle to beat (d) and zero pitch moment.
The movement is generally unstable, however handling of the derivative M_q will affect the rate of divergence: make M_q more negative will reduce the real part of the complex pole and therefore will tend to increase the doubling time.
The movement can be approximated by evaluating the system in u and q such an oscillation whose frequency depends on M_u and M_q [3][4]:

$$\omega = \sqrt{-\frac{M_u g}{M_q}} \qquad \zeta = -\frac{X_u - \frac{M_u g}{M_q{}^2}}{2}\sqrt{\frac{-M_q}{M_u g}} \tag{4.6}$$

4.2.2 Forward flight stability

The characteristic equation in forward flight is not so easy to generalize as in the case with a conventional fixed-wing aircraft.
For the latter, the characteristic equation is solved in pairs of complex conjugate poles representing two oscillatory modes, one short-term and high damping (SP) and a long-term lightly damped (LP).
In the case of a helicopter the characteristic equation is solved in four roots, but depending on the flight conditions can be found two pairs of complex roots, two real and a pair of complex conjugate roots or four real roots.
The reason for this is the large variation of the value of the derivatives in the envelope of flight; however we can find similarities.
Usually the high frequency poles are characterized by two heavily damped subsidence in pitch rate and incidence, like an aircraft.
The phugoid mode of a fixed-wing aircraft is an oscillation in the height and speed at approximately constant incidence.
Now, considering a disturb that causes the helicopter to adopt negative attitude, the component of weight which acts along the longitudinal axis accelerates the helicopter, but the disc automatically rotates upward (speed stability) producing

an angular velocity that rotates the fuselage at an angle of attack greater than the rotor.

The flight path is still downwards and the component of weight causes the speed continues to increase so that the preceding steps are repeated until the traction exceeds the weight and the helicopter starts to rise.

The component weight acting along the flight path now begins to slow down the helicopter and the disc rotor rotates forward producing a negative pitch moment.

The helicopter continues to rise until the weight does not exceed the traction and all this will be repeated until the oscillation eventually damps both (stable dynamic) or increases indefinitely (unstable dynamic).

It is possible to characterize the mode to "long term" [3][4]:

$$\omega = \sqrt{\frac{-\left[Z_u - \frac{M_u}{M_w} Z_w\right] g}{U}} \qquad \zeta = -\frac{X_u - \frac{M_u}{M_w}[Z_w - g]}{2} \sqrt{\frac{-U}{\left[Z_u - \frac{M_u}{M_w} Z_w\right] g}} \qquad (4.7)$$

The frequency of the mode to "long-term" is therefore inversely proportional to the speed U.

An increase of the trim speed reduces the resulting frequency of the oscillation period. An increase of Z_u (relative to the lift coefficient) has the opposite effect.

The damping of the way to "long term" is influenced by the same factors, but in the opposite way; so an increase in trim speed will increase the damping in addition to reducing the frequency of the response.

The resistance of the helicopter (related to Xu) influence the damping of "phugoid".

The following figure 4.3 represent the poles responsible of the pitching oscillatory mode for a generally helicopter.

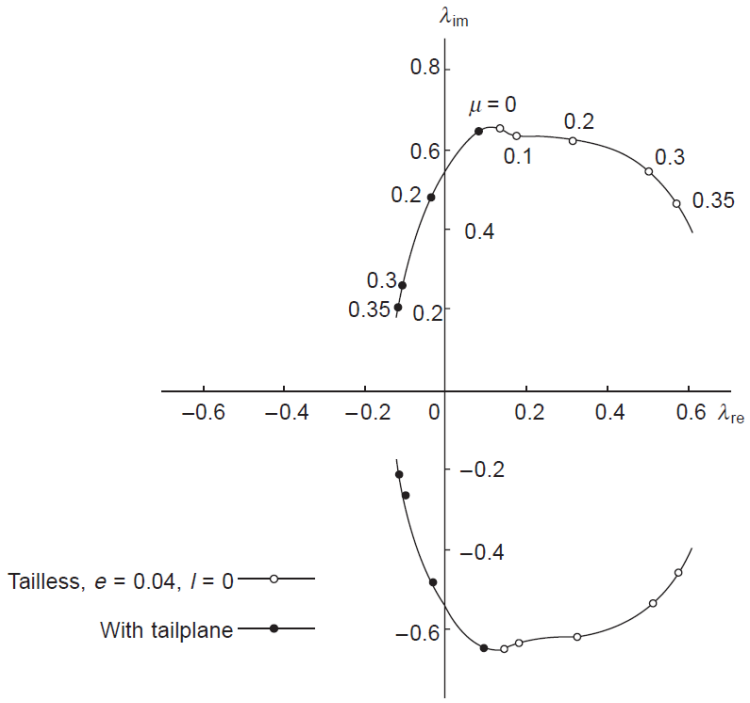

Figure 4.3: Representation of position at different speed flight of pitching oscillatory mode pole in the Gaus's plane [2]

In the example shown is also the contribution of the tail plane, which carries a positive contribution to the stability with increasing speed, making M_q become more negative.

4.3 Lateral plane

The equation are the following and some derivatives such as Y_p, Y_r… are neglected:

$$\begin{cases} \dot{v} + Ur - g\phi\, cos\, \tau_c - g\psi \sin \tau_c = Y_v v + Y_{A1} A_1 + Y_{\Theta_t} \Theta_t \\ \dot{p} = L_v{}' v + L_p{}' p + L_r{}' r + L_{A1}{}' A_1 + L_{\Theta_t}{}' \Theta_t \\ \dot{r} = N_v{}' v + N_p{}' p + N_r{}' r + N_{A1}{}' A_1 + N_{\Theta_t}{}' \Theta_t \\ \dot{\phi} = p + r tan\, \tau_c \\ \dot{\psi} = \frac{r}{\cos \tau_c} \end{cases} \tag{4.8}$$

Where the derivatives with quotes are calculated:

$$\begin{pmatrix} L_i{}' \\ N_i{}' \end{pmatrix} = \frac{1}{\Delta} \begin{bmatrix} 1 & \frac{E}{A} \\ \frac{E}{C} & 1 \end{bmatrix} \begin{pmatrix} L_i \\ N_i \end{pmatrix} \qquad \Delta = 1 - \frac{E^2}{AC}\ [8] \tag{4.9}$$

Passing in the s domain for the calculation of the poles of the system has:

$$\begin{bmatrix} s - Y_v & -g cos\, \tau_c & Us - g \sin \tau_c \\ -L_v{}' & s^2 - L_p{}' s & -L_r{}' s \\ -N_v & -N_p{}' s & s^2 - N_r{}' s \end{bmatrix} \begin{pmatrix} v \\ \phi \\ \psi \end{pmatrix} = 0 \tag{4.10}$$

The quotes will be omitted in the rest of the discussion.

The characteristic equation has the roots [3]:

$$s\left(s + \frac{1}{T_1}\right)\left(s + \frac{1}{T_2}\right)(s^2 + 2\zeta\omega_n s + \omega_n{}^2) = 0$$

From the characteristic equation it is possible define:

1- Heading mode: represented by s=0 that indicates that the aircraft has neutral yaw angle stability.

2- Yawing mode: it is equivalent to the fixed wing, is represented by $\left(s + \frac{1}{T_1}\right) = 0$, the mode is independent of roll and lateral translation and is an exponential motion that can be either convergent or divergent;

3- Rolling mode: described by $\left(s + \frac{1}{T_2}\right) = 0$, is a damped subsidence in pure roll;

4- Lateral/directional oscillation: or Dutch roll, is an oscillation in roll and yaw, which like the pitching oscillation can be flight condition dependent.

4.3.1 Hovering stability

While in the case longitudinal, not only the speed is zero, but also some derivatives are zero, this is definitely not true in the case lateral-directional; however, if the tail rotor is assumed to be located on the roll axis, and then L_r can be considered negligible, we have a situation similar to that of the longitudinal motion [3].

$$s(s - N_r)\left(s^3 - \left(Y_v + L_p\right)s^2 + Y_v L_p s + L_v g\right) = 0 \qquad (4.11)$$

One of the real roots is given by $(s - N_r) = 0$, so that confirms that the yawing mode is independent of the other motions; any disturbance in yaw moment will be damped by the N_r derivative and the root $s = 0$ indicates that the route angle reached consequently to the disturbance remains unchanged.

The other real root is usually negative and very high and represents a very damped roll mode.

The root complex is an oscillation diverging much like the longitudinal case.

In this case however, the presence of the tail rotor, which modifies its traction in the presence of a lateral translation, generates a yaw movement.

The motion can be approximated to an oscillation frequency [3]:

$$\omega = \sqrt{\frac{L_v g}{L_p}} \qquad (4.11)$$

4.3.2 Forward flight stability

The characteristic equation has two real poles, representing a damped roll mode and spiral mode, and two complex conjugate poles that are close to the dutch-roll motion in the fixed-wing aircraft.

As regards the spiral mode there is a variation of the value of the derivative N_v that was neglected in hovering and the equation can be written as follows [3]:

$$\dot{\phi} = p = \frac{g}{U}\frac{[N_r L_v - L_r N_v]}{[L_p N_v - N_p L_v]}\phi \tag{4.12}$$

Usually the term in the denominator is negative and this translates to stability in the relation $N_r L_v > L_r N_v$.

This underlines the influence that the derivative L_v (dihedral effect), which must be negative to ensure the stability of the spiral.

However it is not simple to establish this effect because of the strong variation of the derivatives with the speed of flight.

The roots that develop the "Dutch roll" can be approximated with frequency and damping equal to [3]:

$$\omega = \sqrt{Y_v N_r + U N_v} \quad \zeta = \frac{-(Y_v + N_r)}{2\sqrt{Y_v N_r + U N_v}} \tag{4.13}$$

From this approximation results a damped harmonic mode; but there are not important effects of other aerodynamic derivatives.

Analyzing the same problem constraining the center of gravity of the aircraft and freeing only the rotations (roll and yaw) it highlights the effect of the derivative L_v [3][4]:

$$\omega = \sqrt{\frac{U}{L_p} N_v L_p - L_v N_p} \quad \zeta = \frac{\frac{1}{L_p}\left[N_p L_r - L_p N_r - \frac{U L_v N_p}{L_p}\right]}{2\sqrt{\frac{U}{L_p} N_v L_p - L_v N_p}} \tag{4.14}$$

It is noted that a too high value dihedron effect leads to instability of the system.

The roll rate and yaw rate approximated by $s - L_p = 0$ and $s - N_r = 0$ is not very different from the case of the hovering, remaining exponential damped modes.

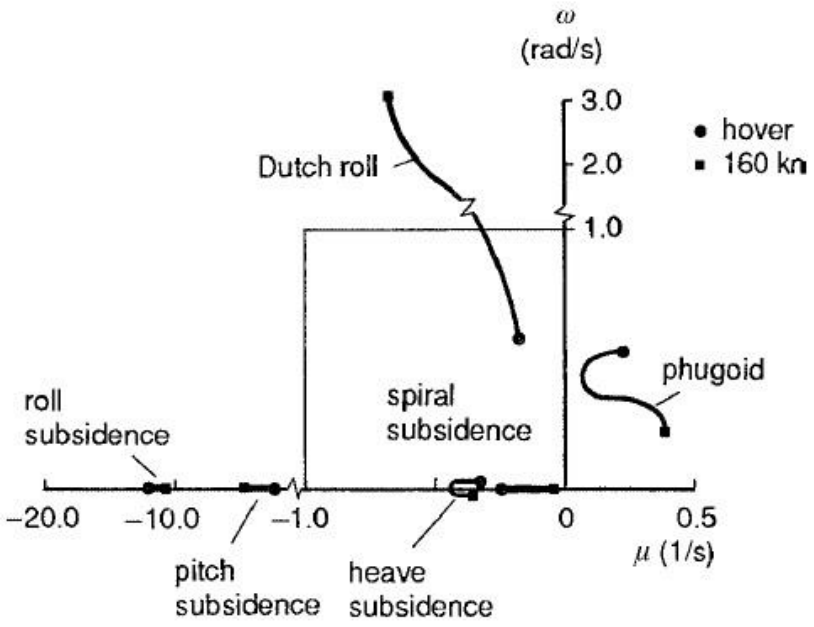

Figure 4.4: Lynx root-loci eigenvalue as a function of forward speed [4]

Of interest is an examples of root loci as a function of forward speed of the "Lynx" from [4] in figure 4.4; however we expect for our model higher pulsation because of the smaller dimensions.

4.4 Fly-bar

We have seen that the helicopter is unstable both laterally and longitudinally in hovering flight and that the longitudinal instability becomes worse with increase of forward speed, particularly when the rotor has hinge-less blades.
Small-size helicopter has a system that increase the stability called fly-bar, that behavior like a mechanical SAS in pitch rate and roll rate.

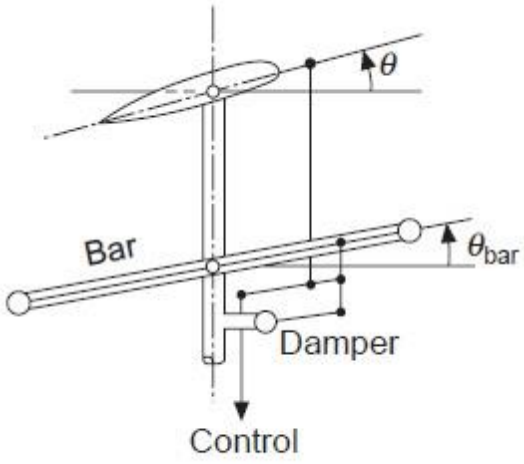

Figure 4.5: Representation of connection between rotor commands and fly-bar [2]

The bar behaves like a gyroscope with lag damping generated from the aerodynamic forces.
The bar is linked to the blade so that a tilt of the bar relative to the shaft causes a change of pitch of the rotor blade.
The dynamic equation of the fly-bar it is the same of the rotor with pitch rate or roll disturbance; considering the only presence of q:

$$\frac{\partial^2 \beta}{\partial \psi^2} + \frac{\gamma}{8}\frac{\partial \beta}{\partial \psi} + \beta = -2q/\Omega \sin\psi + \dot{q}/\Omega^2 \cos\psi \qquad (4.15)$$

where $\beta = \theta_{bar}$ and $\dot{q}/\Omega^2$ is neglectable.

The command $\theta = -A_1 sin\,\psi - B_1 \cos\psi$, $\theta = c_l \theta_{bar}$ ($c_l = 0.5$ for the T-REX 500) and inserting in the 4.15 we obtain regrouping sin and cos:

$$\begin{cases} A_1'' + \frac{\gamma}{8} A_1' - 2B_1' - \frac{\gamma}{8} B_1 = 2c_l q/\Omega \\ 2A_1' + \frac{\gamma}{8} A_1 + B_1'' + \frac{\gamma}{8} B_1' = 0 \end{cases} \tag{4.16}$$

The results of this system to a positive step of pitch rate "q" are the following:

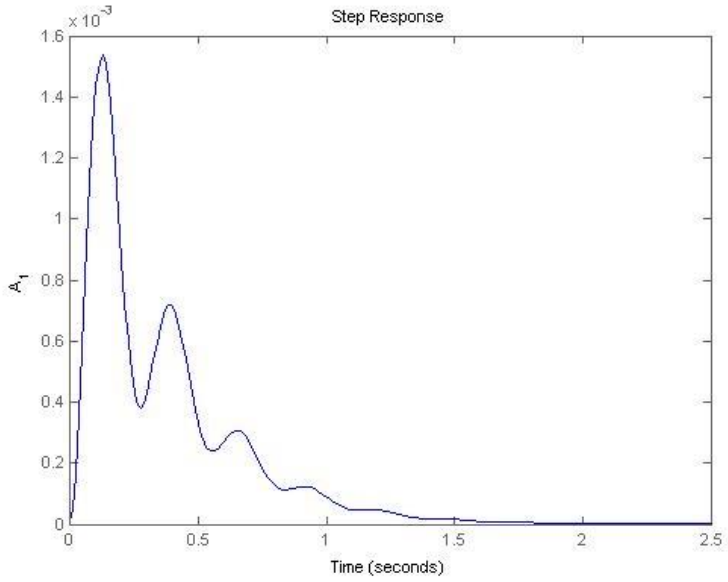

Figure 4.6: A_1 time response at q perturbation

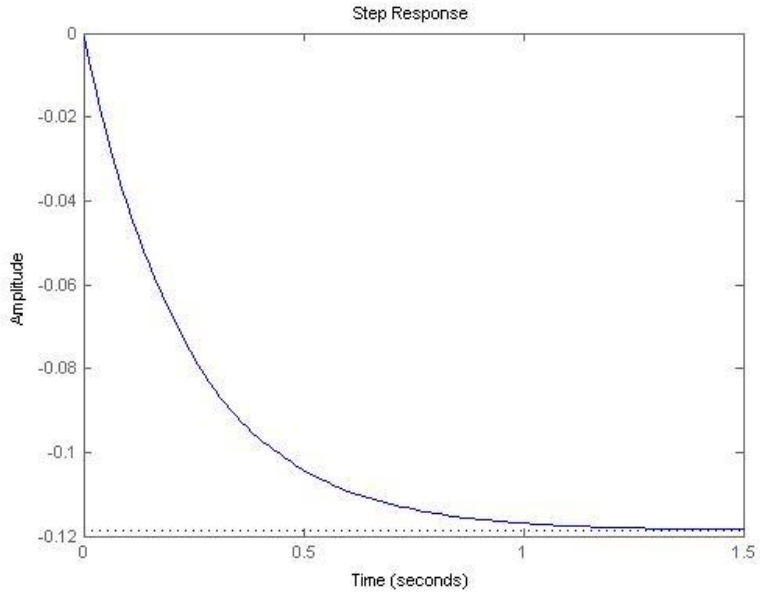

Figure 4.7: B_1 time response at q perturbation

With a disturb of positive q, the fly-bar commands the rotor to tilt back like a first order dynamic, while the command A_1 is near to zero; a good approximation is precisely neglect A_1 and the 4.16 simplify in:

$$B_1{}' + \frac{\gamma}{16} B_1 = -c_l q/\Omega \tag{4.17}$$

$$\left(s + \frac{\gamma\Omega}{16}\right) B_1 = -c_l q \text{ (in Laplace domain)} \tag{4.18}$$

The fly-bar can be treated like a feedback where $B_1 = B_{1p} - \frac{c_l}{T_{fb}s+1} q$; the low-pass filter depends on the fly-bar dynamic ($T_{fb} = \frac{16}{\gamma_{fb}\omega}$).

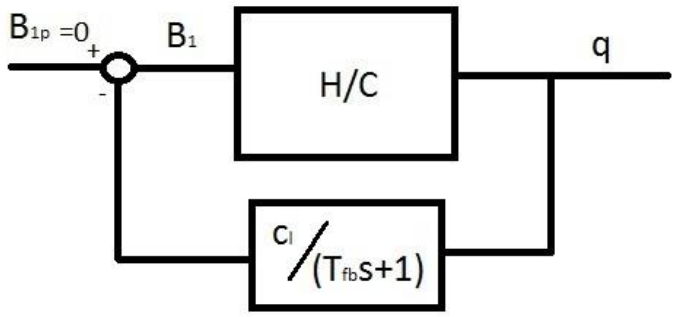

Figure 4.8: Representation of fly-bar feedback

In the Laplace's domain in hovering for example:

$$\begin{bmatrix} s - X_u & g & 0 \\ -M_u & s^2 - sM_q & -M_{B1} \\ 0 & -sc_l & s + \frac{\gamma}{16}\Omega \end{bmatrix} \begin{Bmatrix} u \\ \theta \\ B_1 \end{Bmatrix} = 0 \tag{4.19}$$

The solution gives:

$$\left(s^3 - \left(X_u + M_q\right)s^2 + X_u M_q s\right)\left(s + \frac{\gamma}{16}\Omega\right) - sc_l M_{B1}(s - X_u) + M_u g(s + \frac{\gamma}{16}\Omega) = 0 \tag{4.20}$$

With the false feedback technique it is possible to study the values of poles to the change of the gain c_l:

$1 + KG(s) = 0$, with $K = c_l$

$$G(s) = \frac{-sM_{B1}(s-X_u)}{(s^3-(X_u+M_q)s^2+X_uM_qs+M_ug)(s+\frac{\gamma}{16}\Omega)} \quad (4.21)$$

We can see, in the following figure 4.9, how the high frequency dynamic is not interested by the feedback, but in the low frequency dynamic the poles responsible of the instability in pitch oscillation change their position to the left-half plane with the right value of c_l.

High freq.

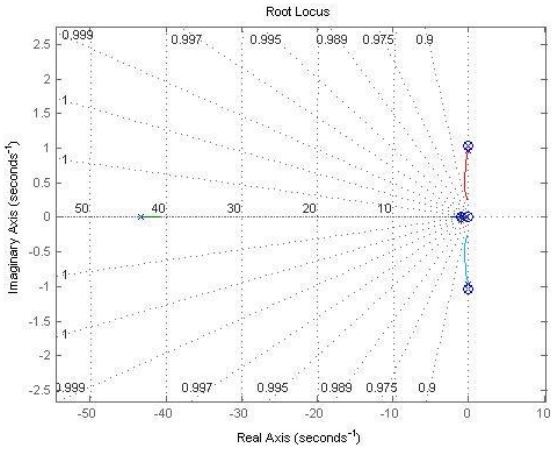

Low freq.

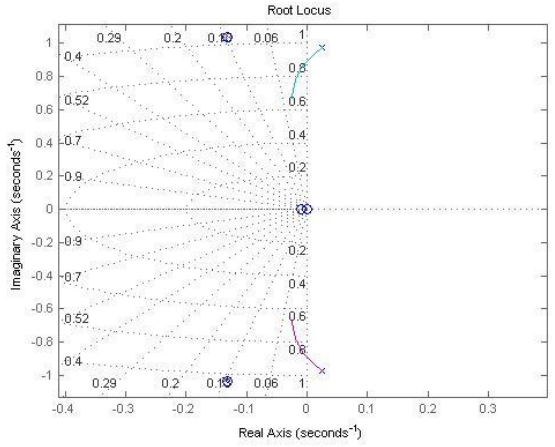

Figure 4.9: Change of position of poles with the fly-bar feedback $c_l = [0, 0.5]$

We have similarly results for the disturb in roll rate but the dynamic is about the command A_1 instead.

4.5 Validation

The development of the linear model has been made in non-dimensional form to be flexible to change of the identification of the RUAV and it allow also the development of control laws in future works.

The identification of the non-linear model has been developed comparing the response registered in a flight test with the response of the simulation on the same story of commands.

This commands has been loaded in the linear system to check the consistency between the two models.

4.5.1 Linear model validation

Following, the response in pitch rate and roll rate show the linear model has an acceptable comparison with the non-linear model.

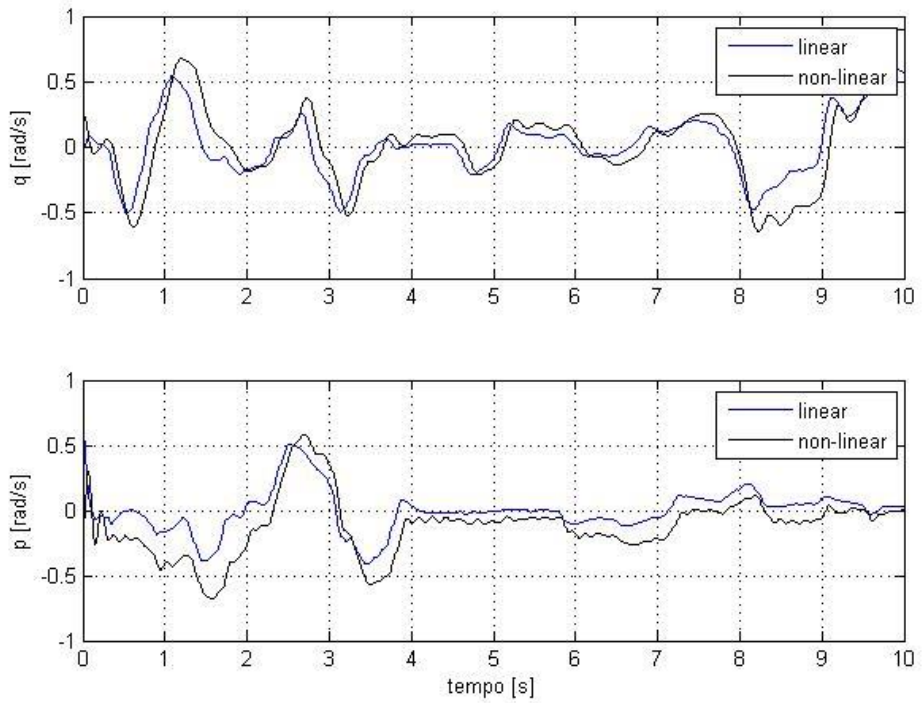

Figure 4.10: Comparison between linear and non-linear models response in pitch rate and roll rate under the same commands

4.5.2 Trim validation

The non-linear model has been evaluate with a Simulink tool that give the possibility to calculate the trim of the vehicle.

The tool is under the route: Tools/Control design/Linear analysis/Trim model.

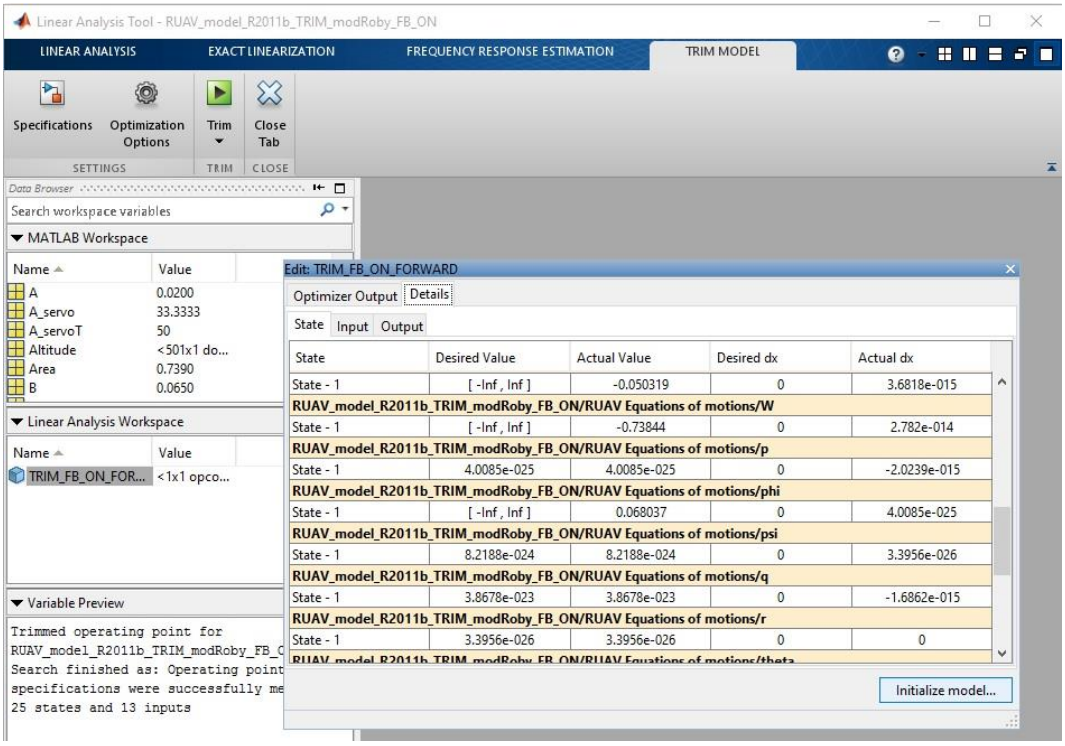

Figure 4.11: Representation of the Simulink trim tool

In "Specifications", the variable known are loaded, such as inputs, outputs and steady state.

The values of the attitude calculated in the chapter 3 has been used to verifying the trim; ones the tool has fended a convergence(TRIM_BF_ON_FORWARD in the figure 4.10), the all variable have been loaded in the non-linear model as initial conditions and a simulation of some seconds has been run to see if the trim is stable.

The hovering condition and three velocity of flight($\mu = 0.04, \mu = 0.06, \mu = 0.1$) have been verified and a corresponding between the two models has been fended.

5. FLIGHT CONTROL

"When evaluating control aspects of rotorcraft the first aspect to consider is the characteristics of the control system. As the pilot must control the swashplate through the flight controls a deficiency in their operation will affect all areas of flight. Even excellent aircraft handling qualities can be masked by poor flight control mechanical characteristics (FCMC). Testing can be divided into quantitative aspects which normally take place on the ground and qualitative aspects which are conducted in flight. As quantitative testing is concerned with the measurement of forces and displacements it can be conducted more easily and safely on the ground. For reversible systems, however, the amount of ground testing that can be undertaken is limited by the requirement to have the rotors turning and by the need to evaluate realistic flight forces. Qualitative testing is concerned with the effect that the control system characteristics have on the conduct of role tasks."[3]

To develop the control laws we have to study the time response of the helicopter to the commands.

5.1 Transfer functions of T-REX 500

First of all it is necessary to extrapolate from the linearized system with the feedback of the fly-bar the transfer functions regarding the dynamics of the T-REX 500.

The system is strongly coupled; however we can suppose that commands like $\theta_0$and B_1 interact primarily with the longitudinal plane, while $A_1$and θ_t affect the lateral plane.

The functions illustrated are the most significant and are about the hovering mode; for the other flight conditions the value of poles are different but the dynamic is still the same; we are interested in flight at fixed point and low flight speed (only at high speed the dynamic change mostly and the helicopter dynamic behavior looks like a plane; i.e. the rotor becomes a wing).

The transfer function illustrated following have been calculated in the hovering condition; in appendix B the transfer function calculated in a range of forward speed have been illustrated.

5.1.1 Command B_1

The transfer function of pitch attitude and pitch rate to a command B_1 are:

$$\frac{\theta}{B_1} = \frac{-814.87(s+4.2)(s+0.0098)}{(s^2+0.48s+0.29)(s^2+47.58s+576.2)} \tag{5.1}$$

$$\frac{q}{B_1} = s\frac{\theta}{B_1} \tag{5.2}$$

The presence of the fly-bar change the dynamic we have seen in the previously chapter: the high frequency pole near to the value of M_q and the fly-bar pole are coalescing giving rise to a second order dynamic and the complex conjugate of the low frequency oscillatory mode are stabilized in the left half plane.

The transfer function in longitudinal and vertical speed are:

$$\frac{u}{B_1} = \frac{9.81(s+4.2)(s^2-21.43s+815.2)}{(s^2+0.48s+0.29)(s^2+47.58s+576.2)} \tag{5.3}$$

$$\frac{w}{B_1} = \frac{-90.34(s+4.2)(s^2-0.065s+2.9)}{(s+1.078)(s^2+0.48s+0.29)(s^2+47.58s+576.2)} \tag{5.4}$$

In the $\frac{w}{B_1}$ function we can see the vertical speed mode pole $(s+1.078)$ that is decoupling from the other dynamics.

The time response are shown in the following figure 5.1 and figure 5.2:

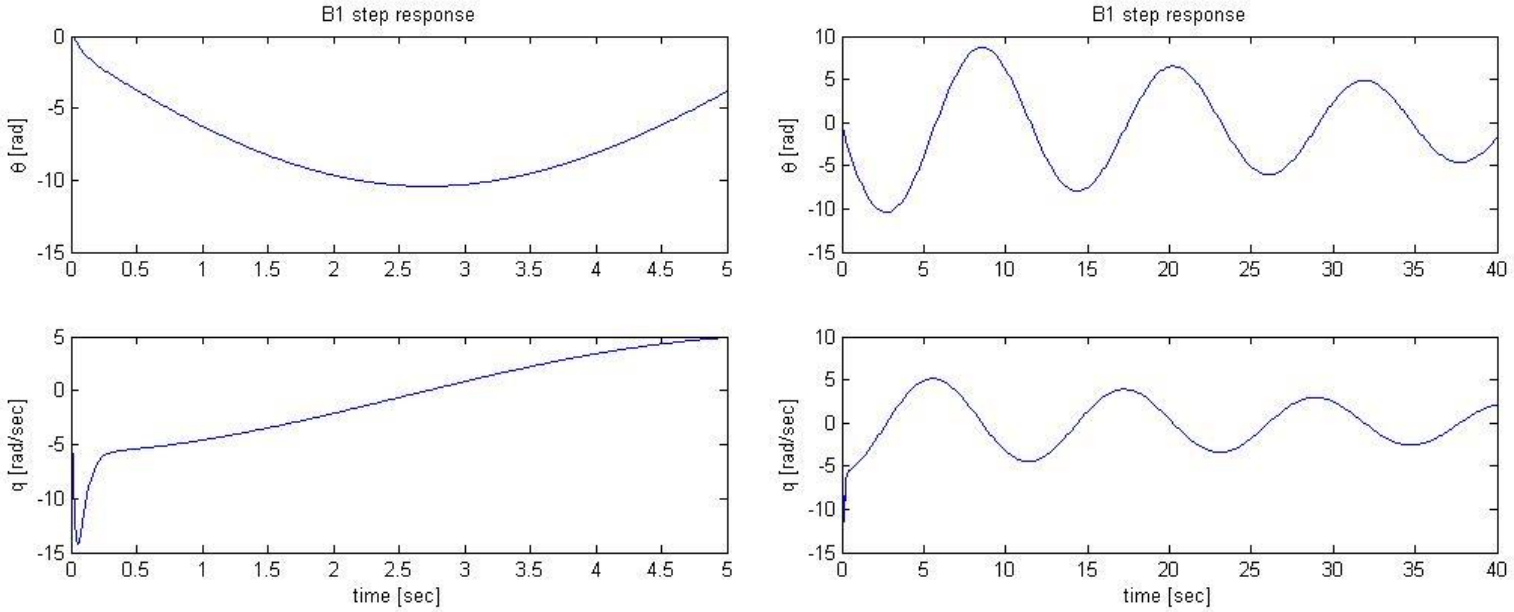

Figure 5.1: Time response in q and θ to step B_1

Be care that the command has given in radiant but the system is linear and we can relate the value very easily.

As we can see the response in pitch rate it's very fast $\dot{q}(0) = M_{B_1}B_1$ but the helicopter does not response in q at regime, because the presence of the zero in the origin; a little bit slow is the response in θ, being the integral of q, that settles itself to a little damped oscillatory mode around the value of -0.2 degrees per 1 degrees command B_1.

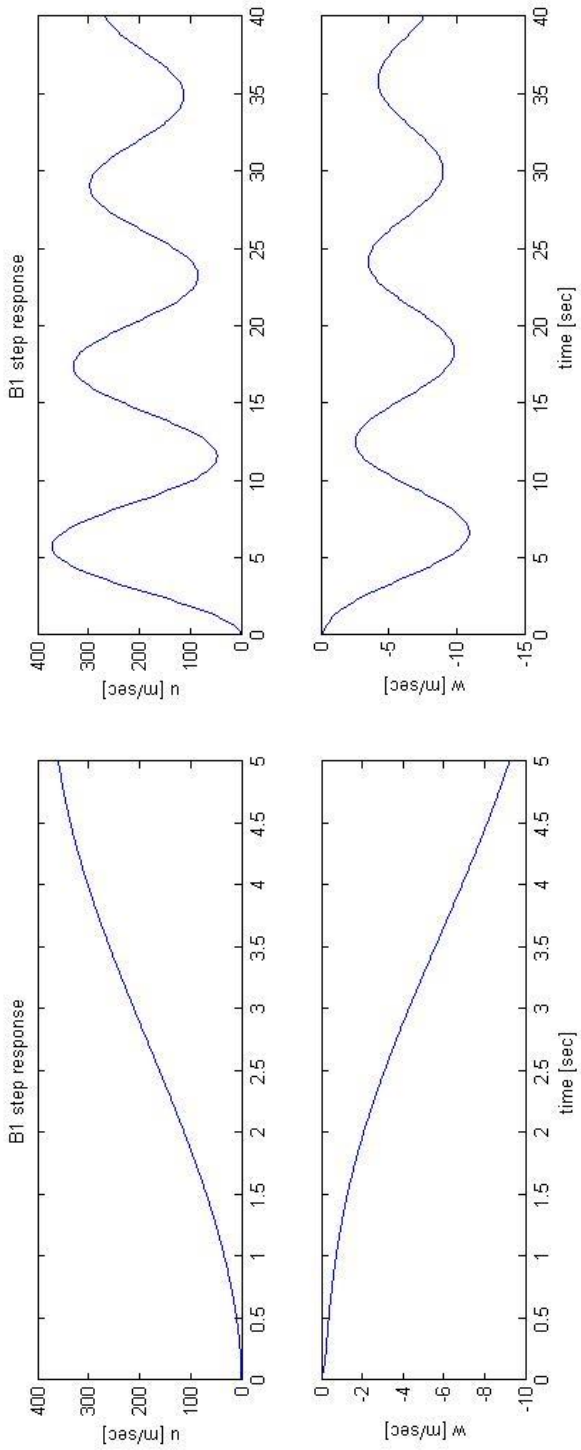

Figure 5.2 Time response in u and w to step B_1

The response in u is more slow compared to the pitch rate, the frontward rotation of the rotor bring a positive acceleration $\dot{u}(0) = 9.81$ and the helicopter takes an oscillatory increment in forward speed around a regime value of 3.5 m/s per 1 degrees of command.
With the rotation of the rotor we expect a loss of lift, but at the same time the increment in longitudinal speed decreases the inflow and the power needed to maintain the helicopter in hovering, see figure 3.3 and 3.7 in "3.3 Trim results", and the helicopter begin to climb; however the amplitude is negligible.

At high speed, as we have already study, the oscillatory poles are more instable because the hinge-less rotor and the fly-bar feedback is less efficient, bringing them only to the marginal stability, in the figure 5.3 we can check how the oscillation is nearly constant, see appendix B to check the values of poles.

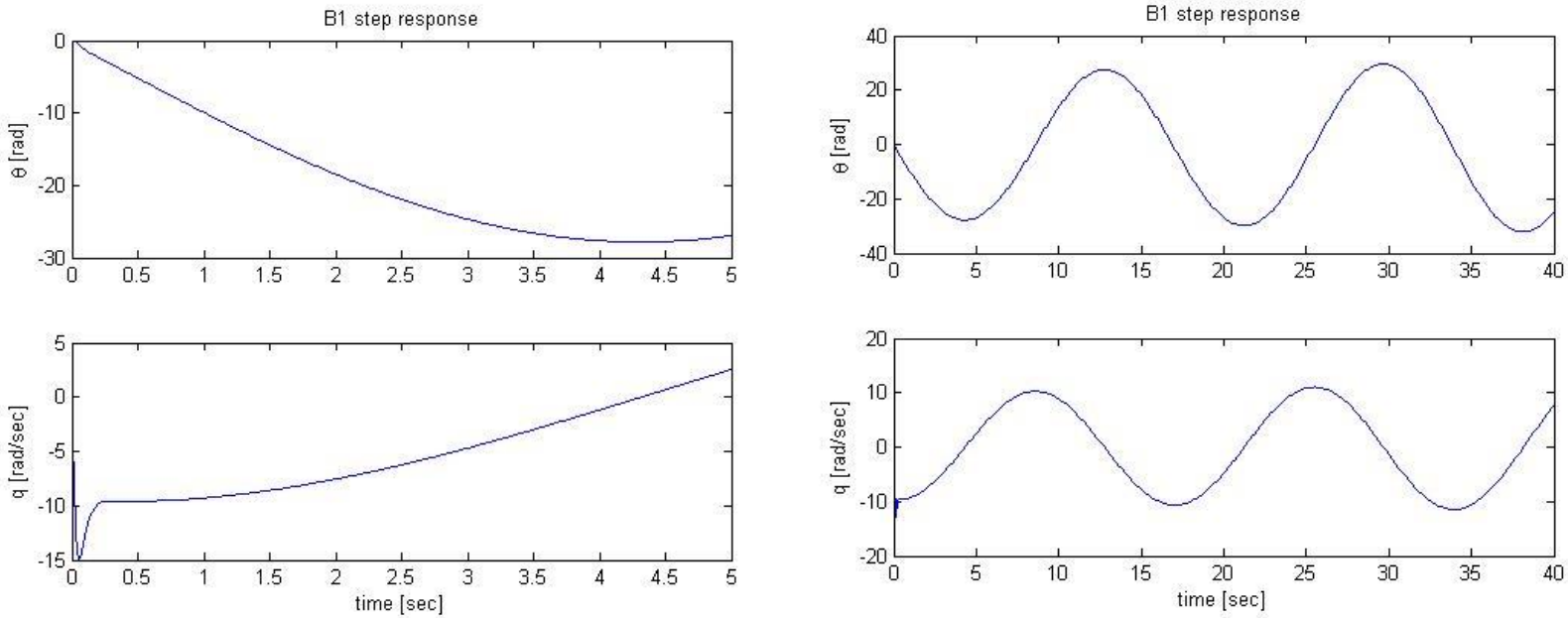

Figure 5.3 Time response in q and θ to step B_1

at high speed

5.1.2 Command θ_0

Being in steady state the resultant of rotor forces pass very near the center of mass so the response in q, θ and u are negligible; of interest are the w and h response instead, where the zero-pole cancellation simplify the transfer function remaining the vertical speed mode only.

$$\frac{w}{\theta_0} = \frac{-76.67}{(s+1.078)} \tag{5.5}$$

$$\frac{h}{\theta_0} = \frac{1}{s}\frac{w}{\theta_0} = \frac{-76.67}{s(s+1.078)} \tag{5.6}$$

In the figure 5.4 is reported also the *u* response in order to see how little is the amplitude to 1 radiant of command.

The response in *w*, or $\alpha = \frac{w}{U}$ if we are in forward flight, is a pure first order and decoupling by the other longitudinal dynamic.

In hovering the response in altitude is simply its integral, in forward motion we should consider the contribute of $V\frac{\theta}{\theta_0}$; however it is negligible and does not change the response.

Following a command θ_0 the altitude grows as ramp.

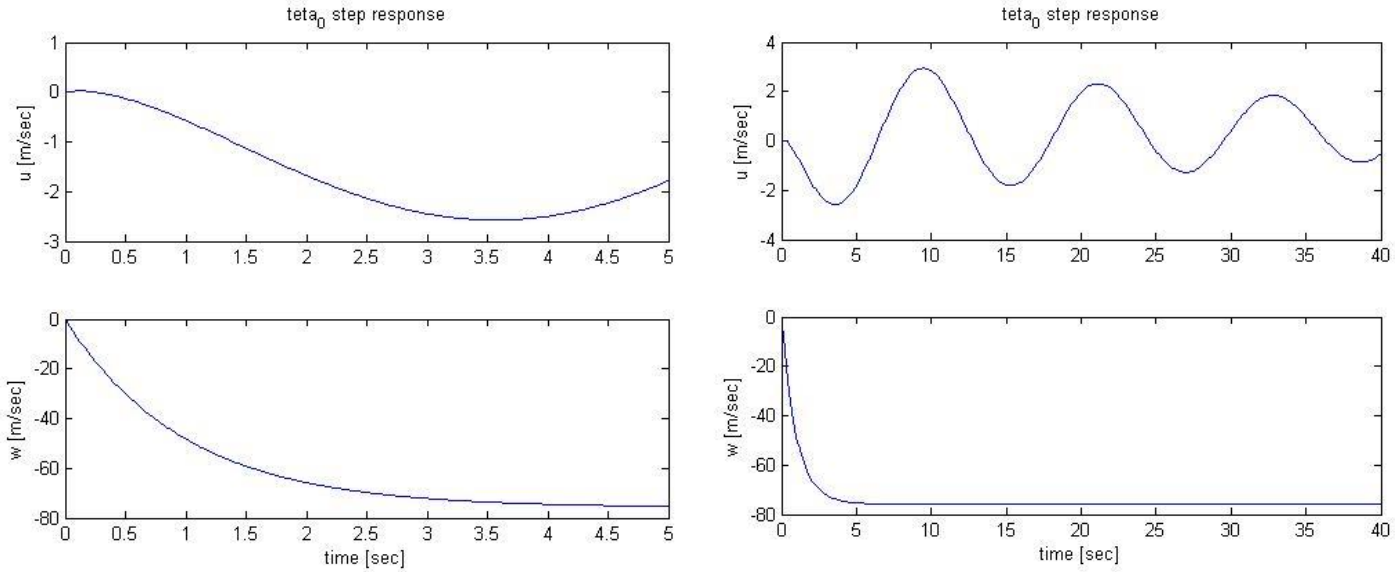

Figure 5.4 Time response in u and w to step θ_0

5.1.3 Command A_1

The command A_1 has effect on the lateral plane.

$$\frac{p}{A_1} = \frac{-2355.2\, s\, (s+4.2)(s+0.75)(s+0.45)}{(s+122.4)(s+14.46)(s+0.89)(s^2+0.37s+0.39)} \tag{5.7}$$

$$\frac{\phi}{A_1} = \frac{1}{s}\frac{p}{A_1} \tag{5.8}$$

$$p = \frac{-2355.2\, s}{(s+122.4)(s+14.46)} \text{ (HF approximation)} \tag{5.9}$$

In the high frequency approximation we can see a highly damped roll dynamic, the spiral mode and the dutch-roll poles are not recognized for the dynamic.

In the first moments the response is governed by the rolling pole and the helicopter reach rapidly a rolling rate; but the presence of the fly-bar and, being in hovering, the high dihedral effect ($\beta = \frac{\pi}{2}$) tilt the rotor and the effect of the zero in the origin bring the rolling rate to zero in a few seconds.

The roll attitude is approximated to a high damped second order response and settles to a constant value, figure 5.5.

With the growing of the forward speed the dihedral effect reduce its self and the spiral pole goes next to the origin; at high flight speed the rolling rate stop to a constant value and the roll attitude grows indefinitely.

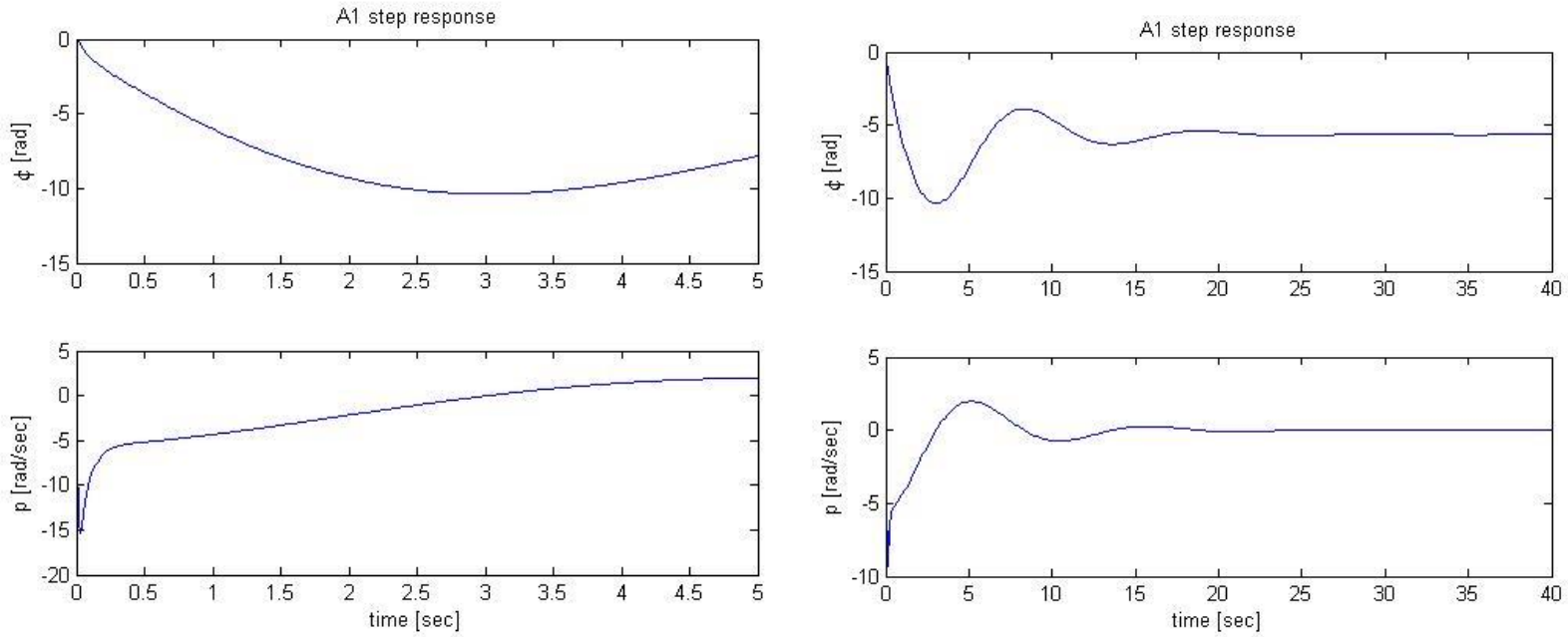

Figure 5.5 Time response in p and phi to step A_1

5.1.4 Command θ_t

The presence of the tail rotor is necessary to balance the torque of the main rotor; a command to its collective influence principally the yaw rate.
Here will be study the behavior in open loop and in a simple closed loop because the control system on the machine is not already been identified.

$$\frac{r}{\theta_t} = \frac{48.34(s^2+0.067s+0.31)}{(s+0.89)(s^2+0.37s+0.39)} \tag{5.10}$$

$$\frac{\psi}{\theta_t} = \frac{1}{s}\frac{r}{\theta_t} \tag{5.11}$$

In hovering the response is almost exclusively in yaw rate with a little oscillation in lateral velocity; in the first moments the helicopter response like a first order, than we have a second order oscillation due the dutch-roll poles and the yaw rate settles to a constant value, while the yaw angle grows to ramp.
With the increasing of the forward speed the effect on lateral velocity becomes more intense; the helicopter response with a constant $\beta = \frac{v}{V}$, while the yaw rate tends to zero at regime.
The gyro mounted on the T-REX 500 measures the yaw rate and ensure the "heading lock" of the helicopter by command the tail rotor collective.

5.2 Controller

The purpose of building the control laws is to allow the helicopter to fly in automatic mode.

That means the pilot assigns the reference values from the radio-controller:

- Hovering mode, the control system set the speed in the three axis to zero;
- Forward flight mode, the pilot can set the speed along the longitudinal and vertical axis and the roll angle by the levers of the radio-controller and the control system work to follow the pilot wish, maintaining always the helicopter in balance.
    - Longitudinal speed: the pilot change the lever of forward speed (*u* figure 5.7) and the controller, not only bring the helicopter to the new speed, but it maintain the altitude and the direction of flight;
    - Vertical speed: the helicopter must perform a climb or a sink with the same forward speed and direction of flight and the control sets as reference the new altitude reached when the pilot set off the ask of vertical speed;
    - Roll angle: if the pilot ask for a turn by setting a roll angle, the helicopter must maintain the altitude and the speed of flight while performing the maneuver.

For these control laws PID controller have been used and they are synthetized by means of SISO techniques.

The figure 5.7 represents how the pilot could set the references for the control:

- the lever on the left side, usually used to command the cyclic B_1 (up and down) and the rotor tail collective θ_t (left and right), now is useful to set a variation of longitudinal velocity *u* or a specific yaw rate;
- similarly for the lever on the right side, where the command of collective θ_0 and cyclic A_1 now corresponds respectively to a request of vertical speed *w* or of a roll angle ϕ.

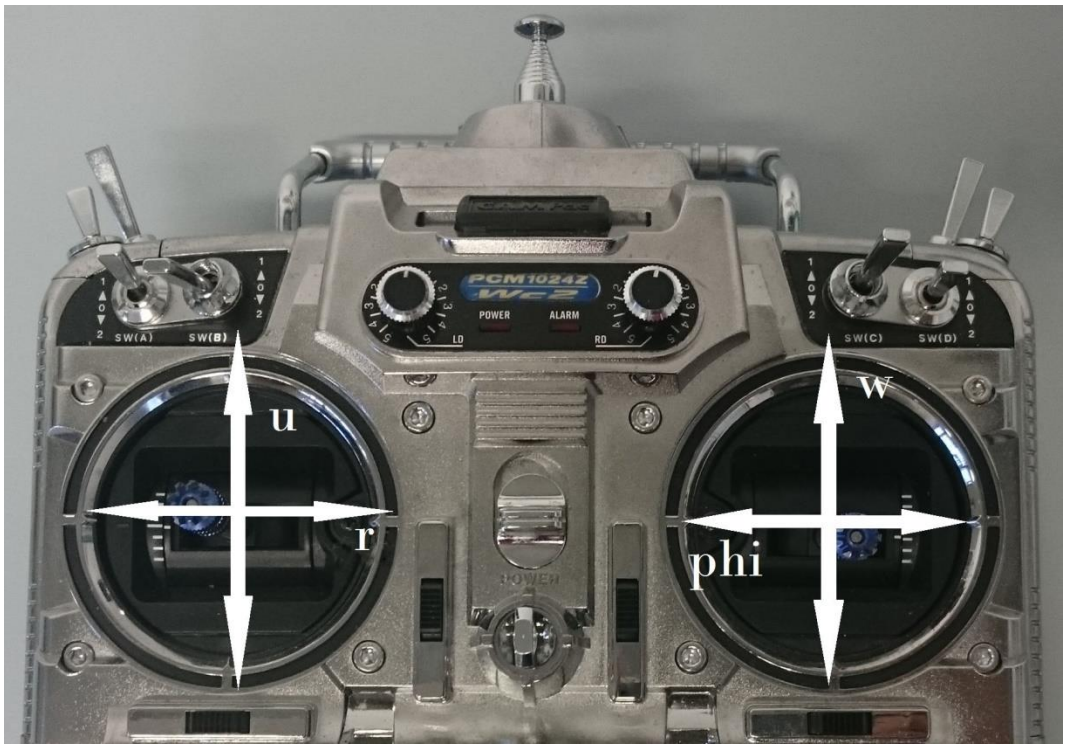

Figure 5.7 Representation of the radio-controller

5.2.1 Autopilot in longitudinal speed and position

This autopilot allow to choose a forward speed or maintain the position along the x body-axes that for small attitude angles can be approximated to the X inertial-axes.

Observing the generalized Bode plot in figure 5.8 the control of the speed along the x body-axes can be realized with a positive proportional (critical phase at 180°) and the addition of an integral action to cancel the asymptotic error [8][9].

Because of the oscillatory poles it is difficult find a value of the gain to maintain a suitable phase margin; to resolve the problem it is possible implementing a derivative control or insert a stability augmentation system by θ and q controller.

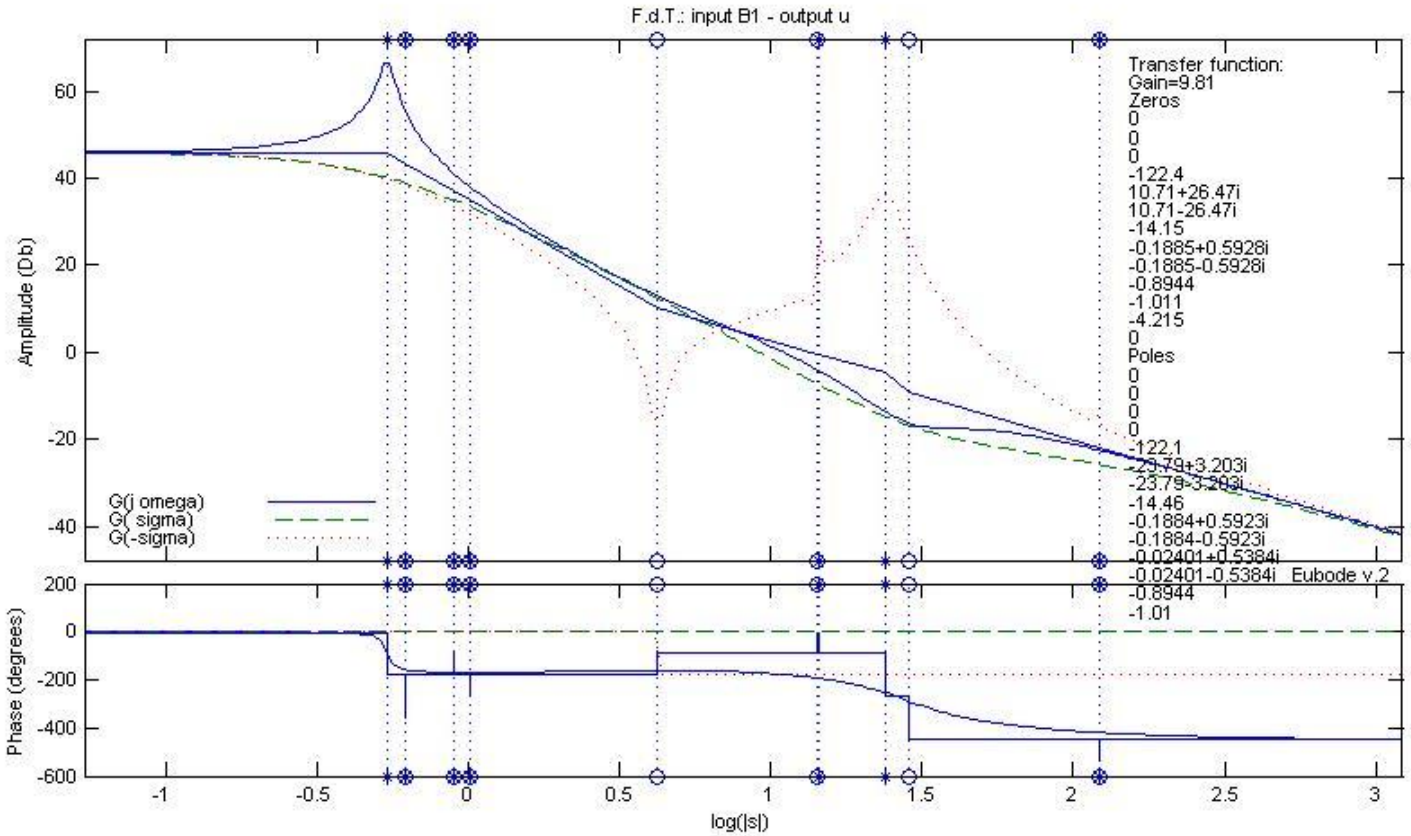

Figure 5.8 Generalized Bode plot $\frac{\mathbf{u}}{\mathbf{B_1}}$

The figure 5.9 represents the electronic control for a common helicopter [4], that can be used on the T-REX too, and the stability effect of a negative proportional control in θ, the upper root locus, and a negative proportional control with lag $(s + \frac{1}{l})$ in q, the lower one, that is exactly the same effect of the fly-bar; therefore we chose to control only the pitch attitude.

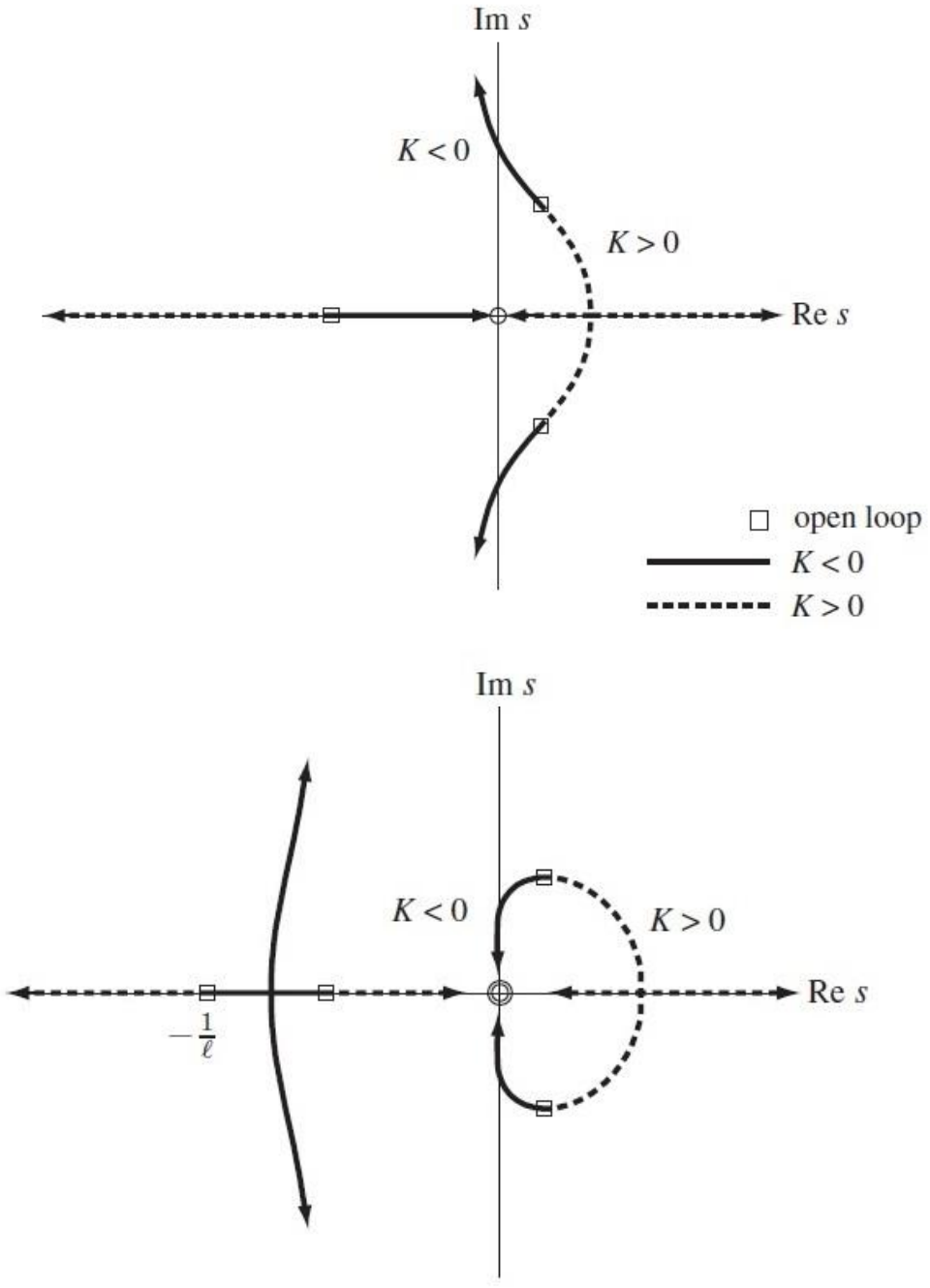

Figure 5.9 Root loci of θ and q controller [4]

Using the figure 5.10 the generalized Bode plot for function $\frac{\theta}{B_1}$ we can see how, choosing a gain $K = -0.2$ (critical phase at 0°), the poles interested by the feedback are only the oscillatory mode and coalescing themselves in to two real roots, while the high frequency poles are not changed by the loop.

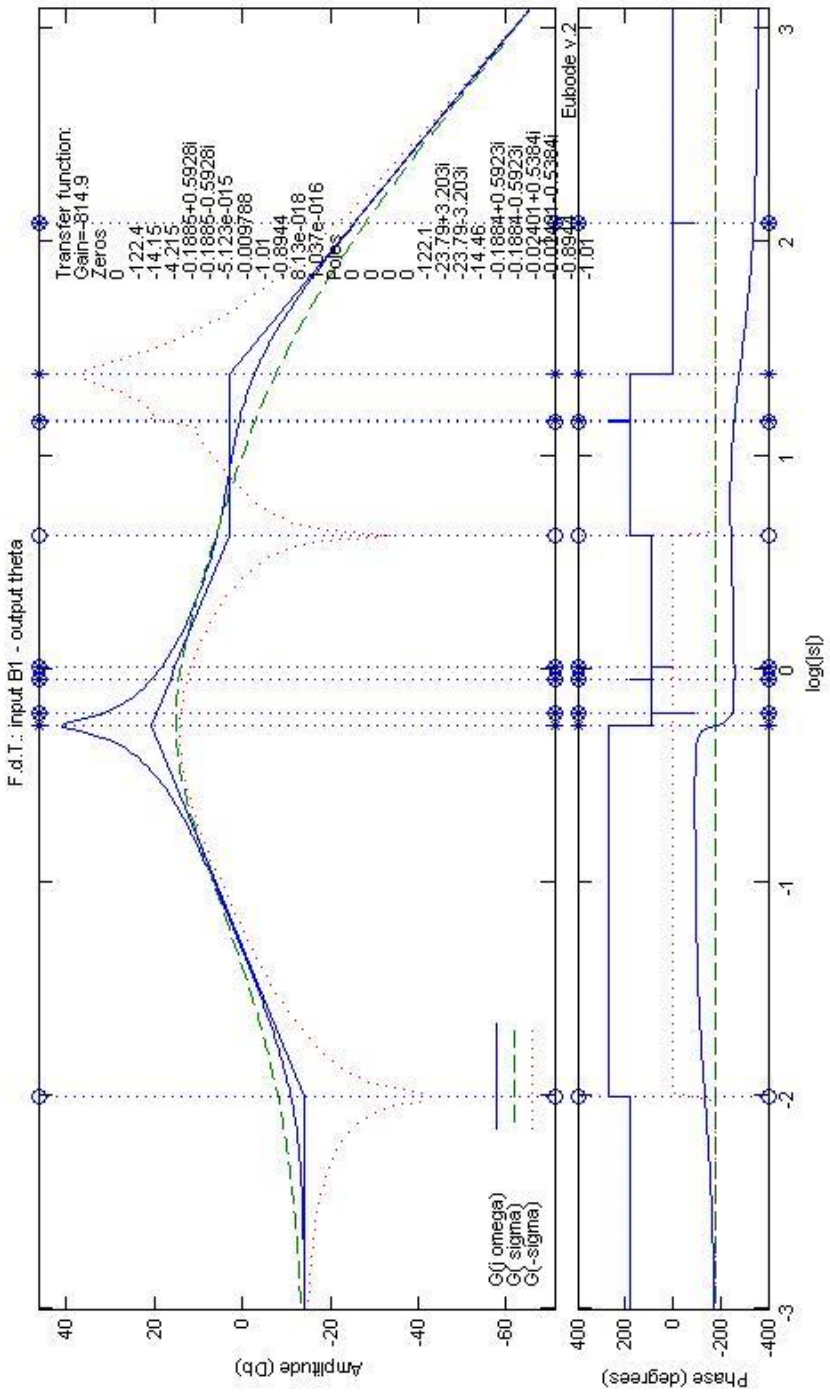

Figure 5.10 Generalized Bode plot $\frac{\theta}{B_1}$

The control chain is the following in figure 5.11.

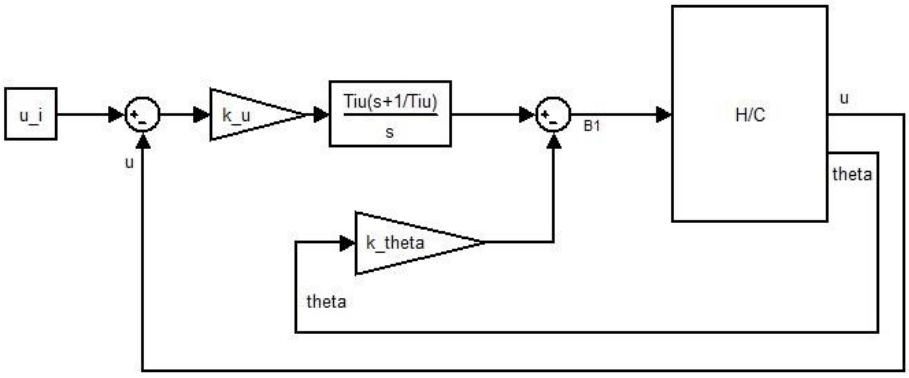

Figure 5.11 Loop chain forward speed control

The transfer function of the position $\frac{X}{\mathrm{B}_1} = \frac{1}{s}\frac{u}{\mathrm{B}_1}$ presents a pole in the origin, so a simply positive proportional control will be able to close the system without an asymptotic error.

The stability augmentation system in θ is still necessary to obtain an acceptable response.

However, as shown in the figure 5.12, the maximum bandwidth reached without destabilizing the system is too low and to improve the velocity of the response it is necessary to implement a derivative control with an high frequency filter or a proportional control in velocity *u* [8].

The proportional control in velocity *u* has been chosen because it is already been developed for the forward speed, but now it is used as a SAS.

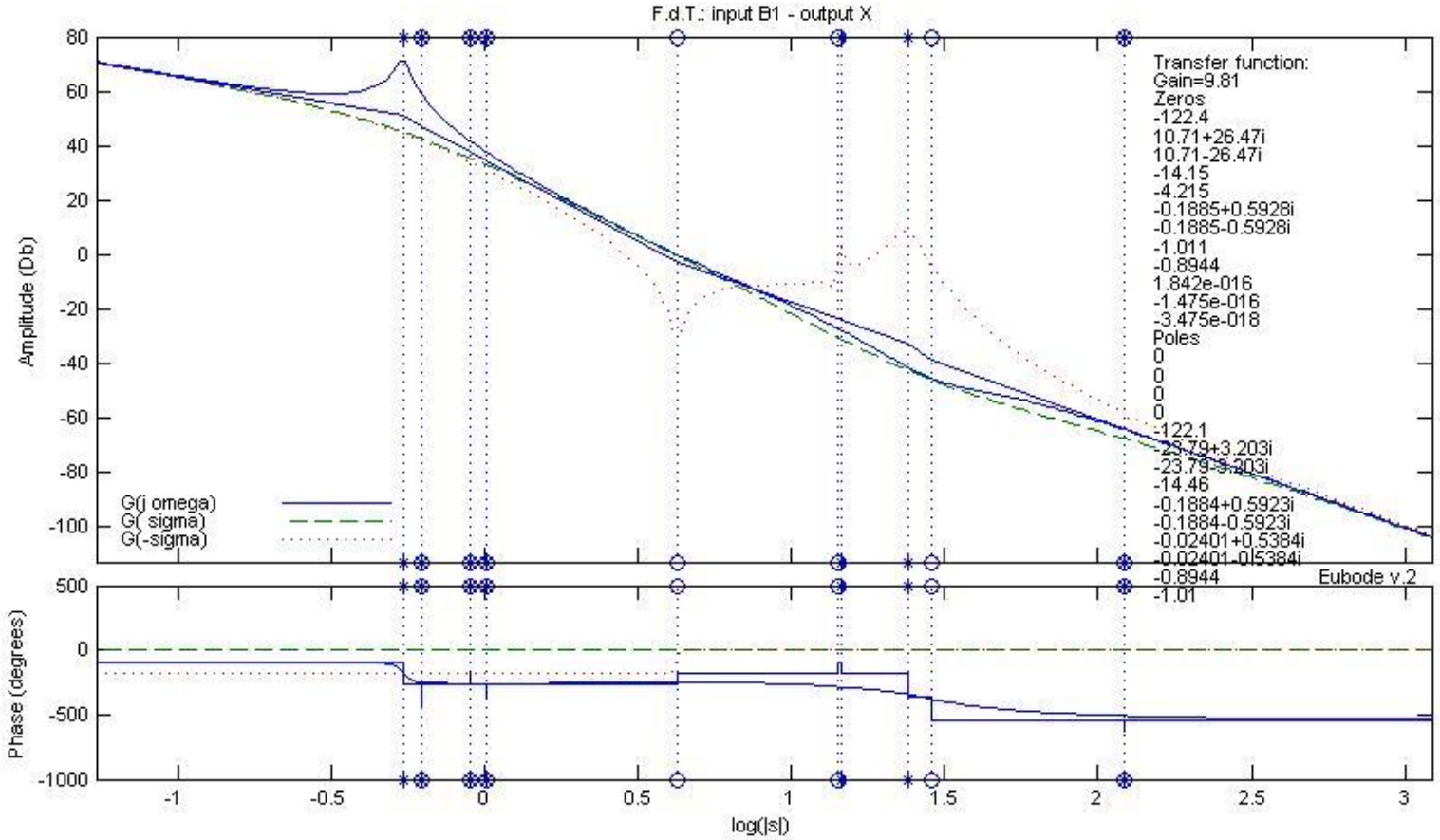

Figure 5.12 Generalized Bode plot $\frac{X}{B_1}$

The control chain is the following in figure 5.13

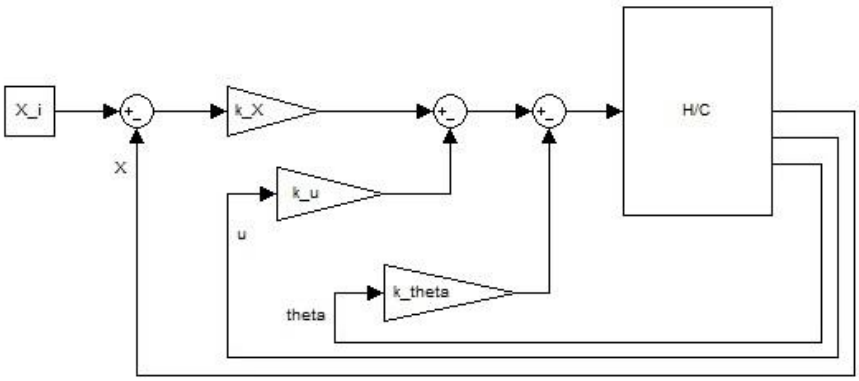

Figure 5.13 Loop chain position X control

5.2.2 Autopilot in vertical speed and altitude

With this autopilot the helicopter is capable of maintain the altitude or reach a new flight level with a vertical velocity set by pilot.

The response in vertical velocity, or incidence α if the helicopter has a forward speed, with a command in collective is a pure first order with an high bandwidth.

A negative proportional feedback with an integral action to ensure the right value request by the pilot it is sufficient to close the system.

The transfer function in altitude is a second order with a pole in the origin; a negative proportional has been developed with a feedback in vertical velocity to increase the bandwidth.

Following are illustrated the Bode diagram of the $\frac{w}{\theta_0}$ and $\frac{h}{\theta_0}$.

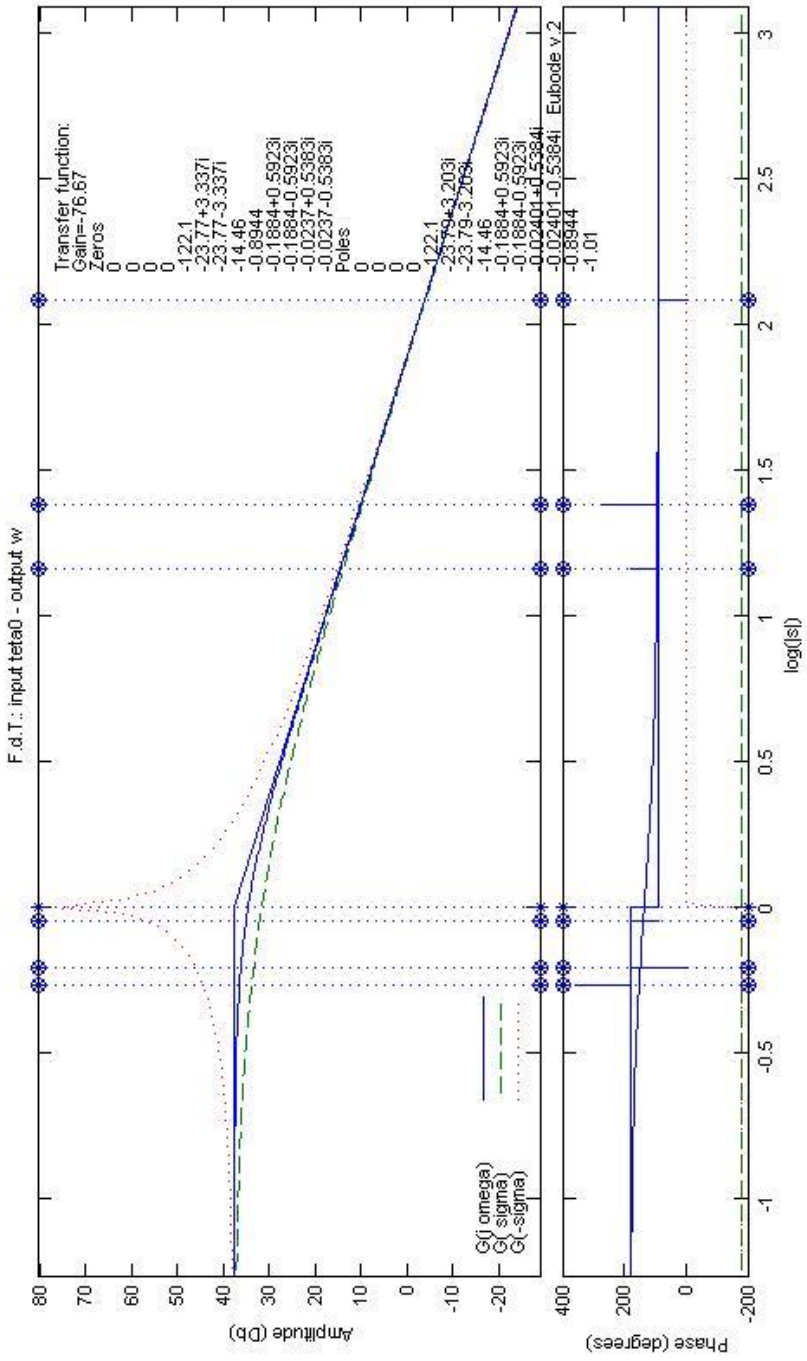

Figure 5.14 Generalized Bode plot $\frac{w}{\theta_0}$

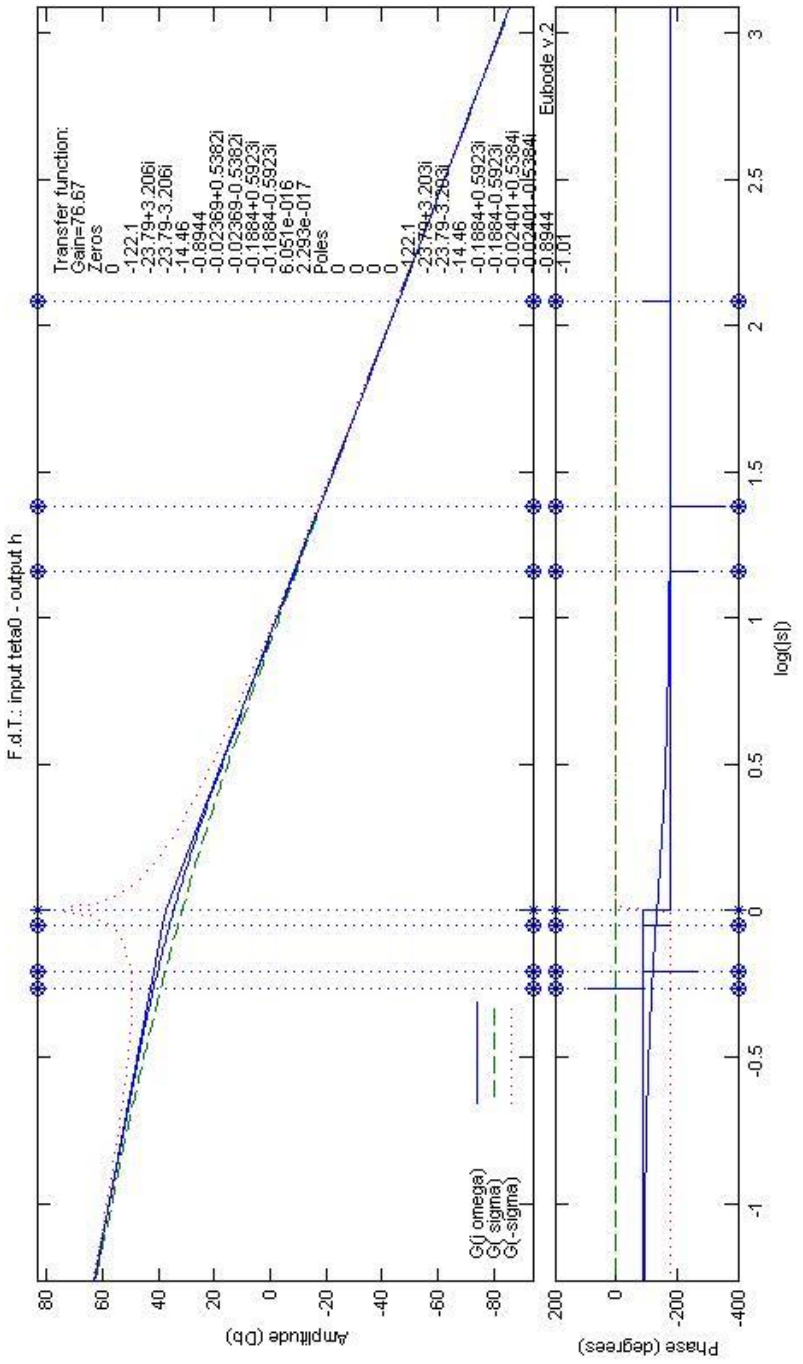

Figure 5.15 Generalized Bode plot $\frac{h}{\theta_0}$

5.2.3 Autopilot in roll angle and lateral position

The behavior of the helicopter in the lateral plane is highly influenced by the forward speed.

In hovering the gyro controller help on the maintaining of the heading, so it is possible remove the degrees of freedom in yaw rate and develop only a controller in position along y axes with the same structure as the previously longitudinal controller, but now the command interested is A_1 and the SAS is based on the ϕ angle to increase the stability and on the lateral velocity v to close the loop with an higher bandwidth [8].

In forward speed we have the relation $Ur = g\phi$, therefore if the pilot is thinking to make a turn, he is asking instead for a specific roll angle.

The controller in ϕ has been developed with a negative proportional and an integral action.

The bandwidth and the phase margin reached, looking the figure 5.13, are satisfactory so the control does not need a derivative or a SAS in roll rate.

The problem to this dynamic is the presence of the "heading lock" control that prevents to perform a correct turn; the resulting motion is a turn with a growing of the dihedral effect, because the increase of the β angle, and a corresponding growth of the command to maintain the roll angle until saturation.

When this autopilot is working it will be necessary a shutdown of the gyro controller that would allow the proper functioning of the autopilot in roll angle.

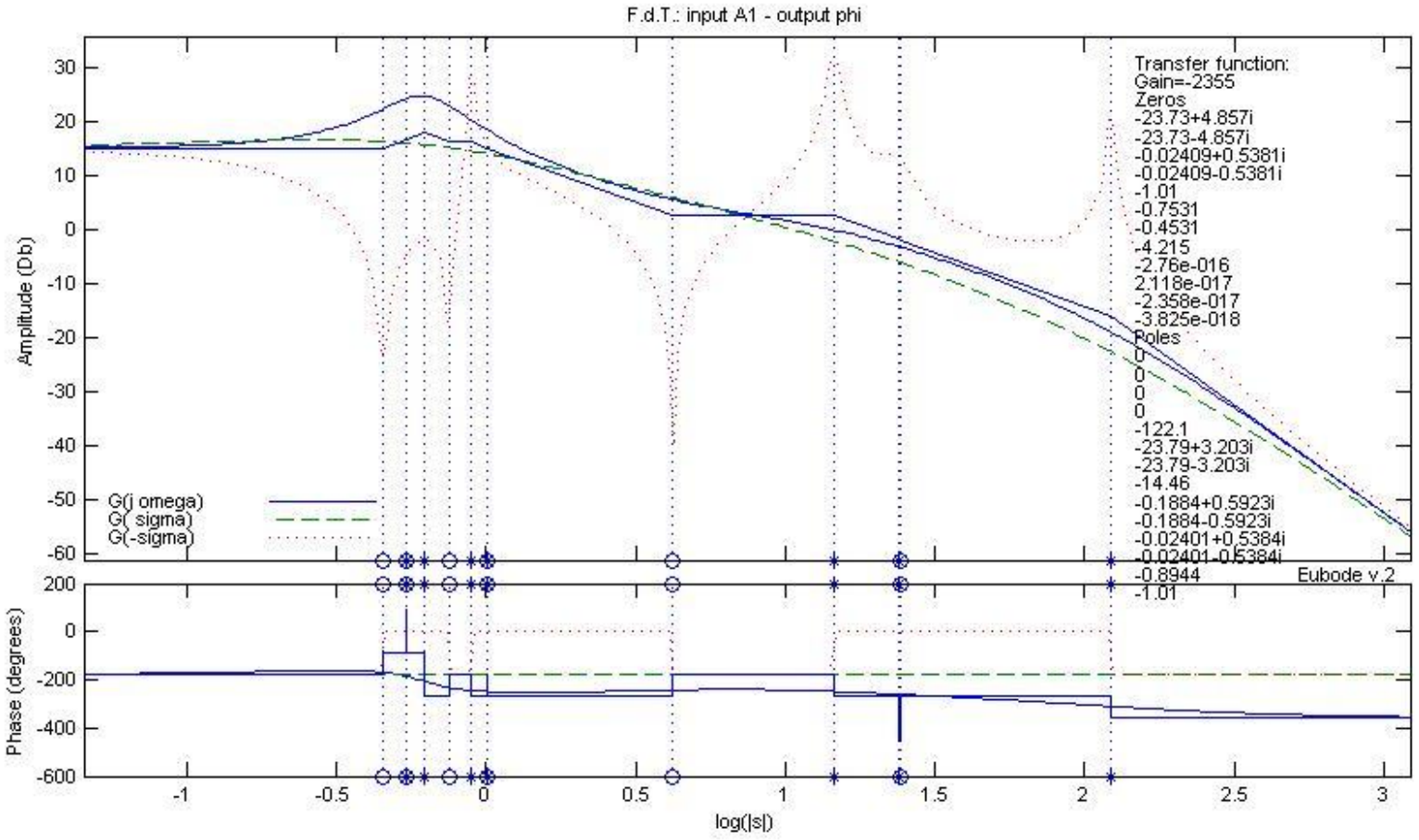

Figure 5.16 Generalized Bode plot $\frac{\phi}{A_1}$

5.3 MIMO system

All the controller are, in a first moment, studied like a SISO system to find the first values of the proportional and integral gains, proceeding in cascade, applying before the SAS feedback and then calculating the autopilot on the new SISO system generated.

Finally all the controller have been implemented in the helicopter linear simulation model to check the interactions effects among the controller themselves.

This step is very important because a strong assumption considered in the synthesis of the controller is that the longitudinal and later dynamic are decoupled, but it is not true in the helicopter dynamics.

Let us suppose the following simple system to evaluate the change of the function $\frac{h}{\theta_0}$ with the presence of a feedback on the longitudinal speed:

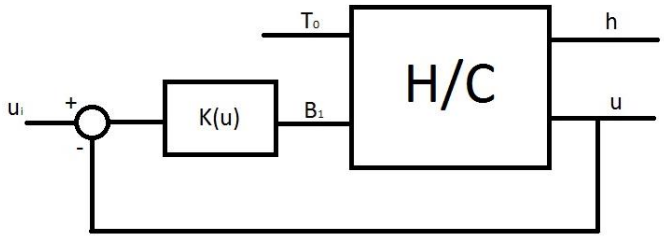

Figure 5.17 Example of MIMO system

Being G_{ij} the transfer function of the *j* input to the *i* output[8]:

$$\begin{Bmatrix} u \\ h \end{Bmatrix} = \begin{bmatrix} G_{u\theta_0} & G_{uB_1} \\ G_{h\theta_0} & G_{hB_1} \end{bmatrix} \begin{Bmatrix} \theta_0 \\ B_1 \end{Bmatrix} \tag{5.12}$$

with the feedback law

$$B_1 = K(u)(u_i - u) \Longrightarrow \; B_1 = K(u)u_i - K(u)(G_{u\theta_0}\theta_0 + G_{uB_1}B_1) \tag{5.13}$$

$$\Delta = 1 + K(u)G_{uB_1} \tag{5.14}$$

$$B_1 = \frac{K(u)}{\Delta}u_i - \frac{K(u)G_{u\theta_0}}{\Delta}\theta_0 \tag{5.15}$$

The system modifying in:

$$\begin{Bmatrix} u \\ h \end{Bmatrix} = \begin{bmatrix} G_{u\theta_0} & G_{uB_1} \\ G_{h\theta_0} & G_{hB_1} \end{bmatrix} \begin{bmatrix} 1 & 0 \\ \frac{-K(u)G_{u\theta_0}}{\Delta} & \frac{K(u)}{\Delta} \end{bmatrix} \begin{Bmatrix} \theta_0 \\ u_i \end{Bmatrix} \tag{5.16}$$

$$\frac{h_{new}}{\theta_0} = \frac{h}{\theta_0} - \frac{K(u)G_{u\theta_0}}{\Delta} G_{hB_1} \tag{5.17}$$

To integrate the all controllers and evaluate the behavior of the helicopter has been developed a code shown in appendix C, that implements the dynamic of the servos of the swash-plate too.

The controller in maintaining of altitude have been resulted ineffective to the pilot's request in change of velocity or in roll attitude because the function $\frac{h}{\theta_0}$ has been modified by others controls and now it is necessary to insert an integral action to cancel the asymptotic error.

The values of the controllers are illustrated in the following table:

Hovering	
k_theta_hover	-0.4
k_u_hover	0.1
k_X_hover	0.15
k_phi_hover	-0.3
k_v_hover	-0.1
k_Y_hover	-0.15
k_w	-0.05
k_h	0.2
Forward speed	
k_theta	-0.4
k_u	0.04
Tiu	1/0.4
k_w	-0.05
Tiw	1/0.15
k_h	0.02
Tih	1/0.1
k_phi	-0.3
Tiphi	1/0.1

Table 5.1: Controller values

5.4 Results

To validate the controllers we need to check the responses in the different flight conditions, applying margins that the responses must be within.

In literature there are not specification about the quality of flight for small-scale helicopter and, with the pilot experience, the following specifics have been settled.

We have auto-pilot controllers, so the responses must be the more as possible like a second order with zero asymptotic error, frequency response flat till the cut off frequency: the specifications chosen are a maximum overshoot of 50% that means for a second order response, in a good approximation, a damping coefficient of about $\zeta > 0.3$ and a settling time of less than 8 s; knowing the minimum ζ we have a limit to the lower bandwidth $\omega_n > 1.6$ s^{-1}, being $T_s = \frac{4}{\zeta \omega_n}$, for a tolerance of ±2%.

In hovering the results obtained with the values of gains in the table 5.1 are the following:

with the controls in longitudinal and lateral positions we within the specifications, because of the marginal stability of the low frequency poles that delay the behavior of the machine; but the control of altitude is well in requests.

We report also the time evolutions of the commands to the swash-plate to check them amplitude is in the limits of saturation of about ±20 deg.

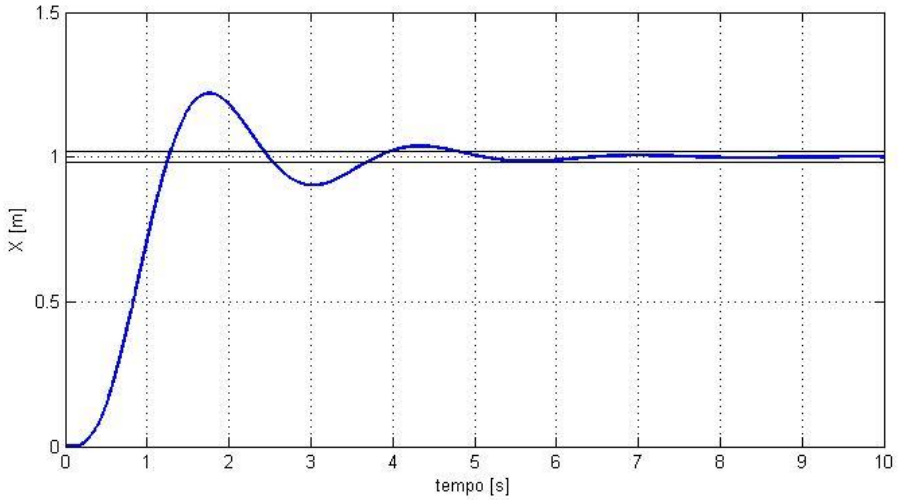

Figure 5.18 Time response of control in longitudinal position

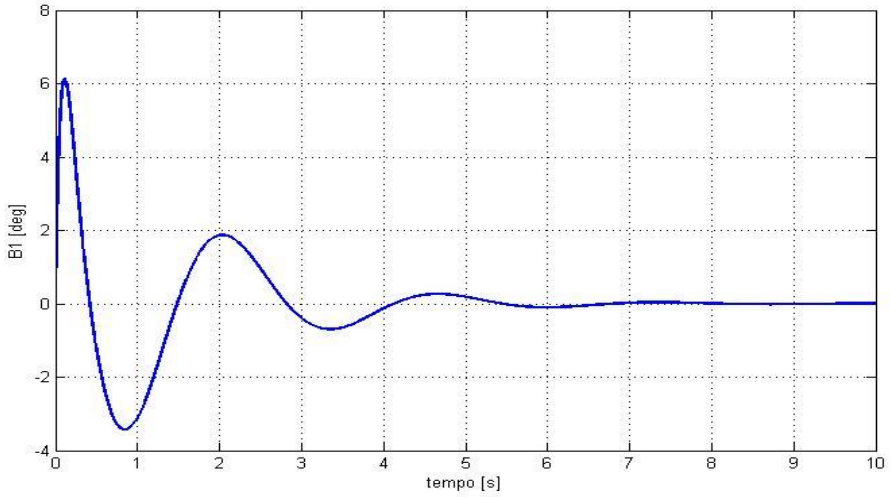

Figure 5.19 Time response of command B_1

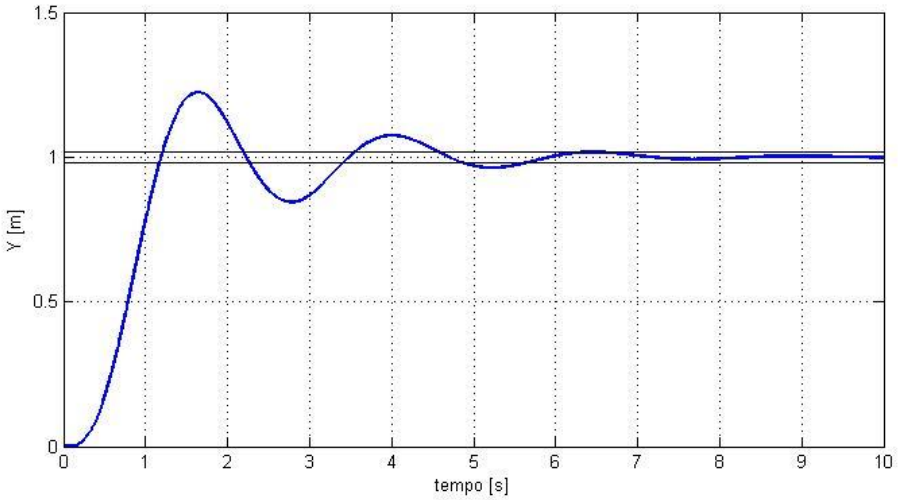

Figure 5.20 Time response of control in lateral position

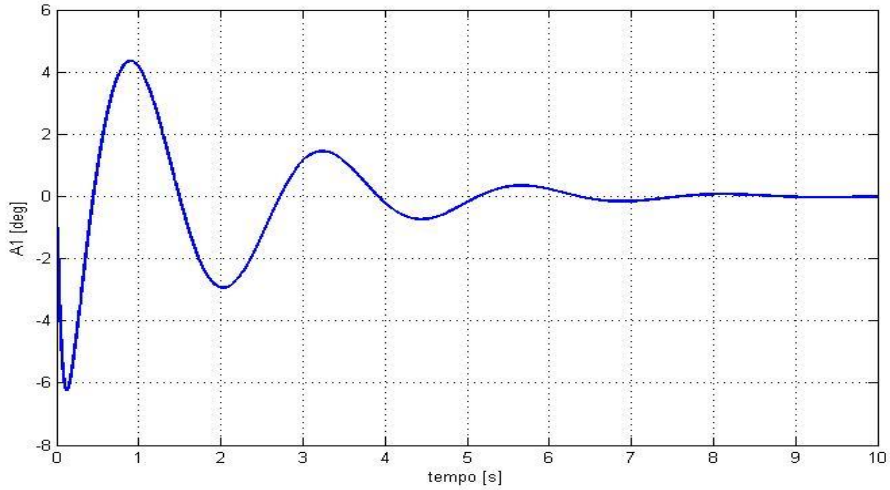

Figure 5.21 Time response of command A_1

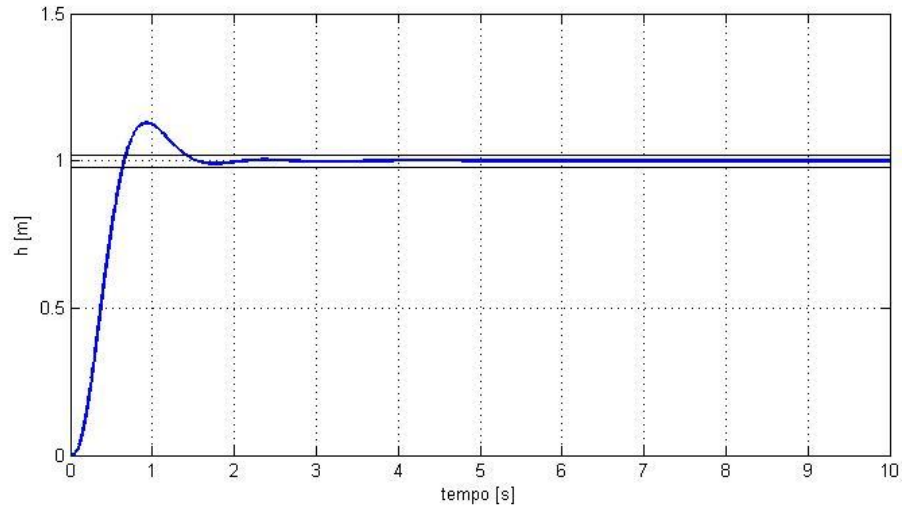

Figure 5.22 Time response of control in vertical position

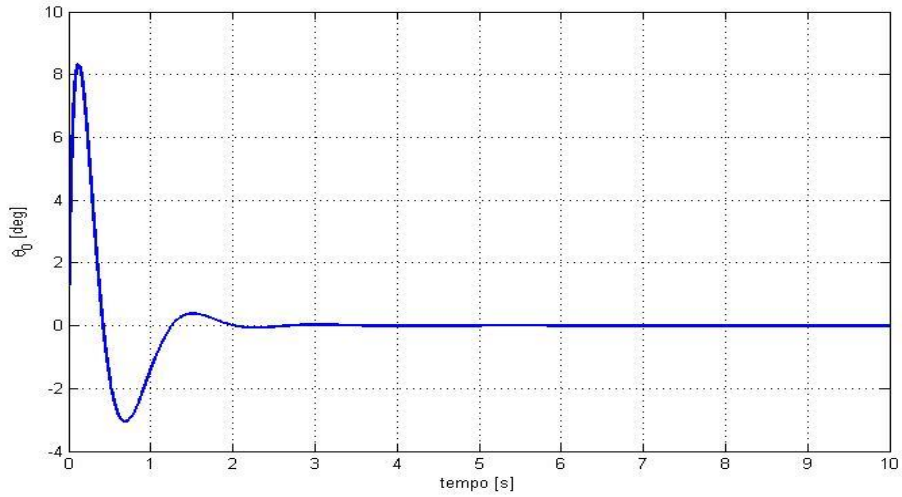

Figure 5.23 Time response of command θ_0

In forward speed we have different flight conditions to analyze and to check the controllers; the purpose is to obtain, without change the controller's gains, all the response consistent with the specification.

Following are illustrated the response at the different forward speed parameters $\mu = 0.04$, $\mu = 0.06$ and $\mu = 0.1$ with the gains of the table 5.1, applying one by one the controllers in forward speed first, in vertical speed and then in roll attitude, while maintaining the others set to zero following.

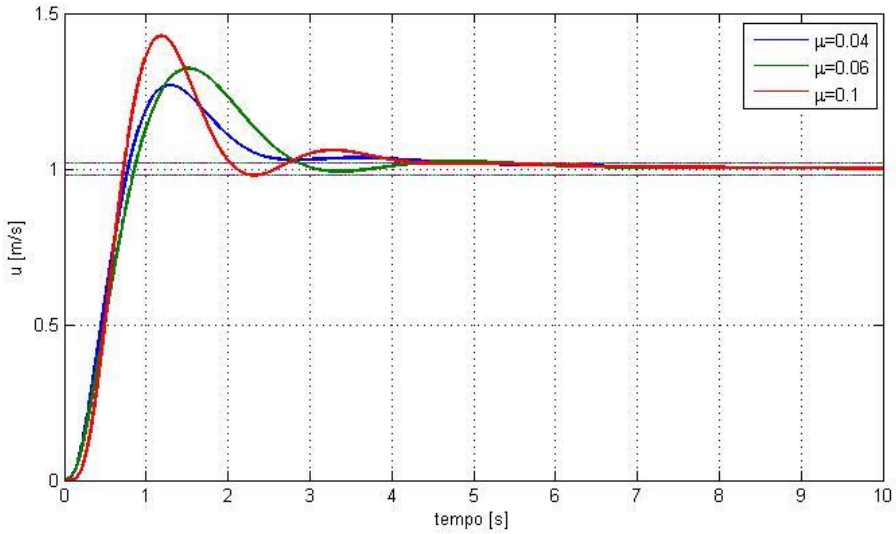

Figure 5.24 Time response of control in forward speed

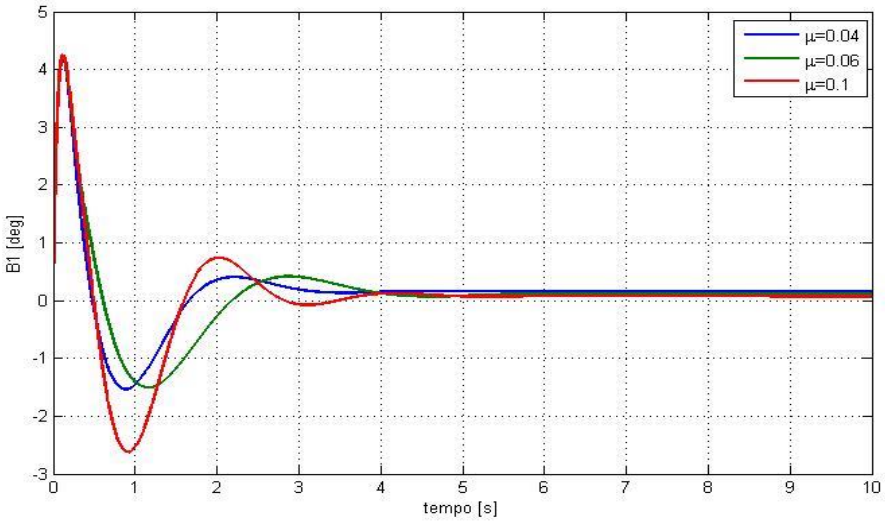

Figure 5.25 Time response of command B_1

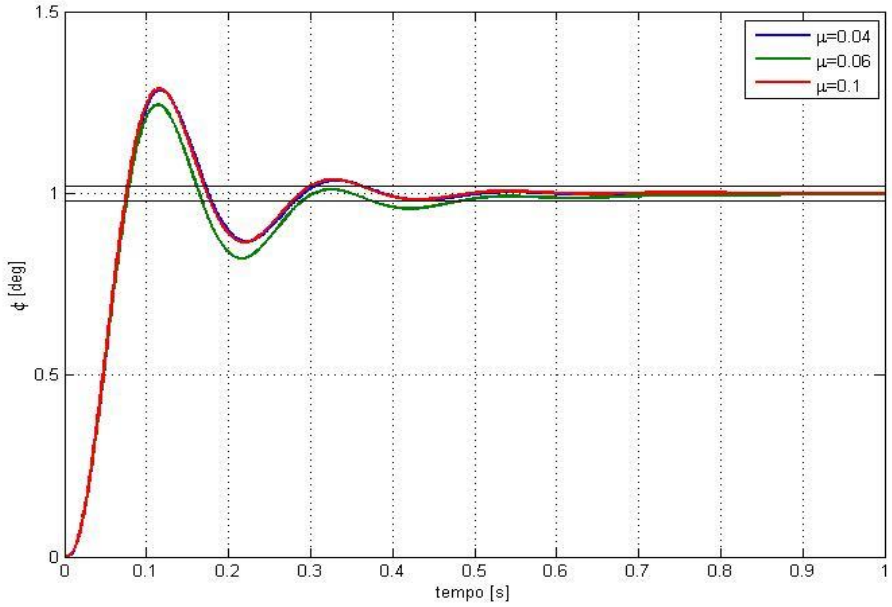

Figure 5.26 Time response of control in ϕ

To note the rapidity of the response in roll due to the very low inertia moment around the x axis.

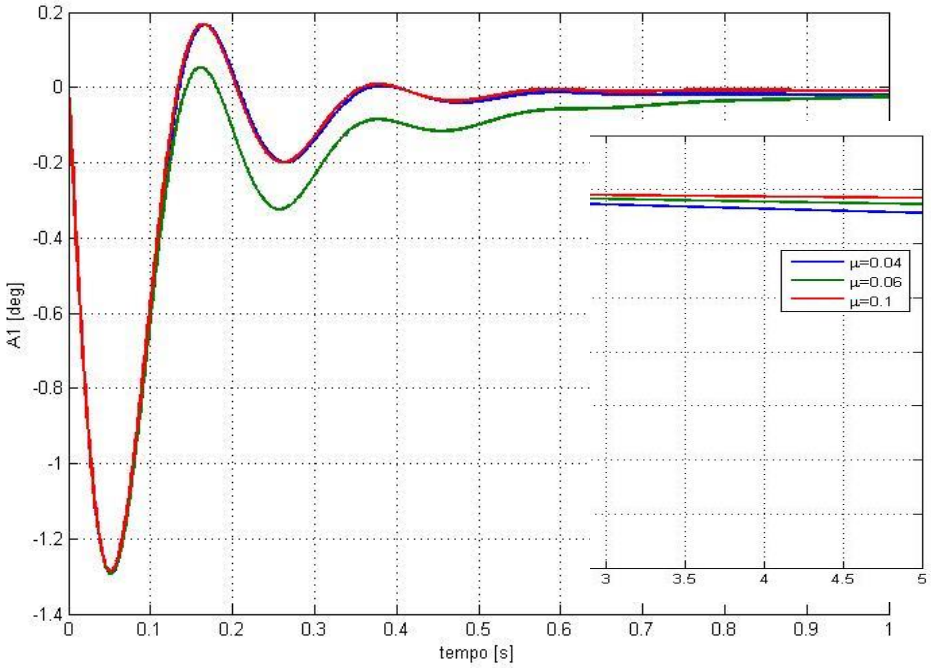

Figure 5.27 Time response of command A_1

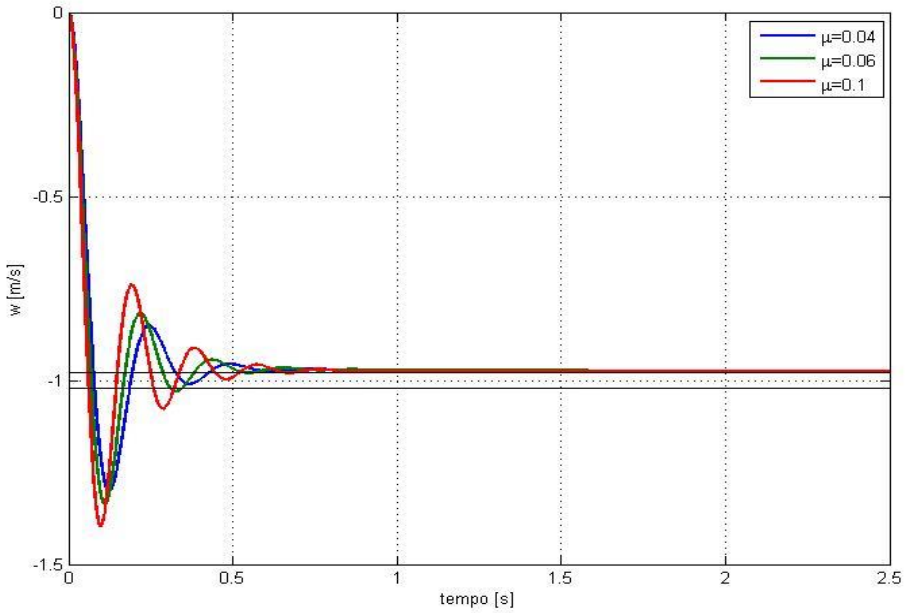

Figure 5.28 Time response of control in w

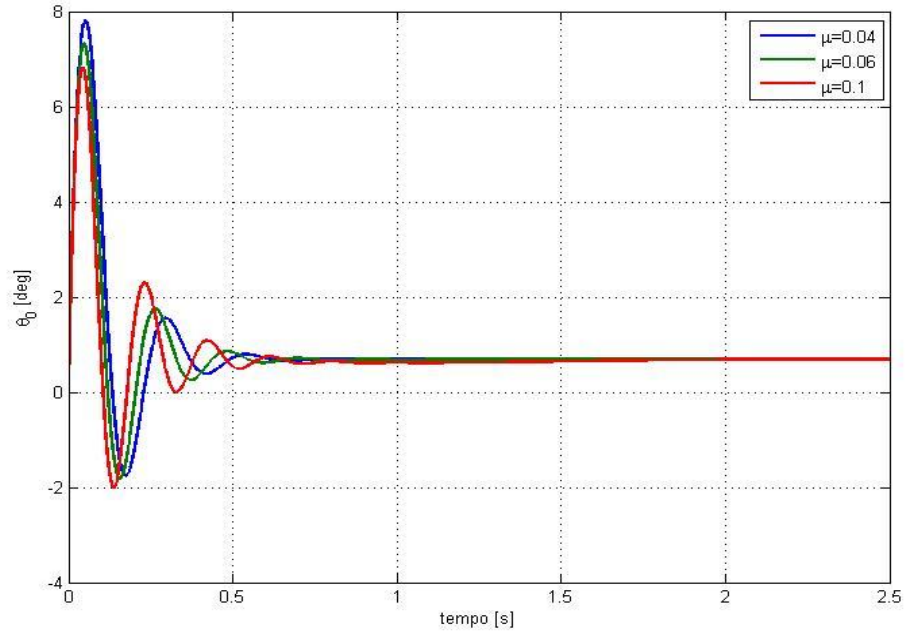

Figure 5.29 Time response of command θ_0

As we can see from the time responses the controllers maintain the specifications in all the flight condition:

- u_control: it is interesting observing the rise of the command with the servo dynamic and the modulation due the fly-bar (SAS in q) and the SAS in θ and finally the integral effect to eliminate the asymptotic error;
- phi_control: we have here the same behavior of the command like in the previously controller on the high frequency, but the presence of the angle $\beta = \frac{v}{V}$ triggers the spiral mode and the control must increase the module of the command till the saturation, like indicated in paragraph 5.2.3; it will be necessary not only deactivate the "heading lock" but also implementing a control to bring the *x* axis of the helicopter tangent to the curve during the turn;
- w_control: we can observe the rapidity of this dynamic, of which we have amply discussed and it does not present particular difficulties, and the integral effect on the command in the low frequencies.

5.5 Controller's architecture

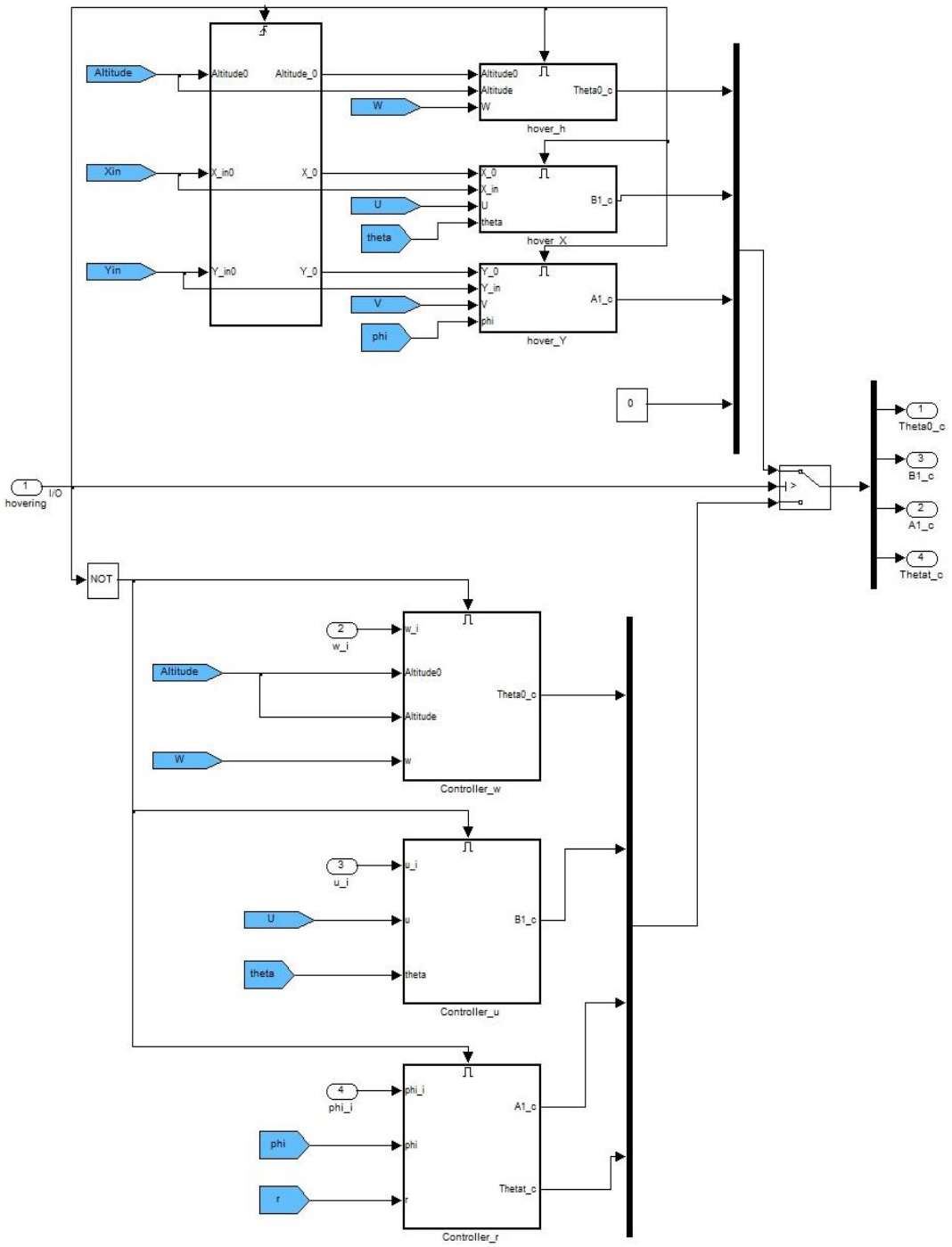

Figure 5.30 Controller's architecture

The complete architecture of the controller that will be implemented in the non-linear system is shown in the figure 5.30.

The inputs are directly from the radio-controller of the pilot, who can choose to maintain the hovering or assign a variation of the velocities.

If the pilot switch on the hovering, the upper blocks are activated; the first block, that is commanded by a trigger, memorize the position of the helicopter at the moment of activation and sets these parameters as references for the controllers in positions and the command to the tail rotor is entrusted to the “heading lock” of the T-REX.

Otherwise is the lower part that is active; in particular the first block maintain the altitude constant as long as the pilot does not request a variation in vertical velocity, only when the input w_i return to zero the block memorize the new altitude as a reference; the second block is the responsible of the longitudinal velocity and the last takes care about the turns.

Unlike the hovering control, the lower provides a command to the tail rotor, if the pilot ask for a turn, to deactivate the “heading lock” by using a simple yaw damper, waiting the identification from the thesis [1], which is adequate for turn of short duration; a better solution will be object of future developments.

6. CONCLUSIONS AND FUTURE DEVELOPMENTS

In conclusion a linear model simulation has been developed with a script that calculate the trim and the aerodynamic derivatives in hovering and in the range of forward speed chosen.

The coincidence for small perturbation of the linear model with the non-linear model has been validate by checking the response to the same commands and by a Simulink tool that calculate the trim.

By the linear model it is possible extrapolate the transfer function to the develop of the control laws that have been validated by the simulation of the model and checking the response to be within the specifications.

The scripts developed to the calculations of the controllers are realized to be useful not only for the T-REX, they will also be useful for future works on different RUAVs or on the same T-REX with an upgrade on its onboard system, like a stereoscopic cams for the “sense and avoid” system, that change the characteristic fended in the identification.

The next step to this work is the substitution of the pilot with a FMS that carries out the mission in autonomous mode and the implementation of a sense and avoid system to the control that is necessary for this kind of flight.

Bibliography

[1] Pietro Rosata “Identification of a small-scale helicopter dynamic model” Master thesis, Univeristà di Pisa, 2015.

[2] A.R.S. Bramwell, George Done, and David Balmford. Bramwell’s Helicopter Dynamics. Butterworth Heinemann, 2001.

[3] Cooke, Fitzpatrick - Helicopter Test and Evaluation

[4] Johnson Wayne. Helicopter theory. Dover Publications, Inc., 1980.

[5] Gareth D. Padfield. Helicopter flight dynamics. Blackwell Publishing, 2007.

[6] Align Corporation, ed. T-REX 500 instruction manual. 2010.

[7] Francesco Schettini and Attilio Salvetti. Dispense di Dinamica del Volo degli Elicotteri. Università di Pisa, 2014.

[8] Eugenio Denti. Dispense di Dinamica del Volo. Università di Pisa, 2014.

[9] Eugenio Denti and Francesco Schettini. Esercitazioni di Dinamica del Volo. Università di Pisa, 2014.

[10] Kane M. Autonomous Systems and Future Capability BAE Systems, Analysts/Fund Managers, 2007.

[11] Manfredi Mazzola. “Modelli di simulazione dinamica, leggi di controllo e strategie di Sense and Avoid per un Remotely Piloted Air System (RPAS)”. Master thesis. Università di Pisa, 2012.

[12] Andrea Zaccaro. “Sviluppo del modello di simulazione dinamica di un elicottero UAV di piccole dimensioni”. Master thesis. Università di Pisa, 2014.

APPENDIX A

In this appendix will be illustrated the script Matlab with the input of the helicopter's characteristics and with the output of the value of the trim and the aerodynamic derivatives at different speed of flight.

Then the possibility of choose a flight speed condition and generate the dimensional aerodynamic derivatives to introduce in the linearized system.

At the end we have the composition of the matrix of the system and the calculation of the fly-bar feedback to obtain the SS system useful to extrapolate the transfer functions.

```
%
=========================================================================
=======

%    TRIM IN HOVERING AND FORWARD FLIGHT AND AERODINAMIC
DERIVATIVES

% Programmed by: Roberto Fiorenzani

%
=========================================================================
=======

%dati di input
m=2.14; %mass
g=9.81;
W=m*g; %weight
s=0.056; %solidity rotor
s_t=0.121; %solidity tail rotor
ro=1.225; %air std
roblade=10; %blade density
R=0.485; %rotor radius
R_fb=0.235;
Mf=0;
Cmf=0; %moment coefficient
tauc=0; %trajectory
A=pi*R^2; %rotor area
xg=0.4*R; %center of mass blade
omega=240.7; %rotor angolar rate
Vtip=omega*R; %tip blade speed
R_t=0.105; %tail rotor radius
A_t=pi*R_t^2; %tail rotor area
Do=0.02; % equivalent drag coeff
do=Do/(s*A); %coefficiente adimensionalyzed
a=4.5; %cl_alfa
```

```
a_t=1.5; %cl_alfa tailrotor
a_fb=1.5; %cl_alfa fly-bar
c=0.0423;%blade chord
c_fb=0.039; % fly-bar chord[m]
B_bl=0.01; % [Kg m^2]inertia blade
delta=0.015; %cd0
gamma=(ro*a*c*R^4)/B_bl;%[ ] %num Lock
B_fb=7.8e-04; % fly-bar inertia[Kg m^2]
gamma_fb=(ro*a_fb*c_fb*R_fb^4)/B_fb;% [ ]
n=2; %Num blade
h=0.289; %center of mass vertical distance
f=-0.025; %center of mass longitudinal distance
l=0; %center of mass lateral distance
ht=-0.012/R; %tail rotor vertical distance
lt=0.575/R; %tail rotor longitudinal distance
e=0; %offset hinge
Sx=0.038;
Sy=0.07;
Sz=0.06;
K_beta=50; % [Nm/rad]
Kbeta_adi=K_beta/(ro*s*A*R^3*omega^2);
% Kbeta_adi=K_beta/(B_bl*omega^2);
epsilon=1.5*e*(1-e);
st_sign=s_t*A_t/s/A;

%data inertia
Ixx=0.02;
Iyy=0.065;
Izz=0.066;
Ixz=-9*10^-4;
Ixy=-7*10^-4;
Iyz=0;
I=[Ixx Ixy Ixz
    Ixy Iyy Iyz
    Ixz Iyz Izz];
j=I/(m*R^2);

Ms=0.5*roblade*R*n*e*xg*omega^2*R^2; %moment due hinge
Cms=Ms/(ro*s*A*R^3*omega^2); %
wc=m*9.81/(ro*s*A*omega^2*R^2); %adim weight
DL=W/A; %disk load
ct=DL/(ro*omega^2*R^2); %coeff thrust
lambdah=sqrt(ct/2); %hovering inflow


% trim per mi=[0,0.18]
mi_look=0:0.1:180;
mi_look=mi_look./1000;
for i=1:length(mi_look);
    %II equation longitudinal trim
    tcd_look(i)=wc-0.5*mi_look(i)^2*do*sin(tauc);
    v0_look=sqrt(W/(2*ro*A));
%%%%
    V_sign_look(i)=mi_look(i)*Vtip/v0_look;
%%%%
    vi0_sign_look(i)=sqrt((-
V_sign_look(i)^2+sqrt(V_sign_look(i)^4+4))/2);                    %%%%
```

```
    vi_0_look(i)=vi0_sign_look(i)*v0_look;
%%%%
    %cicle
    hcd_1_look(i)=0.25*mi_look(i)*delta;
    lambda_i_look(i)=vi_0_look(i)/Vtip;
    alfa_d_1p_look(i)=-
(0.5*(mi_look(i))^2*do*cos(tauc)+hcd_1_look(i))/tcd_look(i)-tauc;
    lambda_d_1_look(i)=mi_look(i)*alfa_d_1p_look(i)-
lambda_i_look(i);
    teta_0_1_look(i)=(4/a*tcd_look(i)-lambda_d_1_look(i)*(1-
0.5*mi_look(i)^2)/(1+1.5*mi_look(i)^2))*1.5*(1+1.5*mi_look(i)^2)/(
1-mi_look(i)^2+2.25*mi_look(i)^4);

hcd_2_look(i)=hcd_1_look(i)+(a*mi_look(i)*lambda_d_1_look(i)/4)*((
teta_0_1_look(i)/3)*(1-
4.5*mi_look(i)^2)/(1+1.5*mi_look(i)^2)+lambda_d_1_look(i)/(1+1.5*m
i_look(i)^2));
    hcd_look(i)=hcd_1_look(i);
    hcditer_look(i)=hcd_2_look(i);
    %contidion to stop iteration hcd
    count(i)=1;
    while abs((-
hcditer_look(i)+hcd_look(i))/hcditer_look(i))>1*10^(-6);
        hcd_look(i)=hcditer_look(i);
        alfa_d_look(i)=-
(hcd_look(i)+0.5*mi_look(i)^2*do*cos(tauc))/tcd_look(i)-tauc;
        lambda_d_look(i)=mi_look(i)*tan(alfa_d_look(i))-
lambda_i_look(i);
        teta_0_look(i)=1.5*(1+1.5*mi_look(i)^2)/(1-
mi_look(i)^2+2.25*mi_look(i)^4).*(4/a*tcd_look(i)-
lambda_d_look(i)*(1-0.5*mi_look(i)^2)/(1+1.5*mi_look(i)^2));

hcditer_look(i)=hcd_1_look(i)+a*mi_look(i)*lambda_d_look(i)/4*((te
ta_0_look(i)/3)*(1-
4.5*mi_look(i)^2)/(1+1.5*mi_look(i)^2)+lambda_d_look(i)/(1+1.5*mi_
look(i)^2));
        count(i)=count(i)+1;
    end
    alfa_d_look(i)=-
(hcd_look(i)+0.5*mi_look(i)^2*do*cos(tauc))/tcd_look(i);
    ni_look(i)=(1-sin(alfa_d_look(i)))/(1+sin(alfa_d_look(i)));
    lambda_d_look(i)=mi_look(i)*tan(alfa_d_look(i))-
lambda_i_look(i);
    teta_0_look(i)=1.5*(1+1.5*mi_look(i)^2)/(1-
mi_look(i)^2+2.25*mi_look(i)^4).*(4/a*tcd_look(i)-
lambda_d_look(i)*(1-0.5*mi_look(i)^2)/(1+1.5*mi_look(i)^2));

a1_look(i)=2*mi_look(i)*(4/3*teta_0_look(i)+lambda_d_look(i))/(1+1
.5*mi_look(i)^2);
    lambda_look(i)=-lambda_d_look(i)+mi_look(i)*a1_look(i);

K_look(i)=(4/3*mi_look(i)/lambda_look(i))/(1.2+mi_look(i)/lambda_l
ook(i));
    %coefficient of flapping

a0_look(i)=gamma/(8*(1+epsilon+K_beta/(omega^2*B_bl)))*(teta_0_loo
k(i)*(1-
19/18*mi_look(i)^2+3/4*mi_look(i)^4)/(1+1.5*mi_look(i)^2)+4/3*lamb
da_d_look(i)*(1-0.5*mi_look(i)^2)./(1+1.5*mi_look(i)^2));
```

```
b1_look(i)=4*(mi_look(i)*a0_look(i)+0.75*K_look(i)*lambda_i_look(i
))/3/(1+0.5*mi_look(i)^2);

a1_look_iter(i)=2*mi_look(i)*(4/3*teta_0_look(i)+lambda_d_look(i))
/(1+1.5*mi_look(i)^2)+((8/gamma)*(epsilon+K_beta/(omega^2*B_bl))*b
1_look(i))/(1-0.5*mi_look(i)^2);

b1_look_iter(i)=4*(mi_look(i)*a0_look(i)+0.75*K_look(i)*lambda_i_l
ook(i))/3/(1+0.5*mi_look(i)^2)-
((8*(epsilon+K_beta/(omega^2*B_bl))*a1_look_iter(i))/(gamma*(1+0.5
*mi_look(i)^2)));
    count_falp(i)=1;
    while abs((-
a1_look_iter(i)+a1_look(i))/a1_look_iter(i))>1*10^(-9) && abs((-
b1_look_iter(i)+b1_look(i))/b1_look_iter(i))>1*10^(-9) ;
        a1_look(i)=a1_look_iter(i);
        b1_look(i)= b1_look_iter(i);
        lambda_look(i)=-lambda_d_look(i)+mi_look(i)*a1_look(i);

K_look(i)=(4/3*mi_look(i)/lambda_look(i))/(1.2+mi_look(i)/lambda_l
ook(i));


a1_look_iter(i)=2*mi_look(i)*(4/3*teta_0_look(i)+lambda_d_look(i))
/(1+1.5*mi_look(i)^2)+((8/gamma)*(epsilon+K_beta/(omega^2*B_bl))*b
1_look(i))/(1-0.5*mi_look(i)^2);

b1_look_iter(i)=4*(mi_look(i)*a0_look(i)+0.75*K_look(i)*lambda_i_l
ook(i))/3/(1+0.5*mi_look(i)^2)-
((8*(epsilon+K_beta/(omega^2*B_bl))*a1_look_iter(i))/(gamma*(1+0.5
*mi_look(i)^2)));
    end
    alfa_nf_look(i)=alfa_d_look(i)-a1_look(i);
    qcshaft_look(i)=(delta/8*(1+4.7*mi_look(i)^2)-
lambda_d_look(i)*tcd_look(i)-mi_look(i)*hcd_look(i));
    Qcshaft_look(i)=qcshaft_look(i)*ro*s*A*omega^2*R^3;
    Tt_look(i)=Qcshaft_look(i)/(lt*R);
    %command longitudinal,coefficient a1s and pitch angle
    B1_look(i)=(a1_look(i)+((hcd_look(i)*h-
f*wc))/(Cms+wc*h+Kbeta_adi));
    a1s_look(i)=a1_look(i)-B1_look(i);
    teta_look(i)=B1_look(i)-a1_look(i)-hcd_look(i)/wc-
0.5*do*mi_look(i)^2/wc;
    %lateral trim
    A1_look(i)=-b1_look(i)+(wc*l-
ht*Tt_look(i)/(W)*tcd_look(i))/(h*tcd_look(i)+Cms+Kbeta_adi);
    fi_look(i)=+b1_look(i)+A1_look(i)+Tt_look(i)/(W);
    Vcap_look(i)=mi_look(i)./cos(alfa_d_look(i));
%
    %aerodinamic derivatives
%
h1(i)=h-f*(alfa_d_look(i)-a1s_look(i));
f1(i)=f+h*(alfa_d_look(i)-a1s_look(i));
ht_p(i)=ht-lt*(alfa_d_look(i)-a1s_look(i));
lt_p(i)=lt;

%
```

```
dlamdai_dmi_look(i)=(2*mi_look(i)*teta_0_look(i)+alfa_nf_look(i)-
(4*tcd_look(i)/(a*lambda_i_look(i)))*V_sign_look(i)*vi0_sign_look(
i)^3)/(1+4/a*tcd_look(i)/lambda_i_look(i)*(1+vi0_sign_look(i)^4));
dlamda_dmi_look(i)=alfa_nf_look(i)-dlamdai_dmi_look(i);
dtc_dmi_look(i)=(2*mi_look(i)*teta_0_look(i)+alfa_nf_look(i)+V_sig
n_look(i)*vi0_sign_look(i)^3/(1+vi0_sign_look(i)^4))/(4/a+lambda_i
_look(i)/tcd_look(i)/(1+vi0_sign_look(i)^4));
if mi_look(i)==0;
    da1_dmi_look(i)=8/3*teta_0_look(i)+2*lambda_look(i)+0.3737;
else
    da1_dmi_look(i)=a1_look(i)/mi_look(i)-
2*mi_look(i)*dlamda_dmi_look(i)/(1-0.5*mi_look(i)^2);
end
dhcd_dmi_look(i)=delta/4;
dlambdai_dw_look(i)=(a/4*lambda_i_look(i)/tcd_look(i)+vi0_sign_loo
k(i)^4)/(1+a/4*lambda_i_look(i)/tcd_look(i)+vi0_sign_look(i)^4);
dlambda_dw_look(i)=1/(1+a/4*lambda_i_look(i)/tcd_look(i)+vi0_sign_
look(i)^4);
dtc_dw_look(i)=a/4/(1+a/4*lambda_i_look(i)/tcd_look(i)+vi0_sign_lo
ok(i)^4);
da1_dw_look(i)=2*mi_look(i)/((1-
0.5*mi_look(i)^2)*(1+a/4*lambda_i_look(i)/tcd_look(i)+vi0_sign_loo
k(i)^4));
dlambdad_dw_look(i)=dlambda_dw_look(i)+mi_look(i)*da1_dw_look(i);
dhcd_dw_look(i)=a/4/(1+a/4*lambda_i_look(i)/tcd_look(i)+vi0_sign_l
ook(i)^4)*(a1_look(i)/2-
mi_look(i)*teta_0_look(i)+mi_look(i)*lambda_look(i)/(1-
0.5*mi_look(i)^2));
db1_dw_look(i)=(16/9*mi_look(i)*dlambda_dw_look(i)+4/3*0.75*K_look
(i)*dlambdai_dw_look(i))/(1+0.5*mi_look(i)^2);
dtc_dq_look(i)=0;
da1_dq_look(i)=-16/gamma/(1-0.5*mi_look(i)^2);
db1_dq_look(i)=-1/(1+0.5*mi_look(i)^2);
dhcd_dq_look(i)=a/4*(lambda_look(i)/2+mi_look(i)*a1_look(i)-
mi_look(i)^2*teta_0_look(i))*da1_dq_look(i);
dtc_dteta0_look(i)=a/6*(1+3/2*mi_look(i)^2)/(1+a*lambda_i_look(i)/
4/tcd_look(i)*(1+vi0_sign_look(i)^4));
da1_dteta0_look(i)=8/3*mi_look(i)/(1-0.5*mi_look(i)^2)*(1-
a*s/2*(1+3/2*mi_look(i)^2)/(8*mi_look(i)+a*s));
dlambdai_dteta0_look(i)=2/3*a*s*(1+3/2*mi_look(i)^2)/(8*mi_look(i)
+a*s);
%
dlambdai_dteta0_look(i)=(lambda_i_look(i)/tcd_look(i)*dtc_dteta0_l
ook(i))/(1+vi0_sign_look(i)^4);
dlambdad_dteta0_look(i)=mi_look(i)*da1_dteta0_look(i)-
dlambdai_dteta0_look(i);
dhcd_dteta0_look(i)=a/8*(a1_look(i)*dlambdad_dteta0_look(i)+lambda
_d_look(i)*da1_dteta0_look(i)-
2*mi_look(i)*(lambda_d_look(i)+teta_0_look(i)*dlambdad_dteta0_look
(i)));
%tail rotor
dtct_dtetat_look(i)=a_t/6*(1+3/2*mi_look(i)^2)/(1+a*lambda_i_look(
i)/4/tcd_look(i)*(1+vi0_sign_look(i)^4));

%longitudinal
xu_look(i)=-tcd_look(i)*da1_dmi_look(i)-
alfa_d_look(i)*dtc_dmi_look(i)-dhcd_dmi_look(i);
```

```
zu_look(i)=-dtc_dmi_look(i);
xw_look(i)=-tcd_look(i)*da1_dw_look(i)-
alfa_d_look(i)*dtc_dw_look(i)-dhcd_dw_look(i);
zw_look(i)=-dtc_dw_look(i);
xq_look(i)=(-tcd_look(i)*da1_dq_look(i)-
alfa_d_look(i)*dtc_dq_look(i)-dhcd_dq_look(i));
xp_look(i)=(-tcd_look(i)*db1_dq_look(i));
zq_look(i)=(-dtc_dq_look(i));
mu_look(i)=(-
h1(i)*xu_look(i)+f1(i)*zu_look(i)+(Cms+Kbeta_adi)*da1_dmi_look(i))
;
mw_look(i)=(-
h1(i)*xw_look(i)+f1(i)*zw_look(i)+(Cms+Kbeta_adi)*da1_dw_look(i));
mq_look(i)=(-
h1(i)*xq_look(i)+f1(i)*zq_look(i)+(Cms+Kbeta_adi)*da1_dq_look(i));
mp_look(i)=(Cms+Kbeta_adi)*db1_dq_look(i);
%lateral
yv_f_look(i)=-0.3*mi_look(i)*Sy/(s*A); %Sy  equivalent lateral
surface
if mi_look(i)==0
    yv_look(i)=-delta/4-st_sign*dtc_dw_look(i)+yv_f_look(i);
    lv_look(i)=(-ht_p(i)*st_sign*dtc_dw_look(i));
else
    yv_look(i)=-tcd_look(i)*a1_look(i)/mi_look(i)-delta/4-
st_sign*dtc_dw_look(i)+yv_f_look(i);
    lv_look(i)=(-
(h1(i)*tcd_look(i)+(Cms+Kbeta_adi))*a1_look(i)/mi_look(i)-
ht_p(i)*st_sign*dtc_dw_look(i));
end
yp_look(i)=(tcd_look(i)*db1_dq_look(i));
yq_look(i)=(-tcd_look(i)*da1_dq_look(i));
lp_look(i)=(-
16/gamma*(h1(i)*(tcd_look(i)+a*lambda_d_look(i)/8)+(Cms+Kbeta_adi)
)/(1+0.5*mi_look(i)^2)-ht_p(i)^2*st_sign*dtc_dw_look(i));
lq_look(i)=-(Cms+Kbeta_adi)*db1_dq_look(i);
lr_look(i)=(ht_p(i)*lt_p(i)*st_sign*dtc_dw_look(i));
nv_look(i)=(lt_p(i)*st_sign*dtc_dw_look(i));
np_look(i)=(ht_p(i)*lt_p(i)*st_sign*dtc_dw_look(i));
nr_look(i)=(-lt_p(i)^2*st_sign*dtc_dw_look(i));
%commands
xB1_look(i)=mi_look(i)*dtc_dw_look(i)*alfa_d_look(i)+tcd_look(i)*(
1+mi_look(i)*da1_dw_look(i))+mi_look(i)*dhcd_dw_look(i);
zB1_look(i)=-mi_look(i)*zw_look(i);
mB1_look(i)=(-h1(i)*xB1_look(i)+f1(i)*zB1_look(i)-
(Cms+Kbeta_adi)*(1+mi_look(i)*da1_dw_look(i)));
xteta_0_look(i)=-tcd_look(i)*da1_dteta0_look(i)-
alfa_d_look(i)*dtc_dteta0_look(i)-dhcd_dteta0_look(i);
zteta_0_look(i)=-dtc_dteta0_look(i);
mteta_0_look(i)=(-h1(i)*xteta_0_look(i)+f1(i)*zteta_0_look(i)-
(Cms+Kbeta_adi)*da1_dteta0_look(i));
yA1_look(i)=-(tcd_look(i)*(1+mi_look(i)*db1_dw_look(i)));
zA1_look(i)=zB1_look(i);
lA1_look(i)=-
(h1(i)*yA1_look(i)+(Cms+Kbeta_adi)*(1+mi_look(i)*db1_dw_look(i)));
nA1_look(i)=0;
yteta_t_look(i)=-st_sign*dtct_dtetat_look(i);
lteta_t_look(i)=-(ht_p(i)*st_sign*dtct_dtetat_look(i));
nteta_t_look(i)=-(-lt_p(i)*st_sign*dtct_dtetat_look(i));
```

```
end

% % grafici
% figure(1)
% plot(mi_look,lambda_i_look,mi_look,-lambda_d_look)
% grid;
% xlabel('\mu');
% ylabel('\lambda_d & \lambda_i');
% legend('\lambda_i','-\lambda_d')
% figure(2);
% plot(mi_look,alfa_d_look*180/pi)
% grid
% xlabel('\mu')
% ylabel('\alpha_d [deg]')
% figure(3)
% plot(mi_look,B1_look*180/pi)
% grid
% xlabel('\mu')
% ylabel('B_1 [deg]')
% legend('f=-0.025')
% figure(4)
% plot(mi_look,a1s_look*180/pi)
% grid
% xlabel('\mu')
% ylabel('a_1s [deg]')
% legend('f=-0.025')
% figure(5)
% plot(mi_look,teta_0_look*180/pi)
% grid
% xlabel('\mu')
% ylabel('\Theta_0 [deg]')
% figure(6)
% plot(mi_look,teta_look*180/pi)
% grid
% xlabel('\mu')
% ylabel('\Theta [deg]')
% legend('f=-0.025')
% figure(7)
%
plot(mi_look,a0_look*180/pi,mi_look,a1_look*180/pi,mi_look,b1_look
*180/pi)
% grid
% xlabel('\mu')
% ylabel('a_0 & a_1 & b_1 [deg]')
% legend('a_0','a_1','b_1')
% figure(8)
%
plot(mi_look,A1_look*180/pi,mi_look,fi_look*180/pi,mi_look,b1_look
*180/pi)
% grid
% xlabel('\mu')
% ylabel('A_1 & \Phi & b_1 [deg]')
% legend('A_1','\Phi','b_1')
% figure(12)
%
plot(mi_look,xu_look,mi_look,xw_look,mi_look,zu_look,mi_look,zw_lo
ok)
% grid
% xlabel('\mu')
```

```
% ylabel('longitud')
% legend('xu','xw','zu','zw')
% figure(13)
% plot(mi_look,mu_look,mi_look,mw_look,mi_look,mq_look./10)
% grid
% xlabel('\mu')
% ylabel('longitud')
% legend('mu','mw','mq/10')
% figure(14)
%
plot(mi_look,yv_look,mi_look,lv_look,mi_look,nv_look,mi_look,lp_lo
ok./10,mi_look,nr_look,mi_look,np_look)
% grid
% xlabel('\mu')
% ylabel('latero')
% legend('yv','lv','nv','lp/10','nr','np & lr')
% figure(15)
% plot(mi_look,xB1_look,mi_look,zB1_look,mi_look,mB1_look)
% grid
% xlabel('\mu')
% ylabel('comand lon')
% legend('xB1','zB1','mB1')
% figure(16)
%
plot(mi_look,xteta_0_look,mi_look,zteta_0_look,mi_look,mteta_0_loo
k)
% grid
% xlabel('\mu')
% ylabel('comand lon')
% legend('xteta_0','zteta_0','mteta_0')
% figure(17)
%
plot(mi_look,yA1_look,mi_look,lA1_look,mi_look,yteta_t_look,mi_loo
k,lteta_t_look,mi_look,nteta_t_look)
% grid
% xlabel('\mu')
% ylabel('comand later')
% legend('yA1','lA1','yteta_t','lteta_t','nteta_t')


% Dimentional aerodinamic derivatives
%choose the value of forward speed
mu=0.01;
%
i=find(mi_look==mu);
V=Vcap_look(i)*Vtip;
teta=teta_look(i);
fi=fi_look(i);
wc=wc*(ro*s*A*omega^2*R^2)/m;
%longitudinal
xu=xu_look(i)*(ro*s*A*omega*R)/m;
zu=zu_look(i)*(ro*s*A*omega*R)/m;
xw=xw_look(i)*(ro*s*A*omega*R)/m;
zw=zw_look(i)*(ro*s*A*omega*R)/m;
xq=xq_look(i)*(ro*s*A*omega*R^2)/m;
xp=xp_look(i)*(ro*s*A*omega*R^2)/m;
zq=zq_look(i)*(ro*s*A*omega*R^2)/m;
mu=mu_look(i)*(ro*s*A*omega*R^2)/Iyy;
mw=mw_look(i)*(ro*s*A*omega*R^2)/Iyy;
```

```
mq=mq_look(i)*(ro*s*A*omega*R^3)/Iyy;
mp=mp_look(i)*(ro*s*A*omega*R^3)/Iyy;

%lateral
yv=yv_look(i)*(ro*s*A*omega*R)/m;
yp=yp_look(i)*(ro*s*A*omega*R^2)/m;
yq=yq_look(i)*(ro*s*A*omega*R^2)/m;
lv=lv_look(i)*(ro*s*A*omega*R^2)/Ixx;
lp=lp_look(i)*(ro*s*A*omega*R^3)/Ixx;
lq=lq_look(i)*(ro*s*A*omega*R^3)/Ixx;
lr=lr_look(i)*(ro*s*A*omega*R^3)/Ixx;
nv=nv_look(i)*(ro*s*A*omega*R^2)/Izz;
np=np_look(i)*(ro*s*A*omega*R^3)/Izz;
nr=nr_look(i)*(ro*s*A*omega*R^3)/Izz;
%commands
xB1=xB1_look(i)*(ro*s*A*omega^2*R^2)/m;
zB1=zB1_look(i)*(ro*s*A*omega^2*R^2)/m;
mB1=mB1_look(i)*(ro*s*A*omega^2*R^3)/Iyy;
xteta_0=xteta_0_look(i)*(ro*s*A*omega^2*R^2)/m;
zteta_0=zteta_0_look(i)*(ro*s*A*omega^2*R^2)/m;
mteta_0=mteta_0_look(i)*(ro*s*A*omega^2*R^3)/Iyy;
yA1=yA1_look(i)*(ro*s*A*omega^2*R^2)/m;
zA1=zA1_look(i)*(ro*s*A*omega^2*R^2)/m;
lA1=lA1_look(i)*(ro*s*A*omega^2*R^3)/Ixx;
nA1=nA1_look(i)*(ro*s*A*omega^2*R^3)/Izz;
yteta_t=yteta_t_look(i)*(ro*s*A*omega^2*R^2)/m;
lteta_t=lteta_t_look(i)*(ro*s*A*omega^2*R^3)/Ixx;
nteta_t=nteta_t_look(i)*(ro*s*A*omega^2*R^3)/Izz;


lu=0; lw=0; lteta_0=0; lB1=0; mv=0; mr=0; mA1=0; mteta_t=0; nu=0;
nw=0;...
    nq=0; nteta_0=0; nB1=0;
I=[1 Ixy/Ixx Ixz/Ixx
    Ixy/Iyy 1 Iyz/Iyy
    Ixz/Izz Iyz/Izz 1];
j_acc=inv(I);
k=[lu lw lq lteta_0 lB1 lv lp lr lA1 lteta_t
    mu mw mq mteta_0 mB1 mv mp mr mA1 mteta_t
    nu nw nq nteta_0 nB1 nv np nr nA1 nteta_t];
%inertial convertion

accop=j_acc*k;
lu=accop(1,1); lw=accop(1,2); lq=accop(1,3); lteta_0=accop(1,4);
lB1=accop(1,5); lv=accop(1,6); lp=accop(1,7);...
    lr=accop(1,8); lA1=accop(1,9); lteta_t=accop(1,10);
mu=accop(2,1); mw=accop(2,2); mq=accop(2,3);
mteta_0=accop(2,4);...
    mB1=accop(2,5); mv=accop(2,6); mp=accop(2,7); mr=accop(2,8);
mA1=accop(2,9); mteta_t=accop(2,10); nu=accop(3,1);
nw=accop(3,2);...
    nq=accop(3,3); nteta_0=accop(1,4); nB1=accop(3,5);
nv=accop(3,6); np=accop(3,7); nr=accop(3,8); nA1=accop(3,9);
nteta_t=accop(3,10);
```

```
% linear system
% open loop
% ==================================
%
%     th0   |--------------------------|
% --------->|                          |-------> u
%     B1    |         Aereo            |-------> w
% --------->|   .                      |-------> q
%     A1    |   x = ALON x + BLON u    |-------> theta
% --------->|   .                      |-------> v
%     tht   |   x = ALAT x + BLAT u    |-------> p
% --------->|   x = [ u w q theta      |-------> r
%           |         v p r fi         |-------> fi
%           |           psi  h  ]'     |-------> psi
%           |                          |-------> h
%           |                          |
%           |                          |
%           |    y = C x + D u         |-------> tau
%           |                          |-------> du
%           |                          |-------> dv
%           |                          |-------> eta
%           |--------------------------|
A=[xu xw xq -wc*cos(tauc) 0 xp 0 0 0 0
    zu zw zq+V -wc*sin(tauc) 0 0 0 0 0 0
    mu mw mq 0 mv mp mr 0 0 0
    0 0 1 0 0 0 0 0 0 0
    0 0 yq 0 yv yp -V +wc*cos(tauc) +wc*sin(tauc) 0
    lu lw lq 0 lv lp lr 0 0 0
    nu nw nq 0 nv np nr 0 0 0
    0 0 0 0 0 1 0 0 0 0
    0 0 0 0 0 0 1 0 0 0
    0 -1 0 V 0 0 0 0 0 0];
B=[xteta_0 xB1 0 0
    zteta_0 zB1 zA1 0
    mteta_0 mB1 mA1 mteta_t
    0 0 0 0
    0 0 yA1 yteta_t
    lteta_0 lB1 lA1 lteta_t
    nteta_0 nB1 nA1 nteta_t
    0 0 0 0
    0 0 0 0
    0 0 0 0];
C=[1 0 0 0 0 0 0 0 0 0
    0 1 0 0 0 0 0 0 0 0
    0 0 1 0 0 0 0 0 0 0
    0 0 0 1 0 0 0 0 0 0
    0 0 0 0 1 0 0 0 0 0
    0 0 0 0 0 1 0 0 0 0
    0 0 0 0 0 0 1 0 0 0
    0 0 0 0 0 0 0 1 0 0
    0 0 0 0 0 0 0 0 1 0
    0 0 0 0 0 0 0 0 0 1
    0 -1/V 0 1 0 0 0 0 0 0
    xu xw xq -wc*cos(tauc) 0 xp 0 0 0 0
    0 0 yq 0 yv yp -V +wc*cos(tauc) +wc*sin(tauc) 0
    0 0 0 0 1/V 0 0 0 1 0];
D=[0 0 0 0
    0 0 0 0
```

```
    0 0 0 0
    0 0 0 0
    0 0 0 0
    0 0 0 0
    0 0 0 0
    0 0 0 0
    0 0 0 0
    0 0 0 0
    0 0 0 0
    xteta_0 xB1 0 0
    0 0 yA1 yteta_t
    0 0 0 0];

sistema_nofb=ss(A,B,C,D,...
                  'inputname',{'Theta0','B1','A1','Theta_t'},...

'outputname',{'u','w','q','theta','v','p','r',...
                  'phi','psi','h','tau','du','dv','eta'});
              zpk(sistema_nofb);

%  % Verifing T.F. in open loop
%   disp(' ')
%   disp(' Verifing T.F. in open loop)
%   for i=1:4
%     [ZERI, POLI, GAINS]= ss2zp(A,B,C,D,i);
%     GAINS
%     ZERI
%   end
%   POLI
% %   damp('POLI')

% flybar (first order)
Tfb=16/gamma_fb/omega; k_fb=-0.5;
  Gain = [k_fb];  Zeri = [ ];  Poli = [-1/Tfb];
  [A_TMP,B_TMP,C_TMP,D_TMP] = zp2ss(Zeri,Poli,Gain);
  fly_bar = ss(A_TMP,B_TMP,C_TMP,D_TMP,...
                'inputname',{'fb_in'},'outputname',{'fb_out'});
% Verifying T.F. fly bar
%   disp(' '),disp('Verifying T.F. fly bar')
%   zpk(fly_bar)

flybar=append(fly_bar,fly_bar);
%   zpk(flybar)
in=[ 2 3 ]; out=[ 3 6 ];
sistema=feedback(sistema_nofb,flybar,in,out);

[Atot,Btot,Ctot,Dtot]=ssdata(sistema);
[Zeri_Theta0,Poli,K_Theta0]  = ss2zp(Atot,Btot,Ctot,Dtot,1);
  [Zeri_B1,Poli,K_B1]  = ss2zp(Atot,Btot,Ctot,Dtot,2);
  [Zeri_A1,Poli,K_A1]  = ss2zp(Atot,Btot,Ctot,Dtot,3);
  [Zeri_Thetat,Poli,K_Thetat]  = ss2zp(Atot,Btot,Ctot,Dtot,4);
  % pulsation and damping of poles
%   disp(' '),disp('System poles with fly_bar:'),damp(Poli)
```

APPENDIX B

Following the transfer function, generated by a Matlab script for the different speed of flight, are illustrated.

The considered flight speed are reported by means of the coefficient of forward speed μ; the transfer function of the hovering case have been shown already in the chapter 5.

$$\boldsymbol{\mu = 0.04}$$

$$\frac{\theta}{B_1} = \frac{-819.14(s+4.2)(s+0.008)}{(s^2+0.03s+0.2)(s^2+47.58s+576.2)}$$

$$\frac{u}{B_1} = \frac{9.7(s+4.2)(s^2-16.31s+816.5)}{(s^2+0.03s+0.2)(s^2+47.58s+576.2)}$$

$$\frac{w}{B_1} = \frac{-3502.8(s+4.2)(s^2-0.03s+1.31)}{(s+1.57)(s^2+0.03s+0.2)(s^2+47.58s+576.2)}$$

$$\frac{w}{\theta_0} = \frac{-131.7}{(s+1.57)}$$

$$\frac{p}{A_1} = \frac{-2395.8\, s\,(s+4.2)(s+0.75)(s+0.45)}{(s+122.8)(s+19.11)(s+0.03)(s^2+2s+15.1)}$$

$$\frac{r}{\theta_t} = \frac{82.97(s^2+0.067s+0.31)}{(s+0.03)(s^2+2s+15.1)}$$

$$\boldsymbol{\mu = 0.06}$$

$$\frac{\theta}{B_1} = \frac{-823.9(s+4.2)(s+0.009)}{(s^2+0.03s+0.09)(s^2+47.58s+576.2)}$$

$$\frac{u}{B_1} = \frac{9.6(s+4.2)(s^2-16.15s+821.1)}{(s^2+0.03s+0.09)(s^2+47.58s+576.2)}$$

$$\frac{w}{B_1} = \frac{-5175.45(s+4.2)(s^2-0.011s+0.5)}{(s+1.92)(s^2+0.03s+0.09)(s^2+47.58s+576.2)}$$

$$\frac{w}{\theta_0} = \frac{-158.34}{(s+1.92)}$$

$$\frac{p}{A_1} = \frac{-2415.9\, s\,(s+4.2)(s^2+2.46s+29.99)}{(s+123.5)(s+14.59)(s+0.009)(s^2+2.47s+27.15)}$$

$$\frac{r}{\theta_t} = \frac{99.67(s^2+0.12s+0.11)}{(s+0.009)(s^2+2.47s+27.15)}$$

$$\boldsymbol{\mu = 0.1}$$

$$\frac{\theta}{B_1} = \frac{-837.59(s+4.2)(s+0.0098)}{(s^2+1.14)(s^2+47.58s+576.2)}$$

$$\frac{u}{B_1} = \frac{7.52(s+4.2)\left(s^2-35.33+867.2\right)}{(s^2+1.14)(s^2+47.58s+576.2)}$$

$$\frac{w}{B_1} = \frac{-8635.2(s+4.2)(s+0.25)(s-0.23)}{(s+2.12)(s^2+0.48s+0.29)(s^2+47.58s+576.2)}$$

$$\frac{w}{\theta_0} = \frac{-186.73}{(s+2.12)}$$

$$\frac{p}{A_1} = \frac{-2499.6\ s\ (s+4.2)}{(s+122.2)(s+19.41)(s+0.0059)}$$

$$\frac{r}{\theta_t} = \frac{117.25(s^2+0.16s+0.12)}{(s+0.89)(s^2+2.95s+53.34)}$$

APPENDIX C

The following scrips are an example of the develop of the MIMO system in hovering to check the effects of the controllers and evaluate the change of the transfer functions with the change of the controller's gains.

```
% Attuatore servo
Ts=1/16;
  Gain = [1/Ts];  Zeri = [ ];  Poli = [-1/Ts];
  [A_TMP,B_TMP,C_TMP,D_TMP] = zp2ss(Zeri,Poli,Gain);
  servo = ss(A_TMP,B_TMP,C_TMP,D_TMP);
% Verifica funzione di trasferimento
%   disp(' '),disp('Funzione di trasferimento dell''attuatore:')
%   zpk(servo)

% Parallelo tra i 4 attuatori
  attuatori = append(servo,servo,servo,servo);
% Verifica funzioni di trasferimento
%   disp(' '),disp('Funzioni di trasferimento del blocco di
attuazione')
%   zpk(attuatori)

% catena loop unitario
  Gain = [1];  Zeri = [ ];  Poli = [ ];
  [A_TMP,B_TMP,C_TMP,D_TMP] = zp2ss(Zeri,Poli,Gain);
  back1 = ss(A_TMP,B_TMP,C_TMP,D_TMP,...
              'inputname',{'anyin'},'outputname',{'anyout'});
% Verifica funzione di trasferimento
%   disp(' '),disp('Funzione di trasferimento unitaria')
%   zpk(back1)

%controllo in theta
Gain = [k_theta];  Zeri = [ ];  Poli = [ ];
  [A_TMP,B_TMP,C_TMP,D_TMP] = zp2ss(Zeri,Poli,Gain);
  theta_damper = ss(A_TMP,B_TMP,C_TMP,D_TMP,...
              'inputname',{'\theta'},'outputname',{'B1'});
% Verifica funzione di trasferimento
%   disp(' '),disp('Funzione di trasferimento dello theta_damper')
%   zpk(theta_damper)

%controllo in phi
Gain = [k_phi];  Zeri = [ ];  Poli = [ ];
  [A_TMP,B_TMP,C_TMP,D_TMP] = zp2ss(Zeri,Poli,Gain);
  phi_damper = ss(A_TMP,B_TMP,C_TMP,D_TMP,...
              'inputname',{'\phi'},'outputname',{'A1'});
% Verifica funzione di trasferimento
%   disp(' '),disp('Funzione di trasferimento dello phi_damper')
%   zpk(phi_damper)

% YAW DAMPER (guadagno)
```

```
  Gain = [k_r];  Zeri = [ ];  Poli = [ ];
  [A_TMP,B_TMP,C_TMP,D_TMP] = zp2ss(Zeri,Poli,Gain);
  yaw_damper = ss(A_TMP,B_TMP,C_TMP,D_TMP,...
               'inputname',{'r'},'outputname',{'Thetat_c'});
% Verifica funzione di trasferimento
%   disp(' '),disp('Funzione di trasferimento dello yaw_damper')
%   zpk(yaw_damper)

% controllo in v (guadagno)
  Gain = [k_v];  Zeri = [ ];  Poli = [  ];
  [A_TMP,B_TMP,C_TMP,D_TMP] = zp2ss(Zeri,Poli,Gain);
  v_damper = ss(A_TMP,B_TMP,C_TMP,D_TMP,...
               'inputname',{'v'},'outputname',{'A1_c'});
% Verifica funzione di trasferimento
%   disp(' '),disp('Funzione di trasferimento del p_damper')
%   zpk(p_damper)

 % controllo in u (solo guadagno)
  Gain = [k_u];  Zeri = [ ];  Poli = [ ];
  [A_TMP,B_TMP,C_TMP,D_TMP] = zp2ss(Zeri,Poli,Gain);
  u_damper = ss(A_TMP,B_TMP,C_TMP,D_TMP,...
               'inputname',{'u'},'outputname',{'B1_c'});
% Verifica funzione di trasferimento
%   disp(' '),disp('Funzione di trasferimento del theta_damper')
%   zpk(theta_damper)

% controllo in w (solo guadagno)
  Gain = [k_w];  Zeri = [ ];  Poli = [ ];
  [A_TMP,B_TMP,C_TMP,D_TMP] = zp2ss(Zeri,Poli,Gain);
  w_damper = ss(A_TMP,B_TMP,C_TMP,D_TMP,...
               'inputname',{'w'},'outputname',{'Theta0_c'});
% Verifica funzione di trasferimento
%   disp(' '),disp('Funzione di trasferimento del w_damper')
%   zpk(w_damper)

% controllo in h (solo guadagno)
  Gain = [k_h];  Zeri = [ ];  Poli = [ ];
  [A_TMP,B_TMP,C_TMP,D_TMP] = zp2ss(Zeri,Poli,Gain);
  auto_h = ss(A_TMP,B_TMP,C_TMP,D_TMP,...
               'inputname',{'h'},'outputname',{'Theta0_c'});
% Verifica funzione di trasferimento
%   disp(' '),disp('Funzione di trasferimento del auto_h')
%   zpk(auto_h)

% controllo in X (solo guadagno)
  Gain = [k_X];  Zeri = [ ];  Poli = [ ];
  [A_TMP,B_TMP,C_TMP,D_TMP] = zp2ss(Zeri,Poli,Gain);
  auto_X = ss(A_TMP,B_TMP,C_TMP,D_TMP,...
               'inputname',{'X'},'outputname',{'B1_c'});
% Verifica funzione di trasferimento
%   disp(' '),disp('Funzione di trasferimento del auto_X')
%   zpk(auto_X)

% controllo in Y (solo guadagno)
  Gain = [k_Y];  Zeri = [ ];  Poli = [ ];
  [A_TMP,B_TMP,C_TMP,D_TMP] = zp2ss(Zeri,Poli,Gain);
  auto_Y = ss(A_TMP,B_TMP,C_TMP,D_TMP,...
               'inputname',{'Y'},'outputname',{'A1_c'});
```

```
% Verifica funzione di trasferimento
%   disp(' '),disp('Funzione di trasferimento del auto_Y')
%   zpk(auto_Y)

% controllo in psi (guadagno)
  Gain = [k_psi];  Zeri = [ ];  Poli = [ ];
  [A_TMP,B_TMP,C_TMP,D_TMP] = zp2ss(Zeri,Poli,Gain);
  auto_psi = ss(A_TMP,B_TMP,C_TMP,D_TMP,...
               'inputname',{'psi'},'outputname',{'Thetat_c'});
% Verifica funzione di trasferimento
%   disp(' '),disp('Funzione di trasferimento del auto_psi')
%   zpk(auto_psi)

% Serie tra il blocco "attuatori" e il blocco "sistema"
% ----------------------------------------------------
  sistema_con_attuatori = series(attuatori,sistema);

% Verifica funzioni di trasferimento dell'aereo in ciclo aperto,
con gli attuatori
%   disp(' '),disp('Funzioni di trasferimento del sistema
attuatori+sistema in ciclo aperto:')
%   zpk(sistema_con_attuatori)

% Schema del blocco theta_damper
%    theta  |         |-------|           |  B1_c
% --------->|-------->|k_theta|---------->|-------->
%           |         |-------|           |
%     phi   |         |-------|           |  A1_c
% --------->|-------->| k_phi |---------->|-------->
%           |         |-------|           |
stabil=append(theta_damper,phi_damper);
ingresso=[ 2 3 ]; uscita=[ 4 8 ];
sistema_aument_stabil =
feedback(sistema_con_attuatori,stabil,ingresso,uscita);
  zpk(sistema_aument_stabil);

% Calcolo e memorizzazione matrici del sistema, zeri, poli e
guadagni in
% ciclo aperto con stabilità aumentata
  [A_CA,B_CA,C_CA,D_CA] = ssdata(sistema_aument_stabil);
  [Zeri_Theta0_CA, Poli_CA, K_Theta0_CA]  =
ss2zp(A_CA,B_CA,C_CA,D_CA,1);
  [Zeri_B1_CA, Poli_CA, K_B1_CA]  = ss2zp(A_CA,B_CA,C_CA,D_CA,2);
  [Zeri_A1_CA, Poli_CA, K_A1_CA]  = ss2zp(A_CA,B_CA,C_CA,D_CA,3);
  [Zeri_Thetat_CA, Poli_CA, K_Thetat_CA]  =
ss2zp(A_CA,B_CA,C_CA,D_CA,4);
% Calcolo e stampa pulsazioni e coefficienti di smorzamento dei
poli in ciclo aperto
%   disp(' '),disp('Poli del sistema attuatori+sistema in ciclo
aperto:'),damp(Poli_CA)

  % Schema del blocco "compensatore"
%           |------------------------------|
%     w     |         |-------|           |  theta0_c
% --------->|-------->|  k_w  |---------->|-------->
%           |         |-------|           |
%     u     |         |-------|           |  B1_c
% --------->|-------->|  k_u  |---------->|-------->
```

```
%           |         |-------|           |
%     v     |         |-------|           |  A1_c
% --------->|-------->|  k_v  |---------->|-------->
%           |         |-------|           |
%     r     |         |-------|           |  Thetat_c
% --------->|-------->|  k_r  |---------->|-------->
%           |         |-------|           |
%           |-----------------------------|
  % Parallelo tra i blocchi del compensatore
  compensatore = append(w_damper,u_damper,v_damper,yaw_damper);
% Verifica funzione di trasferimento
%   disp(' '),disp('Funzioni di trasferimento del compensatore')
%   zpk(compensatore)
  % Schema del blocco "compensatore"

% ****************************** Chiusura
******************************

  ingresso=[ 1 2 3 4]; uscita=[ 2 1 5 7 ];
  sistema_CC =
feedback(sistema_aument_stabil,compensatore,ingresso,uscita);
  zpk(sistema_CC);

% Calcolo e memorizzazione matrici del sistema, zeri, poli e
guadagni con feedback compensatore
  [A_CC,B_CC,C_CC,D_CC] = ssdata(sistema_CC);
  [Zeri_Theta0_CC,Poli_CC,K_Theta0_CC]  =
ss2zp(A_CC,B_CC,C_CC,D_CC,1);
  [Zeri_B1_CC,Poli_CC,K_B1_CC]  = ss2zp(A_CC,B_CC,C_CC,D_CC,2);
  [Zeri_A1_CC,Poli_CC,K_A1_CC]  = ss2zp(A_CC,B_CC,C_CC,D_CC,3);
  [Zeri_Thetat_CC,Poli_CC,K_Thetat_CC]  =
ss2zp(A_CC,B_CC,C_CC,D_CC,4);
  % Calcolo e stampa pulsazioni e coefficienti di smorzamento dei
poli in
%   disp(' '),disp('Poli del sistema con compensatore in ciclo
chiuso:'),damp(Poli_CC)


% Parallelo tra i blocchi controllore
  controllore = append(auto_h,auto_X,auto_Y,auto_psi);
% Verifica funzione di trasferimento
%   disp(' '),disp('Funzioni di trasferimento del compensatore')
%   zpk(controllore)
  % Schema del blocco "controllore"

%           |-----------------------------|
%   hi-h    |         |-------|           |  Theta0_c
% --------->|-------->|  k_h  |---------->|-------->
%           |         |-------|
%   Xi-X    |         |-------|           |  B1_c
% --------->|-------->|  k_X  |---------->|-------->
%           |         |-------|           |
%   Yi-Y    |         |-------|           |  A1_c
% --------->|-------->|  k_Y  |---------->|-------->
%           |         |-------|           |
%   Gyro    |         |-------|           |  Thetat_c
% --------->|-------->| k_psi |---------->|-------->
%           |         |-------|           |
```

```
%           |-----------------------------|

% Serie tra il blocco "controllore" e il blocco "sistema_CC"
% ---------------------------------------------------
  sistema_con_controllo = series(controllore,sistema_CC);
  % Verifica funzioni di trasferimento dell'aereo in ciclo aperto,
con gli attuatori
%   disp(' '),disp('Funzioni di trasferimento del sistema con
controllo in ciclo aperto:')
%   zpk(sistema_con_controllo)

% Calcolo e memorizzazione matrici del sistema, zeri, poli e
guadagni in
% ciclo aperto sistema completo
  [A_CAC,B_CAC,C_CAC,D_CAC] = ssdata(sistema_con_controllo);
  [Zeri_Theta0_CAC, Poli_CAC, K_Theta0_CAC]  =
ss2zp(A_CAC,B_CAC,C_CAC,D_CAC,1);
  [Zeri_B1_CAC, Poli_CAC, K_B1_CAC]  =
ss2zp(A_CAC,B_CAC,C_CAC,D_CAC,2);
  [Zeri_A1_CAC, Poli_CAC, K_A1_CAC]  =
ss2zp(A_CAC,B_CAC,C_CAC,D_CAC,3);
  [Zeri_Thetat_CAC, Poli_CAC, K_Thetat_CAC]  =
ss2zp(A_CAC,B_CAC,C_CAC,D_CAC,4);
% Calcolo e stampa pulsazioni e coefficienti di smorzamento dei
poli in ciclo aperto
%   disp(' '),disp('Poli del sistema con controllo in ciclo
aperto:'),damp(Poli_CA)
loop=append(back1,back1,back1,back1);

%%%%%%%%%%%%%%%%%%%%%%%%%%% chiusura %%%%%%%%%%%%%%%%%%%%%%%%%%%

ingresso=[ 1 2 3 4 ]; uscita=[ 12 10 11 9 ];

sistema_autoCC =
feedback(sistema_con_controllo,loop,ingresso,uscita);
  zpk(sistema_autoCC);
  % Calcolo e memorizzazione matrici del sistema, zeri, poli e
guadagni in
  % ciclo chiso
  [A_autoCC,B_autoCC,C_autoCC,D_autoCC] = ssdata(sistema_autoCC);
  [Zeri_Theta0_autoCC, Poli_autoCC, K_Theta0_autoCC]  =
ss2zp(A_autoCC,B_autoCC,C_autoCC,D_autoCC,1);
  [Zeri_B1_autoCC, Poli_autoCC, K_B1_autoCC]  =
ss2zp(A_autoCC,B_autoCC,C_autoCC,D_autoCC,2);
  [Zeri_A1_autoCC, Poli_autoCC, K_A1_autoCC]  =
ss2zp(A_autoCC,B_autoCC,C_autoCC,D_autoCC,3);
  [Zeri_Thetat_autoCC, Poli_autoCC, K_Thetat_autoCC]  =
ss2zp(A_autoCC,B_autoCC,C_autoCC,D_autoCC,4);
% Calcolo e stampa pulsazioni e coefficienti di smorzamento dei
poli in
% ciclo chiuso
%   disp(' '),disp('Poli del sistema con controllo in ciclo
chiuso:'),damp(Poli_autoCC)
```